Tanta University

Faculty of Engineering

Structural Engineering Department

A Thesis Submitted in Partial Fulfillment of the Requirements for the Degree of

MASTER OF SCIENCE IN ENGINEERING

(STRUCTURAL ENGINEERING)

Entitled

Flexural Behavior of Cold Formed Steel Z-Sections with Edge Stiffened Holes

By

Eng. Nasam Shokry El-Azab Khater

B.Sc. in Civil Engineering, Tanta University, 2017

Under the Supervisor Supervision of

Prof.

Mahmoud H. El-Boghdadi

(Main Supervisor)

Professor of Steel Structures

Structural Eng. Department

Faculty of Eng., Tanta University

Prof.

Nashwa M. Yossef

Professor of Steel Structures

Structural Eng. Department

Faculty of Eng., Tanta University

2023

Abstract

ABSTRACT

For several reasons, cold-formed steel (CFS) beams are usually manufactured with holes. Nevertheless, because of holes, the reduction in the web area causes a decrease in the bending strength. Edge stiffeners are now added around the holes to improve the bending strength of flexural members. This thesis studies CFSZ beams with stiffened holes and investigates how edge stiffener affects the bending strength and failure modes. A nonlinear study was conducted utilizing ABAQUS software and the developed finite element (FE) model was verified against tests from previous studies. Utilizing the verified FE model, a parametric analysis of 104 models was generated to examine the influence of key parameters on the bending capacity of Z-beams. The results indicated that adding edge stiffeners around the holes improves Z-beam flexural capacity and sometimes restores the original bending capacity.

Because the computational techniques to solve the CFS buckling mode with stiffened holes are still unclear, a numerical model for estimating the critical distortional buckling moment for a wide variety of CFSZ sections with stiffened holes using constrained and unconstrained finite strip method (CUFSM) software was suggested.

A numerical method with two procedures was applied and validated. Upon comparison, the numerical method with the two procedures accurately predicted the distortional buckling moment of such sections.

Keywords: Flexural strength; CFSZ sections; Stiffened holes; Distortional buckling moment.

Summary

Summary

In this research, emphasis was placed on the study of cold-formed steel beams with edge stiffened holes, to study the effect of steel thickness, hole size and shape, and the height of the edge stiffener on the flexural strength of this type of beams, and to conduct a numerical study using (ABAQUS) software, to compare previous numerical and experimental results, on a number of cold-formed steel beams, and also to make a parametric study on a number of beams to study the impact of the aforementioned parameters, followed by a numerical and analytical study using CUFSM program to calculate the elastic distortional buckling moment of the sections under study.

ACKNOWLEDGEMENTS

In the Name of Allah The Most Merciful. Praising be to The Almighty God who provided us with determination and support until this research was completed. We praise Him prostrating for Him for the blessings of patience and persistence with our sincere love for His eternal Supreme Being for completing this research so as to be beneficial. We pray and great our noble Messenger who taught the learners and was mercy for the whole world.

I also extend my thanks and gratitude to Prof. Mahmoud H. El-Boghdadi who honored this research with his supervision, thanking him for his advice, guidance, clarification, and detailing.

Many thanks also to Prof. Nashwa M. Yossef for her efforts, kindness, and support to solve the problems I faced while doing this research.

Special thanks to my parents who are the secret of my existence in this life. Were it not for their limitless care, donation, and dedication, this research wouldn't come out to light breathing the blessing of life.

Thanks also are extended to my brothers and sisters who surrounded me with their encouragement and support especially my younger sister, my twin soul who shared me wakefulness during the months and years of this research.

As I started with thanking God, I conclude with His praise and thanksgiving. Glory be to Him.

Nasam Shokry El-Azab Khater

Table of Contents

TABLE OF CONTENTS

ABSTRACT I

ACKNOWLEDGEMENTS III

TABLE OF CONTENTS IV

LIST OF FIGURES VIII

LIST OF TABLES XI

LIST OF SYMBOLS AND NOTATIONS XIII

ABBREVIATIONS XVIII

CHAPTER 1 INTRODUCTION 1

1.1 Overview 1

1.2 Research Objectives 3

1.3 Thesis Organization 3

CHAPTER 2 LITERATURE REVIEW 7

2.1 General 7

2.2 Introduction 7

2.2.1 Methods of manufacturing 10

2.2.2 Shapes of CFS sections and their implementations 12

2.3 Design methods for CFS flexural members in different codes 13

2.3.1 Design of CFS flexural members according to AISI code (2016) [12] 14

2.3.2 Design of CFS beams according to AS/NZS 4600 code (2005) [14] 20

2.3.3 Design of CFS beams according to EN 1993 [13] 22

2.4 Previous studies 23
2.4.1 Experimental studies on CFS beams 24
2.4.2 Theoretical studies on CFS beams 39

2.5 Summary and comments 50

CHAPTER 3 FE ANALYSIS AND VERIFICATION 55

3.1 General 55

3.2 Overview of Finite Element Analysis (FEA) 55
3.2.1 Nonlinear analysis 56
3.2.2 Buckling analysis 57

3.3 Verification Methodology for FE Model 58

3.4 Simulation of CFSC Beams; Specimens of Pham and Hancock [19] 59
3.4.1 FE model configuration 60
3.4.2 Material Model 61
3.4.3 Loading and supports 61
3.4.4 Element type and mesh 62
3.4.5 Imperfection 63
3.4.6 Validation of the FE model 63

3.5 Simulation of CFSZ Beams; Specimen of Haidarali and Nethercot [42] 66
3.5.1 Description of the FE model 66
3.5.2 The comparison of the findings 68

3.6 Simulation of CFSC Beams with Rectangular Stiffened Holes; Specimens of Perampalam et. al [58] 69
3.6.1 FE model arrangement 69
3.6.2 Comparing results 71

3.7 Simulation of CFSC Beams with Circular Stiffened Holes; Specimens of Yu [5] 72
3.7.1 Description of the elastic buckling model 72
3.7.2 Description of the nonlinear buckling model 76

3.8 Summary 79

CHAPTER 4 PARAMETRIC STUDY ON CFSZ SECTIONS WITH STIFFENED HOLES 83

4.1 General 83

4.2 Description of FE Model 83

4.3 Parametric Study 86

4.3.1 List of key parameters 87

4.4 Examination of The Results 90

4.4.1 Effect of the section thickness (*t*) 90

4.4.2 Effect of the hole depth to web height ratio (*R=a/H)* 94

4.4.3 Effect of edge stiffener height (*q*) 96

4.4.4 Effect of hole shape (Rectangular/Circular) 99

4.5 Summary 103

CHAPTER 5 INVESTIGATION ON THE ELASTIC DB MOMENT OF CFSZ SECTIONS WITH STIFFENED OPENINGS 107

5.1 General 107

5.2 Introduction of Finite Strip Method (FSM) 108

5.3 Calculation of the distortional elastic buckling moment (M_{crd}) 110

5.4 Calculating t_r based on the assumption of Grey and Moen [55] 111

5.5 A novel procedure for calculating t_r 114

5.6 The validation of the numerical model 116

5.6.1 Validation with Yu [5] 116

5.6.2 Accuracy of the t_r procedures 119

5.7 Summary 122

CHAPTER 6 CONCLUSIONS AND TRENDS FOR FUTURE RESEARCH..... 126

6.1 General..... 126

6.2 Conclusions 126

6.3 Future works 128

REFERENCES..... 132

List of Figures

LIST OF FIGURES

Figure 1.1 Various openings shapes 2

Figure 2.1 An illustration of members of the CFS with holes [1] 8

Figure 2.2 Different buckling modes of CFSZ beam. (1) Local buckling, (2) Distortional buckling, (3) Global buckling 10

Figure 2.3 Methods of forming of CFS sections: (a) Cold rolling machine, (b) Press brake operation, (c) Bending brake process [10] 11

Figure 2.4 CFS members and decks in different shapes. 12

Figure 2.5 CFSC member with web opening 12

Figure 2.6 Details for calculation of EW of elements with non-circular openings [12] 16

Figure 2.7 Notations for webs subjected to the stress gradient [12] 17

Figure 2.8 Z sections with different stiffener configurations [18] 24

Figure 2.9 Scheme of bending test configuration [18] 25

Figure 2.10 Types of sections [19] 26

Figure 2.11 Sections of tested beams [20] 26

Figure 2.12 RHFB section [21] 27

Figure 2.13 Types of CFS channel sections [23] 28

Figure 2.14 Cross section of SOHS [24] 29

Figure 2.15 Types of sections [25] 30

Figure 2.16 Interior two flange configuration [28] 32

Figure 2.17 Cross section of samples [31] 34

Figure 2.18 Sections used in the experimental test [36] 36

Figure 3.1 An illustration of a cantilever beam used to illustrate boundary nonlinearity [15] 57

Figure 3.2 Test setup configuration [19] 59

Figure 3.3 Definitions for cross-sectional dimensions 60

Figure 3.4 FE model configuration 61

Figure 3.5 Concentrated loads at shear center 62

Figure 3.6 Scheme of the S4R shell element 63

Figure 3.7 The comparison of failure mode between [19] and the FE for C20015 64

Figure 3.8 The comparison of load-deflection behavior between the FE and those in [19] 65

Figure 3.9 The symbols of the Z-section dimensions 67

Figure 3.10 The boundary conditions and the configuration of the FE model 67

Figure 3.11 Material model for D8.5Z120-4 [42] 67

Figure 3.12 The comparison of load-deflection curve obtained from the FE model and those in [42] 69

Figure 3.13 The beam with four-point bending arrangement 70

Figure 3.14 Dimensions of channel section 70

Figure 3.15 The loads and supports of the model 71

Figure 3.16 Details of FE model of elastic buckling analysis 73

Figure 3.17 Cross-section of CFSC beam with stiffened holes 76

Figure 3.18 The nonlinear buckling model of CFSC beam with stiffened holes 77

Figure 3.19 Distortional failure for 600S250-97, 800S250-97 and 1200S250-97 beams with stiffened holes 79

Figure 4.1 Mesh shape of the FE model 85

Figure 4.2 Description of the boundary conditions applied in the FE model 86

Figure 4.3 Finite element model dimensions (a: cross-section, b: unstiffened holes, c: Stiffened hole) 88

Figure 4.4 The hole location in the beam web 90

Figure 4.5 Normalized bending strength for studied beams *G1* and *G2* with rectangular holes ($a/H = 0.6$)..... 91

Figure 4.6 Normalized bending strength for sections with edge stiffened holes ($q = 10$ mm) 93

Figure 4.7 The failure modes of CFSZ beams with varying cross-section thickness 94

Figure 4.8 Relation between bending strength and displacement for CFSZ without holes, with unstiffened holes, and with stiffened edge holes 98

Figure 4.9 Box plot for 80 CFSZ specimens with rectangular web openings showing the effect of edge stiffened height (q) 98

Figure 4.10 The failure modes of the CFSZ section with varying stiffener height 99

Figure 5.1 Finite strip and finite element discretization. 108

Figure 5.2 The buckling curve in CUFSM..... 109

Figure 5.3 Illustration of the numerical model for calculating elastic DB moment 111

Figure 5.4 Illustration of the web hole: a) cross-section, b) web with a rectangular opening, c) web with a circular opening and equivalent rectangular to the circular opening..... 113

Figure 5.5 Rotational stiffness of the web/flange juncture for CFSZ with stiffened hole 114

List of Tables

LIST OF TABLES

Table 3.1 Samples dimensions and properties 60

Table 3.2 The boundary conditions for the FE model 62

Table 3.3 Validation of the FE findings versus the test findings (Pham and Hancock [19])... 64

Table 3.4 Section dimensions 66

Table 3.5 Verification of the FE model against the numerical result of [42] 68

Table 3.6 Boundary conditions 71

Table 3.7 Verification of the FE model against the numerical result (Perampalam et al. [58]) 72

Table 3.8 Details of Yu's [5] sections 73

Table 3.9 The comparison between the FE elastic moment ratios and Yu results [5] 74

Table 3.10 Comparison between the elastic buckling model of Yu [5] and the presented FE for CFSC 1000S162-43 with stiffened circular holes spaced 305 mm 75

Table 3.11 The dimensions of the studied beams 77

Table 3.12 Comparison of the moment strengths determined from the FE and Yu's [5] model. 78

Table 4.1 Dimensions of the adopted Z- section 88

Table 4.2 Reduction in the bending strength of the CFSZ section with the variation of R and q 95

Table 4.3 The effect of hole shape on the bending strength 100

Table 4.4 Influence of hole shape on failure modes of beams 101

Table 4.5 (continued) 102

Table 5.1 Verification of the Numerical model against the results in Yu [5] 118

Table 5.2 The accuracy of the presented model to calculate M_{crd} 121

List of Symbols and Notations

LIST OF SYMBOLS AND NOTATIONS

a	Hole diameter
a/H	Hole diameter - to - web height ratio
B	Flange width
b	Effective width
b_e	Effective width in EN 1993-1-3
b_o	Width of the compression flange
b_1	Effective width
C	Coiled length
D	Lip length
d_h	Hole diameter in AISI
E	Elasticity modulus
F_n	Flexural stress for global buckling
f	Stress in compression element
f_y	Yield stress
f_1	Stress in the compression region

f_2	Stress in the tension region
G	Shear modulus
$G1$	Group 1
$G2$	Group 2
H	Web height
h_o	Height of the web in AISI
J_{we}	St. Venant torsional constant
K	Coefficient of plate buckling
K_σ	Buckling factor
K_θ	Accumulative web stiffness without a hole
$K_{\theta, hole}$	Reduced transverse rotational stiffness of a web with a hole
$K_{\theta, r}$	Equivalent accumulative web rotational stiffness
$K_{\theta, stiffener}$	Rotational restraint of the hole edge stiffener
$K_{\theta we}$	Elastic rotational stiffness provided by effective part of web
L	Span length
L_{cr}	Half-wavelength of distortional buckling of CFS without holes

L_h	Hole length
L_p	Effective hole length
M_{crd}	Critical distortional buckling moment
M_{crdn}	Distortional buckling moment for beams without holes
M_{crdw}	Distortional buckling moment for beams with holes
M_{cre}	Critical LTB moment
M_{crl}	Critical local buckling moment
M_n	Nominal flexural moment
M_{nd}	Nominal distortional buckling moment
M_{ne}	Nominal LTB moment
M_{nl}	Nominal local buckling moment
M_{uh}	Bending strength of beams with holes
M_{us}	Bending strength of solid beams
M_{ynet}	Yield moment of net section
q	Height of hole edge stiffener
R	Ratio of hole depth to web height
S_e	Effective section modulus

S_f	Full section modulus of the outer fiber
S_{fnet}	Net section modulus
t	Thickness of section
t_r	Reduced web thickness
w	Flange width in AISI
ρ	Local buckling reduction factor
λ	Slenderness factor
$\bar{\lambda}_p$	Slenderness ratio of the plate in BS EN1993
ν	Poison ratio
ω	Stress ratio
σ_{cr}	Critical buckling stress
θ	Edge stiffener inclination

Abbreviations

ABBREVIATIONS

AISI	**A**merican **I**ron and **S**teel **I**nstitute
AS	**A**ustralian **S**tandard
CFS	**C**old **F**ormed **S**teel
CFSC	**C**old **F**ormed **S**teel **C**hannel
CFSZ	**C**old **F**ormed **S**teel **Z**ed
DSM	**D**irect **S**trength **M**ethod
DB	**D**istortional **B**uckling
EOF	**E**nd **O**ne **F**lange
ETF	**E**nd **T**wo **F**lange
EWM	**E**ffective **W**idth **M**ethod
FEM	**F**inite **E**lement **M**ethod
FSM	**F**inite **S**trip **M**ethod
IOF	**I**nterior **O**ne **F**lange
ITF	**I**nterior **T**wo **F**lange

LB	**L**ocal **B**uckling
LTB	**L**ateral **T**orsional **B**uckling
NZS	**N**ew **Z**ealand **S**tandard
RHFBs	**R**ectangular **H**ollow **F**lange **B**eams
SD	**S**tandard **D**eviation
SOHF	**S**emi **O**val **H**ollow **F**lange

Chapter 1
Introduction

Chapter 1 Introduction

1.1 Overview

In the 1850s, the United States was the first country to use CFS in the building industry. Since there was a lack of material knowledge and a lack of standard code, this material was limited in applications until 1946 when the American Iron and Steel Institute (AISI) issued the first edition of its standard to design CFS members (AISI, 1946). Today, it is common practice to use CFS members in construction as primary and secondary members of frame systems, including roof purlins, sandwich panels, and walls. CFS is widely used due to several characteristics, including its high capacity-to-weight ratio, wide variety of section shapes, corrosion resistance, and the ease of installation [1].

Z and C purlins are commonly used in steel buildings to carry the roof panels and transmit the roof wind loads to the main frames and provide lateral stability to the main frame parts. It is recommended to use Z-sections over C-sections for shipping purposes since they can be nestled easier and produce a more compact package. Furthermore, the economy of a continued span purlin can be easily attained by lapping and nesting the Z-section. There is no other way to provide continuity for the channel section except through coupling two channel sections cascading. Moreover, the benefit of utilizing Z purlins is due to the unrestricted depth and thickness choice, which provides the necessary freedom for the designer to create the most economical purlin [2].

CFS sections are generally more efficient than hot-rolled sections. Nevertheless, they are exposed to numerous complicated buckling modes since they are often thin sections with unsymmetric or singly symmetric cross sections [3].

Generally, CFS beams (purlins/joists) are exposed to five failure modes and such modes are lateral torsional buckling (LTB), local buckling (LB), distortional buckling (DB), web crippling, and web shear buckling. In the case of CFS members employed as floor beams, floor decks are usually built over such members. Floor decks supply lateral bracing for CFS joists, which prevents them from failing by lateral torsional buckling. Supplying web stiffeners at the support locations can prevent the web crippling of these joists. Consequently, CFS floor joists/purlins are expected to fail due to local buckling, distortional buckling, and shear buckling of the webs.[4]

CFS beams are often manufactured with holes to thread services through (piping, heating ducts, etc.). Figure 1.1 presents varied shapes of openings generated in beams and columns. Web holes in beams reduce the bending strength. Edge stiffeners are sometimes added around openings to improve the bending strength. These edge stiffeners cause stress redistribution in the opening position and alteration in the boundary condition of the web [5].

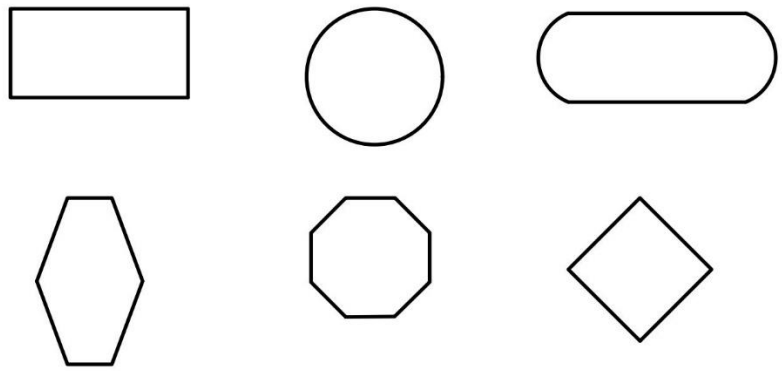

Figure 1.1 Various openings shapes

1.2 Research Objectives

Our knowledge of CFS beams with stiffened holes is largely based on limited data, and the elastic buckling moment has not yet been investigated in depth (as will be seen in Chapter 2). Moreover, motivated by the lack of information about CFSZ beams with stiffened holes, the aim of this thesis was to study the behavior of CFSZ beams with stiffened holes numerically and observe the hole edge stiffener impact on the flexural capacity, as well as failure modes. Hence, the elastic distortional moment of such beams will be proposed utilizing numerical and analytical procedures. So, the Direct Strength Method (DSM) based design equations could be extended to indicate the bending strength of such beams. Since the DSM for calculating the distortional buckling strength of CFS beams with holes is primarily based on the elastic distortional buckling moment, introducing a numerical model to accurately calculate the elastic distortional buckling moment, for the beams under consideration, can improve the DSM.

1.3 Thesis Organization

The thesis contains six chapters, and the contents of such chapters are briefly depicted as follows:

Chapter 1: This chapter highlights the content and the purpose of this thesis and provides a brief introduction on cold-formed steel members.

Chapter 2: This chapter presents an introduction of CFS members in more detail. Moreover, different design procedures, according to different standard codes, to estimate the bending capacity of CFS flexural members with /without openings are presented. Finally, a summary of the current literature review associated with CFS beams (experimental, numerical, and analytical studies) is introduced in this chapter.

Chapter 3: A definition of the numerical modeling approach, which is adopted in this thesis, is included in this chapter as well as a validation study on the used finite element model.

Chapter 4: This chapter describes the adopted FE model in more detail and develops a parametric investigation on CFSZ beams to study the effect of a group of parameters such as steel thickness, opening size, opening shape, and stiffener height on the bending capacity and failure modes.

Chapter 5: A numerical method with two different procedures utilizing the finite strip method is suggested in this chapter to estimate the elastic distortional buckling moment of the studied beams.

Chapter 6: The major findings of this research as well as suggestions for forthcoming research are highlighted in this chapter.

Chapter 2

Literature Review

2Chapter 2 Literature Review

2.1 General

This chapter summarizes experimental and theoretical researches relevant to this thesis, which are available in the literature. Previous studies conducted on different configurations of CFS beams are widely discussed. Furthermore, this chapter considers a variety of design formulas as suggested by a code of practice and previous research. In general, this chapter provides the necessary background for this thesis.

2.2 Introduction

Steel structures are mostly made of hot-rolled and cold-formed members. Members made of hot-rolled steel are fabricated at high temperatures, whereas those made of CFS are fabricated at room temperature [6]. The CFS members are made up of sections that have been cold formed from steel strips, sheets, flat bars, and plates, using roll-forming equipment, press braking, or bending brake processes. Steel sheets or strips with a thickness between 0.4 and 6.4 mm are typically utilized in CFS members. Cold forming can be used to successfully create structural shapes out of bars up to 25 mm thick [7].

Openings are usually set in the webs of CFS members such as purlins/beams to permit installing a plumbing system, piping, and bracing. Also, because the effective width approach considers the removal of parts which exposed to the local buckling from the calculations; it can be achieved from the beginning by making holes in the web. Figure 2.1 presents an illustration of members of the CFS with holes [1].

Figure 2.1 An illustration of members of the CFS with holes [1]

CFS members have a lot of advantages in building structures. Some of these advantages are listed below:

1- Cold-formed steel light sections can handle comparatively light loads and/or small lengths, as compared to heavier hot-rolled sections.
2- Load-bearing decks can offer practical surfaces for the construction of a floor, roof, and walls. Under different circumstances, such decks could even supply enclosed partitions for conduits.
3- Cold-forming processes enable the economically efficient production of unique sectional shapes, leading to the achievement of good strength/weight ratios [7].

The following characteristics of CFS structural members can be achieved in comparison with other materials, for example, concrete and wood:

1- Lightness.
2- High stiffness and capacity.
3- It is easy to prefabricate and mass produce.
4- Installation is fast and straightforward.
5- Greater accuracy in the details.
6- Transportation and handling costs are reduced.
7- Incombustible.
8- Recyclable material.
9- At ambient temperatures, the material does not shrink or creep. [7]

Although CFS members have many advantages, there are several disadvantages such as weak torsional stiffness, low resistance to fire, and lowered ductility [8]. A major drawback of the CFS member is its raised slenderness, which allows it to be buckled primarily through one or more of the following modes [9]:

- Local buckling (does not include any translation only rotation of the intersection between the web and the flange. The flange and web deformation generally take the form of a sine wave with a half wavelength equal to or smaller than the biggest dimension of the element subjected to compressive stress) [9].
- Distortional buckling (includes rotation and translation at the flange-web junction, resulting in significant deformation of both the web and the flange.

The web is exposed to a flexural distortion corresponding to a sine wave shape. The half wavelength lies between the half wavelength of local and overall buckling [9].

- Global buckling (LTB or/and flexural buckling) happens with no deformation of the cross-section parts at long half-wavelengths. The cross-section is translated and/or rotated as a rigid body) [9]. Figure 2.2 shows the different buckling modes of the Z-beam.

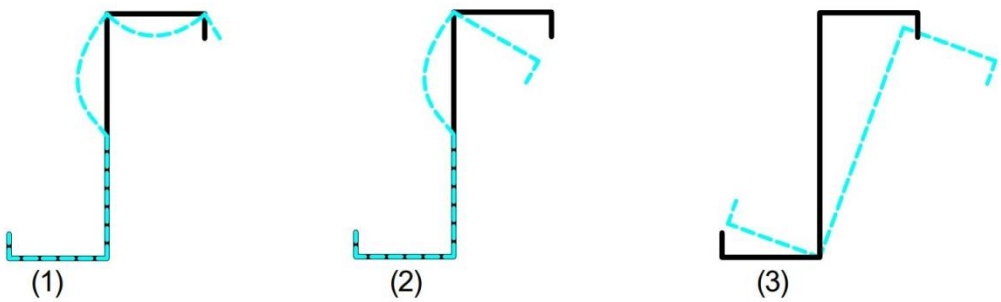

Figure 2.2 Different buckling modes of CFSZ beam. (1) Local buckling, (2) Distortional buckling, (3) Global buckling

To manufacture the CFS sections, several methods can be used as will be shown in the next subsection.

2.2.1 Methods of manufacturing

Cold-formed sections are produced using one of three techniques:

1. Cold roll forming (construction parts including individual members, floor, and wall panels are produced using this technique). The machine of cold roll forming is shown in Figure 2.3 (a).
2. Press brake process (Figure 2.3 (b)). This method is used under some restrictions such as:

- The section is of uncomplicated configuration.
- The section to be created is comparatively broad (typically larger than 457 mm).
- The required amount is less than 91.5 m/min).

Using a press brake, simple shapes like angles, C-channel, and Z-sections can be created in a maximum of two processes. Sections with greater complexity might require multiple processes [7].

3. Bending brake process (Figure 2.3 (c)).

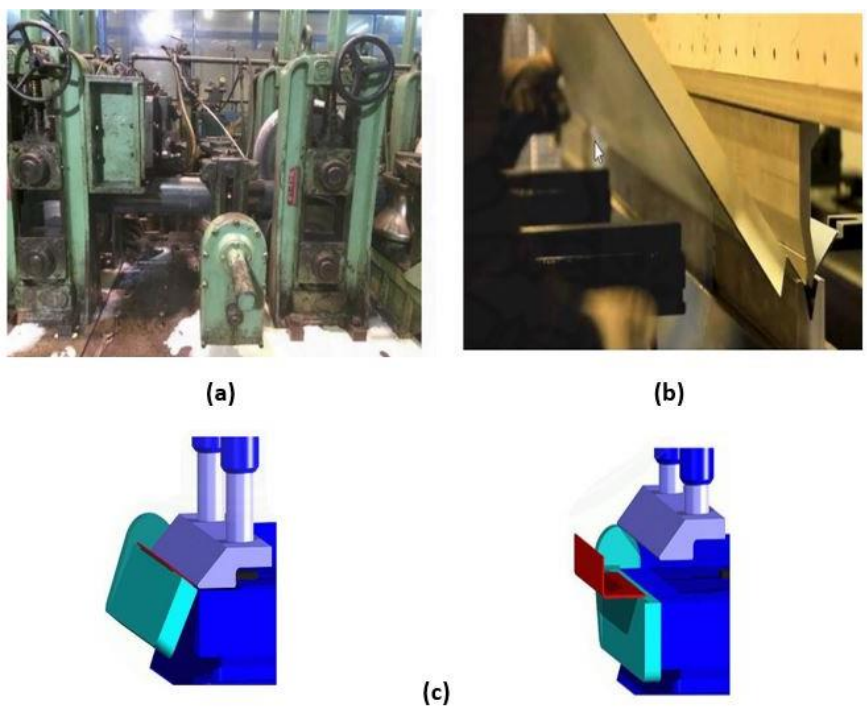

Figure 2.3 Methods of forming of CFS sections: (a) Cold rolling machine, (b) Press brake operation, (c) Bending brake process [10]

These methods can produce different shapes of CFS sections as will be presented in the next subsection.

2.2.2 Shapes of CFS sections and their implementations

There are a lot of shapes that can be produced for CFS sections. Some of them are used to produce the individual members such as channels, Z-sections, angles, hat sections, I-sections, T-sections, and tubular sections, and others are used to produce panels and decks as shown in Figure 2.4 [7]. Sometimes, there is a need to create holes in the CFS members, as shown in Figure 2.5.

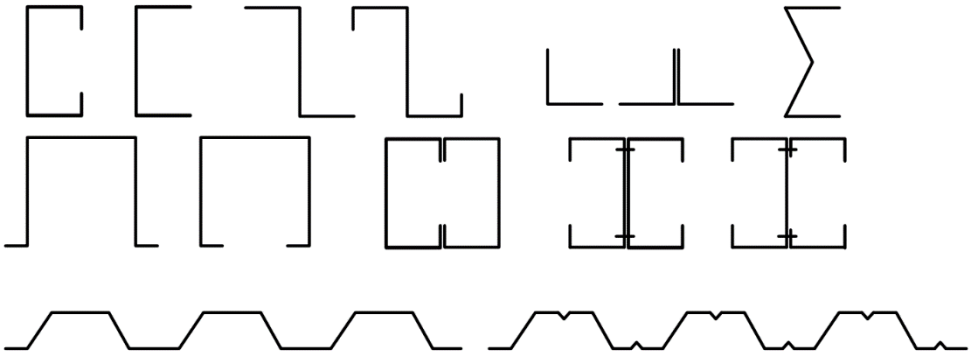

Figure 2.4 CFS members and decks in different shapes.

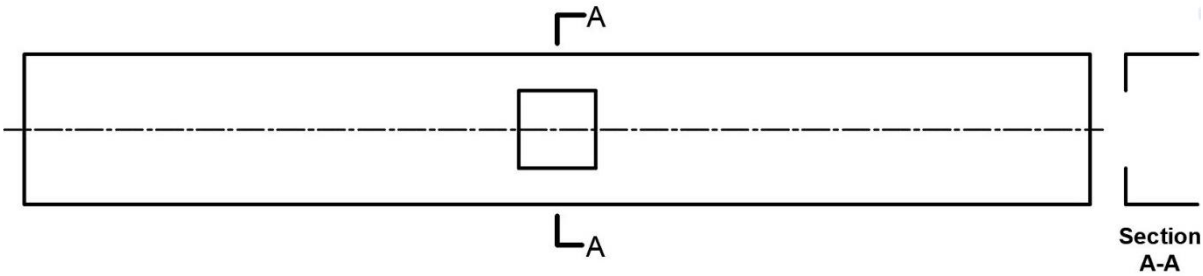

Figure 2.5 CFSC member with web opening

CFS members are used in the following implementations [11]**:**

1. Systems for the roof and walls of commercial, industrial, and agricultural structures.
2. Structural components for plane or space trusses.
3. Residential structures.
4. Roof deck or steel floor.
5. Utility poles.
6. Automotive implementations.

The existing standards, including the AISI-16 [12], EN 1993 [13], and the Australian and New Zealand Standards (AS/NZS) [14], handle the flexural capacity of CFS sections with solid webs and with web holes. In contrast, they don't supply procedures for determining the bending capacity of CFS sections with edge-stiffened openings. So, a design method is needed to consider the impact of adding edge stiffener around openings. The following subsections provide an overview of the different standards used to design the CFS flexural members.

2.3 Design methods for CFS flexural members in different codes

In the current CFS design codes, there are two primary design procedures, the effective width method (EWM) and the direct strength method (DSM). The EWM depends on the reduction area supplied by each element in the cross-section undergoing to local buckling. However, the DSM considers the stability of the whole cross-section along with the interaction among the elements. [15]

2.3.1 Design of CFS flexural members according to AISI code (2016) [12]

Two design procedures are presented by the AISI for CFS members, the DSM provided in the Main Specification (AISI-S100-16, Chapter F) and the EWM in the (AISI-S100-16, Appendix 1). The detailing of each procedure is presented below.

2.3.1.1 EWM for CFS beams

The calculations of effective width (b) for CFS members are summarized in the following equations:

1) <u>The effective width (EW) of uniformly compressed stiffened elements</u>

b should be determined such that:

$$b = w \quad \text{when} \quad \lambda \leq 0.673 \qquad \textbf{Eq. (2.1)}$$

$$b = w\rho \quad \text{when} \quad \lambda > 0.673 \qquad \textbf{Eq. (2.2)}$$

Such that

$w =$ Flat width

$\rho =$ Local reduction factor

$$= \frac{(1 - 0.22/\lambda)}{\lambda} \qquad \textbf{Eq. (2.3)}$$

$\lambda =$ Slenderness factor

$$= \sqrt{\frac{f}{Fcrl}} \qquad \textbf{Eq. (2.4)}$$

$f =$ Stress in compression element

$$F_{crl} = k\ \frac{\pi^2 E}{12(1-\mu^2)}[t/w]^2 \qquad \textbf{Eq. (2.5)}$$

Such that

$K =$ Coefficient of plate buckling

t = Thickness of compressed parts.

E = Elasticity Modulus

μ = Poisson's ratio.

2) <u>The EW of uniformly compressed unstiffened elements</u>

b should be considered as the b of stiffened elements, with the exception that, k, shall be taken equal to 0.43.

3) <u>The EW of uniformly compressed stiffened elements with holes</u>

b for circular openings is defined as:

when $0.5 \geq d_h/w \geq 0$, and $w/t \leq 70$, and the opening spacing $\geq 0.5w$ and $\geq 3d_h$

$$b = w - d_h \quad \text{when} \quad \lambda \leq 0.673 \qquad \textbf{Eq. (2.6)}$$

$$b = \frac{w\left(1 - \frac{0.22}{\lambda} - \frac{0.8d_h}{w} + \frac{0.085d_h}{w\lambda}\right)}{\lambda} \quad \text{when} \quad \lambda > 0.673 \qquad \textbf{Eq. (2.7)}$$

Where d_h represents the hole diameter.

While for a uniformly stiffened element with openings that are not circular, the element should be comprise of two unstiffened strips of flat width (c) neighboring to the openings as shown in Figure 2.6. Then, b of each unstiffened strip should be calculated as b of stiffened elements as mentioned earlier. But here the coefficient of plate buckling should be taken = 0.43.

Some limits must be taken into account when using these provisions, these limits are presented in AISI (Appendix 1).

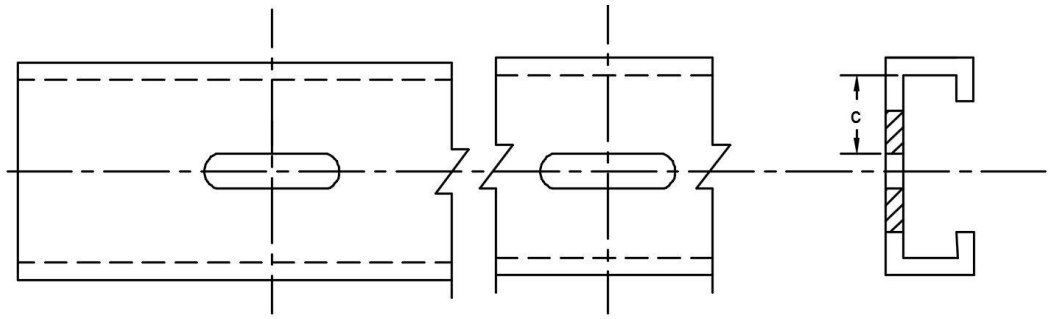

Figure 2.6 Details for calculation of EW of elements with non-circular openings [12]

4) <u>The EW of stiffened elements exposed to a stress gradient</u>

For webs exposed to a stress gradient, the coefficient of plate buckling and EW should be defined such that:

$$k = 4 + 2(1+\omega)^3 + 2(1+\omega) \qquad \textbf{Eq. (2.8)}$$

When $h_o/b_o \leq 4$

$$b_1 = b_e/(3+\omega) \qquad \textbf{Eq. (2.9)}$$

$$b_2 = b_e/2 \qquad \text{For } \omega > 0.236 \qquad \textbf{Eq. (2.10)}$$

$$b_2 = b_e - b_1 \qquad \text{For } \omega \leq 0.236 \qquad \textbf{Eq. (2.11)}$$

For $h_o/b_o > 4$

$$b_1 = b_e/(3+\omega) \qquad \textbf{Eq. (2.12)}$$

$$b_2 = b_e/(1+\omega) - b_1 \qquad \textbf{Eq. (2.13)}$$

Such that

b_e = Effective width calculated as the b of uniformly compressed stiffened element, with the exception that, k, shall be taken equal to Eq. (2.8)

b_1, b_2, and are effective widths (as defined in Figure 2.7).

b_o = The width of the compression flange (out-to-out) (Figure 2.7).

h_o = The web depth (out to out) (Figure 2.7).

$\varphi = |f_2/f_1|$,

where

f_1 = Stress in compression region (Figure 2.7).

f_2 = Stress in tension region (Figure 2.7).

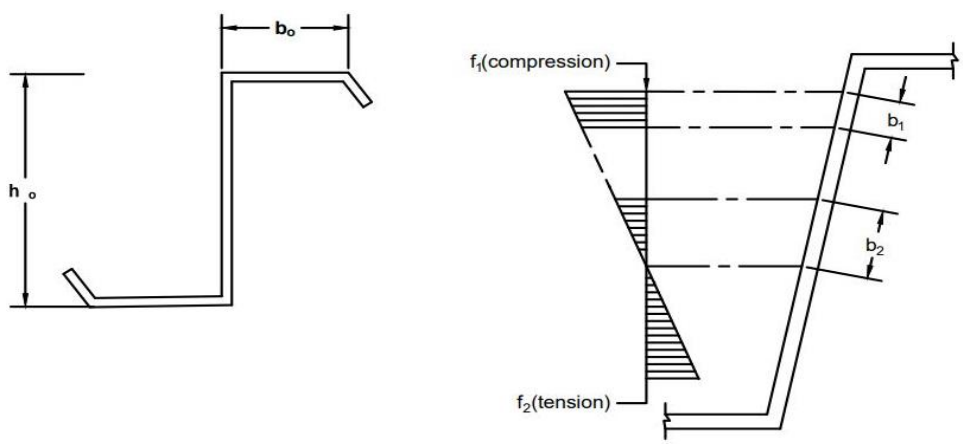

Figure 2.7 Notations for webs subjected to the stress gradient [12]

After calculating the effective width in the previous ways (as mentioned before), the nominal flexural capacity could be determined such that:

$$M_n = S_e F_n \leq S_{et} f_y \qquad \textbf{Eq. (2.14)}$$

Such that

S_e = Effective section modulus estimated at outer fiber compressive stress of F_n.

F_n = Flexural stress for global buckling. The detailing of the calculation of the (F_n) is presented in AISI standard (section F2.1).

S_{et} = Effective section modulus estimated at outer fiber tension stress of f_y.

f_y = Yield stress.

Note: S_e is calculated for members without openings using the EW of each component in the cross-section. For sections with unstiffened openings, the parts neighboring the opening should be handled as unstiffened elements.

2.3.1.2 DSM for CFS beams

DSM is an appropriate way for determining the strength of CFS members. Regarding the design of CFS flexural members with openings, it will be summarized below:

The nominal flexural strength (M_n) is equal to the minimum of M_{ne}, M_{nl}, and M_{nd} (LTB strength, LB strength, and DB strength) respectively.

1) <u>LTB moment (M_{ne}):</u>

For $M_{cre} < 0.56M_y$

$$M_{ne} = M_{cre} \qquad \textbf{Eq. (2.15)}$$

For $2.78M_y \geq M_{cre} \geq 0.56M_y$

$$M_{ne} = 10/9\, M_y \left[1 - \frac{10M_y}{36M_{cre}}\right] \qquad \textbf{Eq. (2.16)}$$

For $M_{cre} > 2.78M_y$

$$M_{ne} = M_y \qquad \textbf{Eq. (2.17)}$$

Where

M_{cre} = Critical elastic LTB moment (including the impact of openings).

2) <u>LB moment (M_{nl})</u>:

For $\lambda_l = \sqrt{M_{ne}/M_{crl}} \leq 0.776$ **Eq. (2.18)**

$$M_{nl} = M_{ne}$$ **Eq. (2.19)**

For $\lambda_l > 0.776$

$$M_{nl} = \left[1 - 0.15\left[\frac{M_{crl}}{M_{ne}}\right]^{0.4}\right]\left[\frac{M_{crl}}{M_{ne}}\right]^{0.4} M_{ne}$$ **Eq. (2.20)**

M_{crl} = Critical elastic LB moment (including the impact of openings).

3) <u>DB moment (M_{nd}):</u>

For $\lambda_d \leq \lambda_{d1}$

$$M_{nd} = M_{ynet}$$ **Eq. (2.21)**

For $\lambda_{d1} < \lambda_d \leq \lambda_{d2}$

$$M_{nd} = M_y - \left(\frac{M_{ynet-M_{d2}}}{\lambda_{d2} - \lambda_{d1}}\right)(\lambda_d - \lambda_{d1})$$ **Eq. (2.22)**

For $\lambda_d > \lambda_{d2}$

$$M_{nd} = \left[1 - 0.22\left[\frac{M_{crd}}{M_y}\right]^{0.5}\right]\left[\frac{M_{crd}}{M_y}\right]^{0.5} M_y$$ **Eq. (2.23)**

Where

M_{crd} = Critical elastic DB moment (including the impact of openings)

$\lambda_d = (M_y/M_{crd})^{0.5}$

$\lambda_{d1} = 0.673(M_{ynet}/M_y)^3$

$\lambda_{d2} = 0.673(1.7(M_y/M_{ynet})^{2.7} - 0.7)$

M_{ynet} = Yield moment (for net section) = $S_{fnet}f_y$, where S_{fnet} = net section modulus.

Note: Critical elastic moment is calculated according to Appendix 2 in AISI (2016) or from CUFSM software as will be presented in Chapter 5 [16].

2.3.2 Design of CFS beams according to AS/NZS 4600 code (2005) [14]

The EWM and DSM that are provided by the AISI standard are presented likewise in the AS/NZS 4600 code for CFS members. The detailing of each method is discussed here.

2.3.2.1 EWM

The M_n for C and Z - sections is the minimum of the $M_n$calculated according to initiation of yielding, LTB, and DB.

1) <u>According to the initiation of yielding</u>

$$M_{ny} = S_e f_y \qquad \textbf{Eq. (2.24)}$$

Where

f_y = Yield strength.

S_e = The effective section modulus defined at the yield stress.

2) <u>According to LTB</u>

The $M_n$of the laterally unbraced sections is determined as follows:

$$M_{nLTB} = S_c f_c \qquad \textbf{Eq. (2.25)}$$

Where S_c is the effective section modulus computed at a stress f_c and $f_c = \frac{M_c}{S_f}$, where S_f represents the full unreduced section modulus for the outer compression fiber and M_c is the critical LTB

moment. The detailing of the calculation of the (M_c) is presented in AS/NZS standard in section 3.3.3.2.1.

3) According to DB

The M_n of sections is determined such that:

$$M_{nDB} = S_c f_c \qquad \textbf{Eq. (2.26)}$$

The detailing of calculations of the S_c and f_c, for DB, are presented in AS/NZS standard in section 3.3.3.3.

As mentioned before, to determine the effective section modulus of the cross-section, the EW of each compression element should be defined first. The procedures and the equations of calculation of the effective width are the same as those provided by AISI.

2.3.2.2 DSM

The M_n is the minimum of the M_n for LTB, LB, and DB strengths (M_{ne}, M_{nl}, M_{nd}) respectively.

1) For LTB (M_{ne})

For $M_{cre} < 0.56\ M_y$

$$M_{ne} = M_{cre} \qquad \textbf{Eq. (2.27)}$$

For $2.78M_y \ \geq \ M_{cre} \geq \ 0.56M_y$

$$M_{ne} = 10/9M_y\left[1 - 10M_y/36M_{cre}\right] \qquad \textbf{Eq. (2.28)}$$

For $M_{cre} > \ 2.78M_y$

$$M_{ne} = M_y \qquad \textbf{Eq. (2.29)}$$

Such that

M_{cre} = Elastic LTB moment.

$M_y = S_f f_y$, where (S_f) is the full section modulus of the outer fiber.

2) For LB (M_{nl})

For $\lambda_l = \sqrt{M_{ne}/M_{crl}} \leq 0.776$

$$M_{nl} = M_{ne} \quad \textbf{Eq. (2.30)}$$

For $\lambda_l > 0.776$

$$M_{nl} = \left[1 - 0.15\left[\frac{M_{crl}}{M_{ne}}\right]^{0.4}\right]\left[\frac{M_{crl}}{M_{ne}}\right]^{0.4} M_{ne} \quad \textbf{Eq. (2.31)}$$

M_{crl} = Elastic LB moment.

3) For DB (M_{nd})

For $\lambda_d = \sqrt{M_y/M_{crd}} \leq 0.673$

$$M_{nd} = M_y \quad \textbf{Eq. (2.32)}$$

For $\lambda_d > 0.673$

$$M_{nd} = \left[1 - 0.22\left[\frac{M_{crd}}{M_y}\right]^{0.5}\right]\left[\frac{M_{crd}}{M_y}\right]^{0.5} M_y \quad \textbf{Eq. (2.33)}$$

Where

M_{crd} = Elastic DB moment.

2.3.3 Design of CFS beams according to EN 1993 [13]

2.3.3.1 EWM

The detailing of the EWM is developed in Clause 4.4 of BS EN 1993-1-5, and presented as follows:

$$b_e = \rho b \quad \textbf{Eq. (2.34)}$$

$$\rho = 1 \qquad \text{For } \bar{\lambda}_p \leq 0.673 \qquad \textbf{Eq. (2.35)}$$

$$\rho = \frac{\bar{\lambda}_p - 0.055(3+\varphi)}{\bar{\lambda}_p{}^2} \leq 1 \qquad \text{For } \bar{\lambda}_p > 0.673 \qquad \textbf{Eq. (2.36)}$$

$\bar{\lambda}_p$ = Slenderness ratio of plate

$$= \sqrt{\frac{f_y}{\sigma_{cr}}} = \frac{b/t}{28.4\varepsilon\sqrt{k_\sigma}} \qquad \textbf{Eq. (2.37)}$$

Such that

$\varepsilon = \sqrt{\frac{235}{f_y}}$, k_σ, represents the buckling factor, and (ρ) represents the reduction factor.

φ = the stress ratio determined according to clauses 4.4(3) and 4.4(4) in BS EN 1993-1-5.

σ_{cr} = the critical buckling stress of the plate.

For an unstiffened element, the same way is used to calculate its effective width with some changes:

$$\rho = 1 \qquad \text{For } \bar{\lambda}_p \leq 0.748 \qquad \textbf{Eq. (2.38)}$$

$$\rho = \frac{\bar{\lambda}_p - 0.188(3+\varphi)}{\bar{\lambda}_p{}^2} \qquad \text{For } \bar{\lambda}_p > 0.748 \qquad \textbf{Eq. (2.39)}$$

2.4 Previous studies

The following subsections summarize experimental, numerical, and analytical research available in the literature relevant to the subject being discussed.

2.4.1 Experimental studies on CFS beams

2.4.1.1 Experimental studies on CFS beams with solid web

In 2003, Yu and Schafer conducted an experimental investigation on C and Z sections [17]. The study focused on local buckling failure. All samples were simply supported and loaded at 1/3 point of the span. A comparison was made between the bending strengths defined by the test and those determined by the DSM. By comparison, for thin and thick specimens, it was found that the DSM provides satisfactory capacity predictions.

The behavior of CFSZ beams with different stiffener configurations was carried out by Nguyen et al. in 2006 [18] (see Figure 2.8). Four points loading test was carried out as presented in Figure 2.9. All specimens were simply supported. From the test, it was observed that at the maximum load, the LB and DB failures were noticed in all samples. Moreover, compared to thinner samples, thicker samples reached the maximum moment more slowly. The bending strengths obtained from the test were compared with those obtained from the AISI [12], and AS/NZS [14] standards. In general, the strengths predicted by those standards were conservative for the studied samples.

The study involved a numerical analysis using ABAQUS program to verify the experimental results, and it presented a reasonable agreement with the experimental findings.

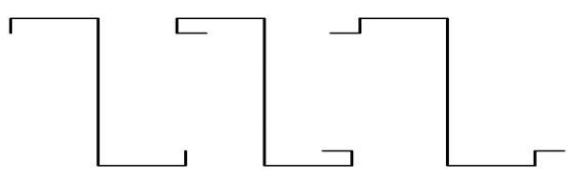

Figure 2.8 Z sections with different stiffener configurations [18]

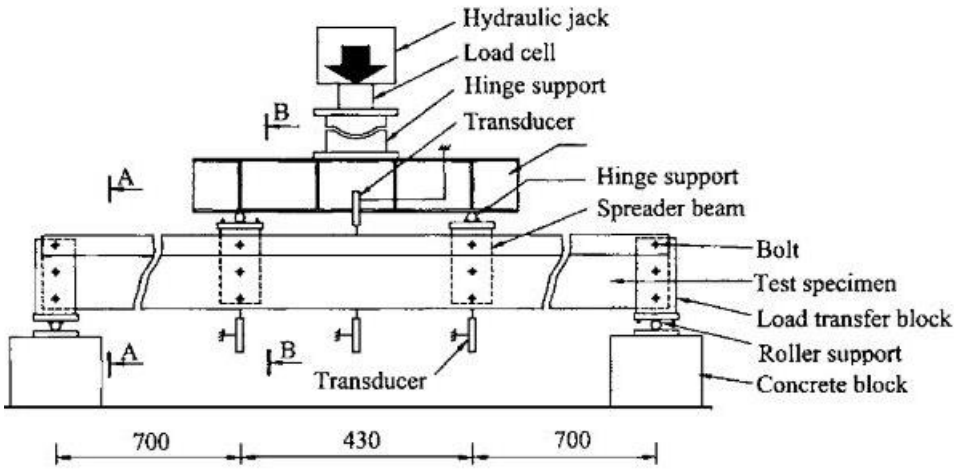

Figure 2.9 Scheme of bending test configuration [18]

An experimental study was adopted by Pham and Hancock (2013) to determine the flexural capacities of CFS build-up sections with high-strength steel [19]. Figure 2.10 shows the section types used in this investigation. An arrangement consisting of four-point bending was used for the test. Two sets of samples were used in the test. A set of them was restricted from the failure of DB by attaching the straps between the two loading points in the bending area whereas the other group was not restricted (to fail under DB). From the findings, it was found that the bending strengths of type 2 sections were improved by 4.5% to 22.4% compared to type 1 sections, with the thin sections showing the greatest improvement.

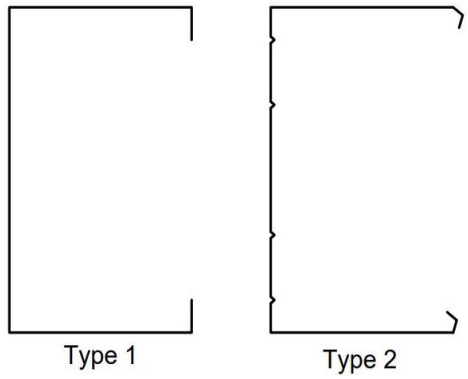

Figure 2.10 Types of sections [19]

In 2013, Laim et al. investigated experimentally the bending strength of four types of sections as shown in Figure 2.11 [20]. In this study, structural performance and the modes of failure of these types of sections were compared. All samples were loaded at 1/3 points of the beam length. The authors concluded that, in comparison with other types of studied beams, type 4 demonstrated a significantly higher on average maximum load capacity. Moreover, Type 2 could increase the bearing capacity of beams by 1.45 times when compared with type 3. In addition, beams with type 1 and type 3 failed due to the LTB, but type 2 and type 4 beams failed due to the DB.

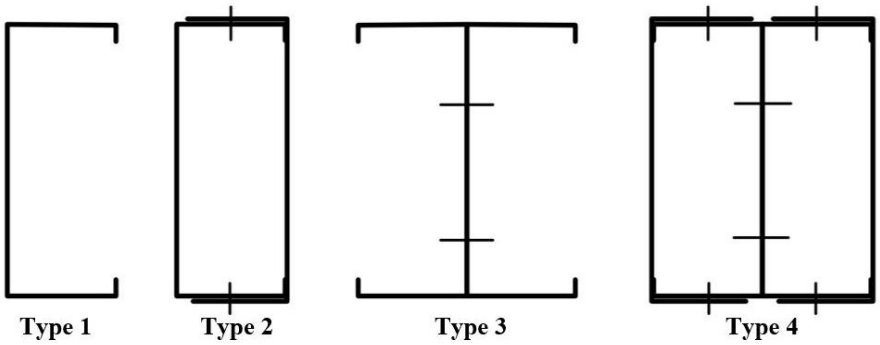

Figure 2.11 Sections of tested beams [20]

The research presented by Wanniarachchi and Mahendran (2017) discussed experimentally the flexural strength of CFS beams with rectangular hollow flange (screw-fastened) RHFBs [21] (see Figure 2.12). All samples were simply supported and loaded by four-point bending. Test findings were compared with the capacities determined by AISI S100 [12] and AS/NZS 4600 [14] standards. From the comparison, the moment strengths of the RHFBs which are intermittently screw fastened can be determined using the AS/NZS 4600 and AISI S100 design rules, that are relied on effective width rules. Furthermore, a comparison between test findings and the capacities obtained from DSM was conducted. When DSM is used, it is possible in most cases to obtain the bending strengths of adopted beams (which screw fastened) with reasonable accuracy.

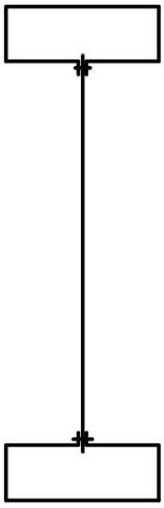

Figure 2.12 RHFB section [21]

An experimental study of CFS tubular beams was adopted by Li and Young (2017) [22]. The effectiveness of tubular sections exposed to web crippling was studied. Both rectangle and square hollow sections were tested.

Comparisons were made between the test findings and AS/NZS, EC3, and AS4100 strengths. From the findings, the authors stated that the web-crippling equations in the existing codes are not appropriate to estimate the web-crippling strength of such sections.

In 2019, Muftah et al. studied experimentally the deflection and bending capacity of bolted built-up sections [23]. Two types of channel profiles were under investigation as shown in Figure 2.13. To create the first built-up section, two CFS channels from type 1 (extended stiffener) were connected face to face by using a screw on web element. To create the second one, two CFS channels from type 2 (outstand stiffener) connected face to face by using a screw on stiffener. The samples were examined by using four-point loading tests. After testing, it was observed that the bending resistance of the built-up section with outstand stiffener was higher than the built-up section with extended stiffener. Moreover, the flexural resistance of the built-up section with outstand stiffener was dependent on the load location.

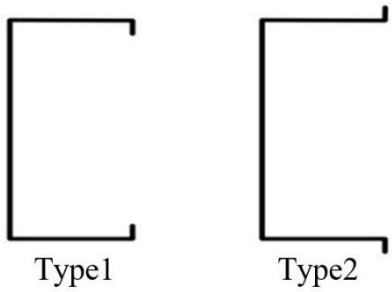

Figure 2.13 Types of CFS channel sections [23]

The research reported by Chen and Young (2019) studied the flexural capacity of CFS semi-oval hollow sections (SOHS) (see Figure 2.14) [24]. In the experimental investigation, the tested beams were loaded in two ways. Three points and four points loading configurations were performed on studied beams. The test results showed that no shear failure was noted in all studied beams.

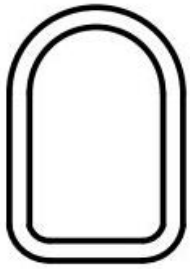

Figure 2.14 Cross section of SOHS [24]

In addition to the experimental test, the authors created a FE model to verify the test results using the ABAQUS program. Furthermore, the performance of the studied section under flexural strength was examined in a parametric study. A comparison of the experimental and numerical findings with DSM strengths was conducted. From the results, it was found that the DSM gives quite conservative predictions. Therefore, some modifications were made to DSM.

In 2019, Manikandan and Thulasi examined how CFS built-up beams performed under flexural moment [25]. In the Experimental investigation, there are different kinds of sections were tested (see Figure 2.15). Simply supported C-channel sections connected back-to-back and loaded in two points on the beam length were generated.

The authors noted that the use of a channel section with both intermediate web and edge stiffeners enhanced the capacity of the section.

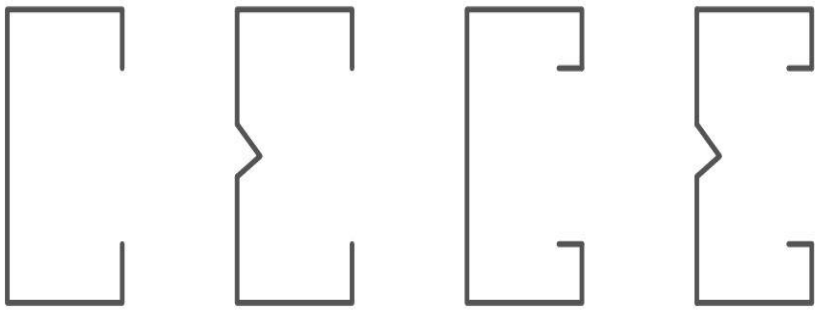

Figure 2.15 Types of sections [25]

The authors, also, created a FE model to verify the experimental test by using the ABAQUS program. Also, a parametric analysis was performed to study the impact of the change of section dimensions and bolt spacing on the bending capacity of adopted beams. It was observed that the section dimensions and bolt spacing considerably affect the capacity of the section. Results from both the experimental test and FE model were compared with the DSM and the convenient modifications were elaborated.

The impact of fastener arrangement on the bending rigidity of CFS members was studied by Phan and Rasmussen (2019) [26]. In the experimental test, the samples were two C-sections linked back-to-back. The beams were simply supported. All samples were loaded about the weak axis (four-point loading test).

The authors, also, conducted a numerical study using the ABAQUS program and an analytical study on the same samples used in the experimental study. From the results of all these studies, the authors observed that when the stiffness of the fastener was increased, the flexural rigidity was also increased. In addition, the flexural rigidity of the members was increased by increasing the fastener rows number.

2.4.1.2 Experimental studies on CFS flexural members with openings

The research developed by Schudlich et al. (2011) [27] studied experimentally the moment resistance of CFS C-sections with rectangular perforations. All tested beams were simply supported and loaded at 1/3 points along beam length. From the findings, it was stated that the existence of web perforations in the tested sections reduced section capacity as well as increased distortional buckling deformation. A comparison was made between test strengths and DSM strengths for flexural members with perforations. The findings showed that the DSM was accurate to predict flexural strength when I_{net}/I_g = 0.9. On the other hand, the DSM was unconservative when I_{net}/I_g = 0.8 (I_{net} and I_g describe the inertia moment of the net and gross section).

In 2012, Uzzaman et al. studied experimentally the performance of CFS channel beams with circular holes under web crippling [28]. The test was arranged under interior two flange loading conditions (ITF) as presented in Figure 2.16.

A nonlinear analysis was also created by the authors to verify the experimental test using the ANSYS program. The significance of hole size and hole position on the web crippling was examined using parametric studies. The web-crippling capacity of the studied sections is primarily influenced by the hole size and location.

Depending on the findings of both numerical and experimental analyses, the reduction factor of web crippling strength was predicted for the ITF.

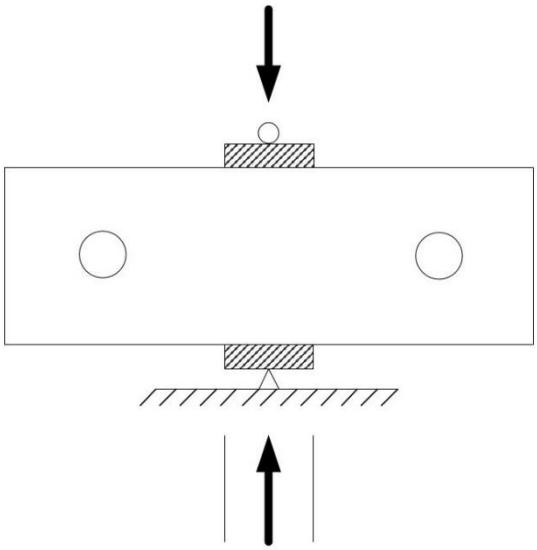

Figure 2.16 Interior two flange configuration [28]

The shear behavior of CFS built-up sections with circular holes was presented by Keerthan and Mahendran (2013) [29]. The samples were simply supported and loaded at mid-span. Experimental shear resistances were compared with the shear resistances obtained by AS/NZS 4600. It was noted that, according to AS/NZS 4600, the equations are conservative for studied sections with small openings and unconservative for studied sections with large openings. The authors made some modifications to the shear strength design equations.

They found that the suggested formulas are accurate to determine the shear strength of channel beams with perforations.

An experimental investigation on the elastic buckling moments of CFS channel sections with rectangular perforations was conducted by Moen et al. (2013) [30]. All specimens were loaded at 1/3 points of the specimen length. According to the results of the experiment, there was unstiffened strip buckling of the compressed web associated with the distortional buckling deformation. This was when the hole depth was about 2/3 of the web depth. In addition, when the hole height approached the web height, the compressed flange above the hole buckled suddenly.

The behavior of CFS sections with different edge stiffeners and web perforations under LB and DB was studied by Wang et al. (2013) [31]. The study concentrated on C and Σ sections as illustrated in Figure 2.17. The samples were simply supported at their two ends. It was observed that the flexural strength of the Σ-sample was increased by 6.06% more than C-sample. Moreover, the stiffness of the Σ-section decreased the effect of the openings as compared to samples of the C-section. A numerical investigation was also performed by the authors on the same samples. Regarding buckling modes and flexural strength, the FE findings were reasonably consistent with the experimental findings.

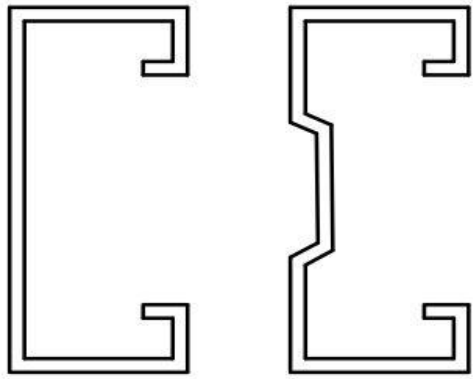

Figure 2.17 Cross section of samples [31]

In 2013, Karmazinova studied the performance of CFS Σ – sections with circular holes according to lateral flexural torsional buckling [32]. All samples were under four points bending condition. A comparison was made between the lateral-torsional buckling strengths determined from tests and those determined from EN 1993-1-1 code.

In (2013), Uzzaman et al. extended their experimental research to study the impact of openings on web crippling under end two flange loading conditions (ETF) [33]. All samples were C-sections. The authors, also, established a FE model to verify the experimental test by using ANSYS program. It was found that the findings of the FE model agreed with the findings of the experimental study. Furthermore, the main parametric effect on web crippling was the hole depth and the hole location. A comparison was made between the web crippling strengths determined from both the FE model and experimental and those determined by NAS specification. From this comparison, the authors proposed the reduction factor for the ETF.

In 2015, Wang and Young investigated the moment strength and modes of failure of two kinds of CFS built-up sections with circular perforations [35]. One of them was two channels connected back-to-back and the second one was two channels connected face-to-face. An experimental examination was created to obtain the bending resistance and study the effect of hole size on the bending resistance. A simply supported beam was tested and loaded in four points bending. The circular perforations were positioned in the moment region. The results indicated that the ultimate moment decreased when the value of hole depth/web height increased. A Comparison was made between the test bending strengths and DSM strengths. It was found that the DSM is suitable for designing CFS built-up open and closed sections with openings.

In 2016, Degtyareva and Degtyarev introduced an experimental test on CFS C-sections with slotted web exposed to shear strength [36]. The sections that were tested are presented in Figure 2.18. A concentrated load was applied at mid span for all samples. The results indicated that the ultimate shear resistance of the adopted sections was reduced by 50% to 71%. In addition, substantial plastic deformation of the steel strips among the slots resulted in a more ductile behavior of the slotted sections than the solid sections.

A set of tentative equations was presented for the shear strength of the slotted sections with and without tension field action. The tested shear strength and the formulas that take tension field action into account demonstrated reasonable agreement.

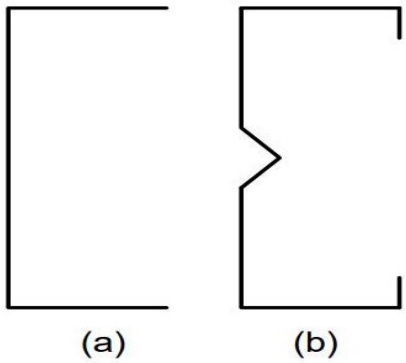

Figure 2.18 Sections used in the experimental test [36]

The bending behavior of CFSC sections with rectangular openings was investigated by Zhao et al. (2019) [37]. In the experimental investigation, a group of samples with different sizes of openings and lip of flange were examined under four points bending. Simply supported channel beams were linked back-to-back. From the findings, it was stated that the holes modify the modes of failure of members from just LB or just DB to distortional-local buckling interaction (restricted by DB or LB).

A numerical investigation was conducted by the authors to verify the experimental test using the ANSYS program. The capacities evaluated from tests and FE analyses were compared with those estimated by DSM. The DSM was unconservative to calculate the capacities of CFS channels with opening. Some modifications were made on DSM to improve the design of beams with perforations.

2.4.1.3 Experimental studies on CFS flexural members with stiffened openings

In 2006, Sivakumaran et al. examined the moment resistance of C-sections with openings accompanied by stiffeners around the openings [38]. The test sample assembly was constructed by putting the channel sections face-to-face. The samples were loaded in four points bending. The shapes of the openings under investigation were square, circular, and rectangular. Two reinforcement schemes were performed (scheme A and scheme B) as shown in Figure 2.19. The results demonstrated that the influence of the stiffener (reinforcement) was based on the type of stiffener and it is length, bolt spacing, and bolt pattern. In addition, CFS sections with large holes can be reinforced with cost-effective schemes.

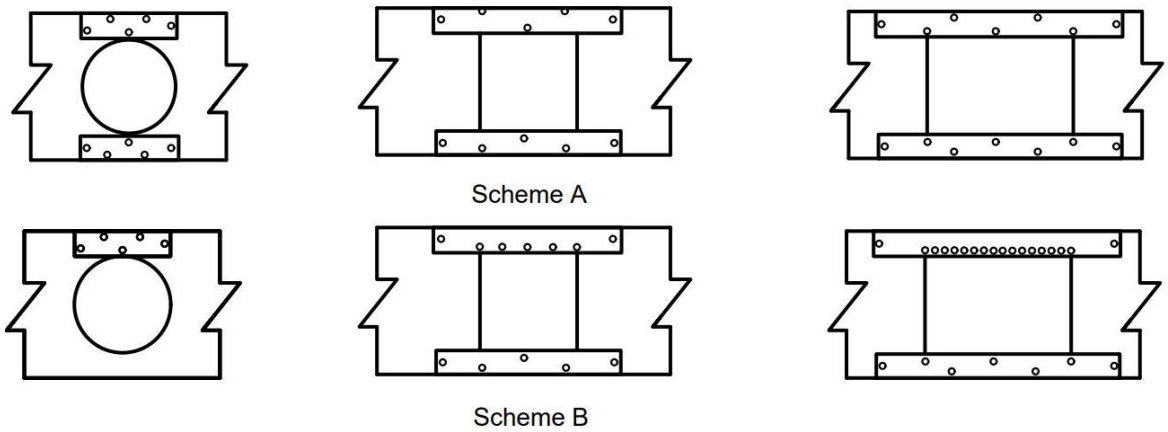

Figure 2.19 Reinforcement schemes [38]

An experimental study of C-sections with stiffened circular perforation was created by Keerthan and Mahendran (2015) [39]. The study was to explore the strength of CFS beam with large web opening when a plate attached around it. A concentrated load was applied at a mid-span of all simply supported samples. Different web stiffening configurations were used around holes. A numerical study was created by the authors using the ABAQUS program to verify the test findings.

The experimental and numerical findings displayed that AISI recommendations for plate stiffeners are insufficient for restoring the original shear strength of CFS beams with holes. An alternative plate stiffener system with appropriate dimensions and screw-fastening configurations has been presented by Keerthan and Mahendran to restore the original shear capacity.

The moment resistance of C-sections with circular stiffened perforations was examined by Chen et. al. (2020) [40]. In the experimental investigation, all samples were examined under a four-point loading condition. It was noted from the test findings that most of the studied samples with stiffened openings failed under DB failure. On contrary, for studied samples without stiffened openings, combined local and distortional buckling was noted. Thereafter, the authors performed a numerical model using the ABAQUS program to verify the experimental results. In addition, the influence of stiffener length, perforation size, and beam length on the bending strength of such sections was investigated. It was demonstrated that, when compared to a solid beam, the presence of five stiffened perforations enhanced the bending strength by 14.5%. Moreover, when the ratio of perforation diameter to web depth was raised from 0.1 to 0.5 and the strength increased by 2.7%. Since the LB near the perforations provides better performance. The strengths calculated by the experimental and numerical investigation were compared with those estimated by the AISI, AS/NZS standards for C- sections without perforations. Moreover, they were also compared with strengths calculated by formulas for C- sections with unstiffened perforations presented by Moen and Schafer [41]. These comparisons indicated that AISI and AS/NZS bending strengths for C- sections without perforations were found to be conservative.

Using the formulas of Moen and Schafer [41], the determined bending strengths of C- sections with stiffened/unstiffened perforations were very conservative and hence not suitable for stiffened openings.

2.4.2 Theoretical studies on CFS beams

2.4.2.1 Theoretical studies on CFS beams with solid web

In 2011, Haidarali and Nethercot discussed numerically the bending strength of Z-beams [42]. Single and double sections were examined. The ABAQUS program was utilized to conduct a nonlinear FE investigation. The behavior of Z-beams was studied utilizing two sets of nonlinear models. The first allows combined local and distortional buckling, and the second only allows local buckling. Two concentrated loads implemented at 1/3 points of the loaded length were performed on simply supported beams. The authors concluded that a combined purlin/sheeting configuration can be effectively represented using the generated FE model.

In (2012) Haidarali and Nethercot extended their numerical study to investigate the performance of CFSZ sections with intermediate stiffeners [43] as presented in Figure 2.20. The study was to examine the bending strength under LB and DB.

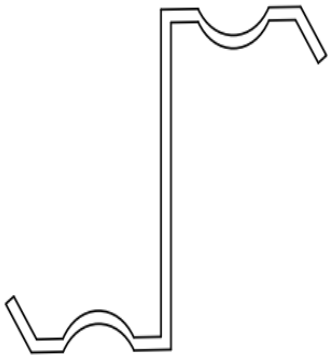

Figure 2.20 Z section with stiffened flanges [43]

The beams were loaded at 1/3 points of the beam length. The effect of intermediate stiffener size and its location in compression was examined. From the FE results, it was found that in response to changes in the location of the intermediate stiffener, the maximum change in the bending strength ranged from 1% to 5% with a general average of 3%. In addition, the capacity of the Z-section increased with increasing dimensions of the intermediate stiffener; however, the increase rate was reduced when the intermediate stiffener became larger. A comparison of the numerical strengths with the strengths predicted by Eurocode was conducted. It was concluded that the equations of the Eurocode need to modify for intermediate stiffeners.

Law et al. (2012) proposed new simplified procedures for predicting the critical distortional loads of C and Z sections [44]. The authors observed that the new simplified procedures predicted by them were more consistent and precise predictions for the critical distortional load than the existing AISI results.

A nonlinear FE analysis using ANSYS on hollow flanged Z-sections was conducted by Karunakaran and Santhi (2013) [2]. All models were simply supported and tested under four points bending. In comparison to the Z-section with a solid flange, the hollow flanged Z-section exhibited better deformation properties. However, the stiffness of the hollow flanged Z-beam was four times higher than that of the solid one.

The research conducted by Yerudkar and Vesmawala (2017) studied the capacity and buckling behavior of CFS-stiffened beams [45]. FE analyses were created using the ANSYS program. All sections were Z- sections with different shapes of stiffeners as shown in Figure 2.21. All studied beams were simply supported and loaded at 1/3 points along beam length. From the results, it was obvious that for sections with a ratio of flange width-to-section thickness >20 and a ratio of web depth-to-section thickness ≤ 100, it was appropriate to provide stiffeners in both the web and the flange.

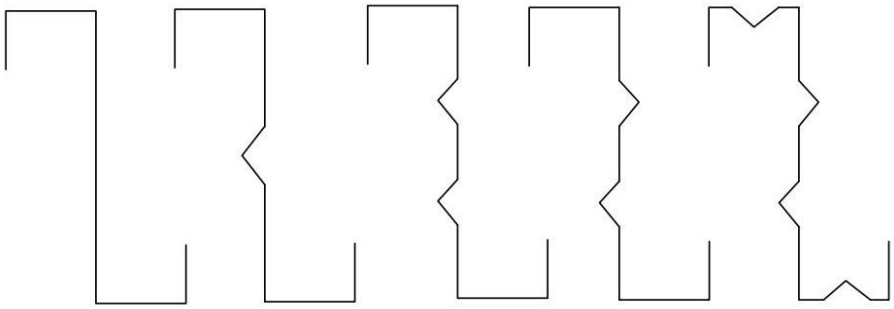

Figure 2.21 Different shapes of sections [45]

The research presented by Ghannam (2018) studied the bending strength of CFS built-up sections [9]. Two profiles were under study as illustrated in Figure 2.22. A numerical investigation using the ANSYS program was used to investigate the moment strength of such profiles. In the FE model, a simply supported beam was created.

All beams were loaded at two points on the loaded length. A parametric investigation was made to study the impact of material thickness, yield strength, and the distance among the vertical components (to generate the built-up profile). Based on this investigation, it was concluded that as yielding stress and steel thickness increase, the bending moment capacity also increases. Furthermore, there was no substantial difference in bending strength when the length among vertical components was increased.

Moreover, the moment strength of the web with stiffeners is higher than the moment strength of the web without stiffeners. The author used the EWM and DSM to evaluate the moment capacity of such sections. It was found that the EWM and DSM gave conservative results. So, some modifications were applied to the DSM.

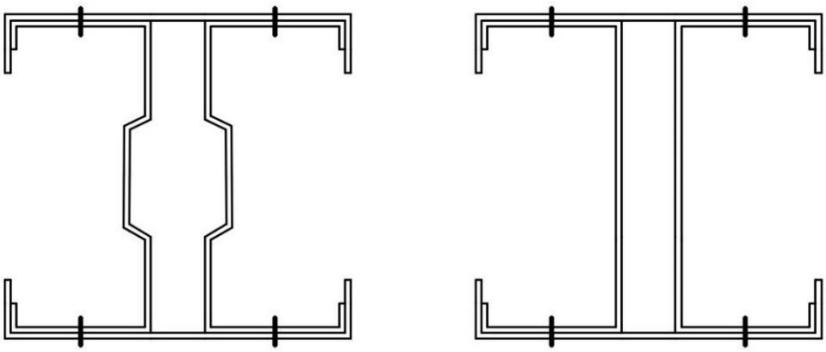

Figure 2.22 The studied built-up profiles [9]

In 2018, Ye et al. presented a numerical study to analyze the bending resistance and deflection of C-sections [46]. The FE model was created using the ABAQUS program. Simply supported C- sections connected back-to-back were generated. A comparison was performed between the numerical findings and the experimental findings created by Ye (2016) [47]. In addition, the FE results were used to measure the precision of EC3 and DSM equations.

The authors found that the FE predictions can be changed by approximately 7% when geometric imperfections are taken into account. Moreover, flexural strengths predicted by both EC3 and DSM were accurate.

2.4.2.2 Theoretical studies on CFS beams with openings

In 2010, Moen and Schafer presented some modifications on the DSM to determine the moment resistance of CFS flexural members with perforations [41]. Finite strip method utilizing the CUFSM software and manual calculations were involved to derive the equations used to estimate the moment resistance of such beams. It was demonstrated that the modified DSM was accurate and suitable to calculate the moment resistance of beams with perforations.

It must be pointed out that the DSM equations for flexural members with holes that were predicted by Moen and Schafer (2010) [41] were added to the current AISI standard. These equations were presented previously in sub-section 2.3.1.2.

The research performed by Keerthan and Mahendran (2014) examined the behavior of C-sections with circular perforations [34]. Experimental and numerical analyses were created to examine the shear performance of such sections. In the experimental test, all samples were two-channel sections connected back-to-back. The samples were loaded at mid-span. A numerical study using the ABAQUS program was conducted by the authors to verify the experimental studying. A comparison of the test and FE model shear strengths with AS/NZS 4600 and AISI shear strengths was conducted.

It was found that the design formulas from AS/NZS 4600 were conservative for beams with small perforations and unconservative for beams with large perforations. New equations were suggested by the authors to obtain the shear capacity of C- beams with circular openings.

In 2015, a numerical investigation of the LTB behavior of C-purlin with web perforations was addressed by Ling et al [48]. The LUSAS program was used to create the finite model. A uniformly distributed load was applied along the beams. Fixed support was generated for all models. The shapes of the openings under investigation were C-hexagon, circle, regular octagon, elongated circle, and diamond shapes. From this investigation, it was found that the sections with small holes showed a negligible difference in the bending strength. Moreover, a web with C-hexagon holes presented the smallest reduction in LTB strength compared to other opening shapes. Also, the buckling strength decreased whenever the opening size increased.

In 2017, the influence of web openings on the DB moment of CFS C-sections was studied by Yuan et al. [49]. The numerical investigation was created by using the ABAQUS program. simply supported boundary conditions were applied for all models. All models were subjected to the concentrated moment at their ends about the major axis. The authors created an analytical investigation by using the DB model of EN1993-1-3. They found that the impact of circular perforations on the critical stress of such sections can be explained as their influence on the rotational constraint to the compressed system of flange-lip by utilizing the DB model of EN1993-1-3.

In 2017, Wang and Young presented the failure modes and moment resistance of CFS built-up beams with circular openings [50]. A numerical investigation was used to calculate the moment strengths by using the ABAQUS program. In the FE model, A simply supported beam was generated and subjected to four-point bending. The numerical model was created to verify the experimental results created by the authors [35]. A comparison was made between the moment strengths calculated from numerical and experimental results and those determined by DSM for sections with holes. From the results, it was stated that DSM is suitable to design built-up open sections with holes and conservative to design built-up closed sections with holes. Some modifications were made on DSM to improve the design of CFS built-up beams with holes.

The research addressed by De'nan et al. (2017) investigated the shear capacity of Z-beams with perforations [51]. FE analyses were created using the LUSAS program to examine the impact of perforation size, perforation shape, and section type. Fixed-pinned supports were the boundary conditions in this investigation. From the results of analyses, it was noted that as the perforation size is increased, the shear strength is reduced. In addition, the performance of diamond shape perforation under shear loading was better than the performance of the circle-hole shape. Furthermore, the shear buckling strength of Z beams with smaller section depths was higher than that of Z beams with larger section depths.

The behavior of web crippling strength on Z-beams with circular openings was highlighted by Kumar et al. (2018) [52]. A nonlinear FE analysis was created using the ANSYS program. All models were subjected to uniform load with simply supported boundary conditions.

In comparison with the test findings conducted by the authors, the resistance determined from the numerical model was compared. From the comparison, it was demonstrated that the ratios of perforation diameter to web depth and web depth to section thickness were the main variables that affect the web crippling resistance of Z-beams with openings.

In 2019, Lawson and Basta studied the deflection of C-sections with circular perforations [53]. Two formulas were derived by the authors. Such formulas were compared with the results of the test created by the authors and FE using the ABAQUS program. The restrictions of the deflection formulas were presented.

In 2019, Yu et al. reported a numerical and analytical investigation to evaluate the DB moment for C-sections with circular perforations (see Figure 2.23) [54]. The authors presented a simple analytical formulation based on the DB model introduced by Hancock (for solid beam) to evaluate the DB moment of the studied sections. Linear buckling analysis was generated using the ANSYS program. A simply supported beam was performed under a pure moment. A comparison was generated between the findings from the numerical analysis and those from the analytical formulation. The authors noted that the modified formulation was accurate to evaluate the DB moment for the CFS C-sections with circular perforations.

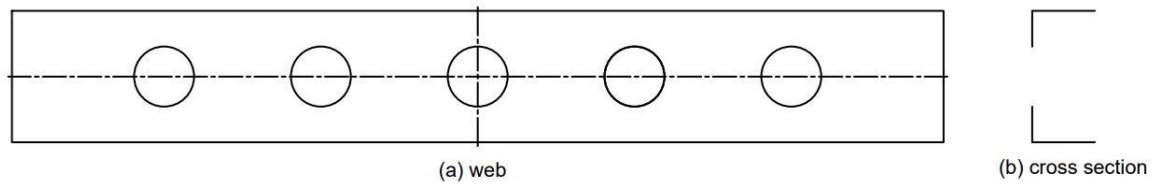

Figure 2.23 CFSC beam with circular holes [54]

2.4.2.3 Theoretical studies on CFS beams with stiffened openings

The equations for estimating the elastic buckling load/moments of members with stiffened perforations were proposed by Grey and Moen in 2011 [55]. They were among the first to suggest using reduced thickness to calculate the distortional buckling capacity of CFSC beams with stiffened holes. However, their suggested equation requires justification to be more applicable, especially for CFSZ beams (as will be presented in Chapter 5). The elastic buckling load/moment of global, local, and distortional buckling predicted by their equations was compared with the FE eigen buckling analysis by using the ABAQUS program.

The bending resistance of the C-sections with stiffened perforations was reported by Yu (2012) [5]. The FE model was created utilizing the ABAQUS program. Linear and post-buckling analyses were performed. The linear buckling model was generated to find the optimized profile of the holes, then used such profile in post-buckling analysis. In the nonlinear buckling model, the beams were simply supported and loaded at two 1/3 points of the loaded length. The author proposed a new procedure (see Eq. (2.40) and Eq. (2.41)) according to DSM to compute the local buckling strength of C-members with stiffened perforations.

When the suggested method was compared with the FE model findings, the authors observed that the new procedure can be use to obtain the LB capacity of C-members with stiffened openings for edge stiffener length to web depth less than 0.06.

$$M_{nl} = M_y \qquad \textit{when} \qquad \lambda_l \leq 0.925 \qquad \textbf{Eq. (2.40)}$$

$$M_{nl} = \left(1 - 0.05\left(\frac{M_{crl}}{M_y}\right)^{0.35}\right)\left(\frac{M_{crl}}{M_y}\right)^{0.35} M_y \qquad \textit{when} \qquad \lambda_l > 0.925 \qquad \textbf{Eq. (2.41)}$$

In 2015, Garifullin et al. presented numerically the impact of stiffeners around perforations on the local buckling of C-sections [56]. They examined the influence of perforation spacing and perforation size on elastic buckling moment. The FE model was created using the SCAD program. Simply supported beams were performed and loaded at two L/3 points of the loaded length. From the results, it was found that creating edge stiffeners around holes improved the LB moment of such sections. Moreover, if the spacing between the holes is sufficiently large, the buckling will appear at the region between openings and the tested beams will perform similarly to the solid beams.

The impact of stiffeners around perforations on the behavior of web crippling for C-beams was reported by Uzzaman et al. (2017) [57]. The numerical study was generated utilizing the ABAQUS program. The results of the FE model were validated by an experimental test performed by the authors. Parametric studies were generated to examine the influence of perforation size, stiffener height, and perforation position on the web crippling capacity. The authors concluded that a substantial increase in web crippling resistance is shown by adding

edge stiffeners around holes in such sections. In addition, web crippling resistance is significantly affected by the stiffener height-to-web depth ratio.

The DB strength of C-sections with edge stiffeners around perforations was investigated by Perampalam et. al in 2019 [58]. The numerical model was performed utilizing the ABAQUS program. Two concentrated loads were applied to all models and boundary conditions were simply supported. The impact of material thickness, hole depth, and stiffener length was examined. From the findings, it was demonstrated that the edge stiffener increased the bending strength significantly beyond the original capacity of the solid sections. The authors made some modifications on DSM for the distortional buckling strength of solid members to be suitable to estimate the strength of C-members with stiffened rectangular openings. The authors stated that the proposed DSM equation was applied at opening width and yield strength equal to 150 mm and 450MPa, respectively. Hence, they recommended conducting more studies to expand the application of the proposed DSM equations.

A novel model to predict the bending strength of CFS C-sections with edge-stiffened holes was presented by Dai et al. (2022) [59]. The authors use a machine learning model to compute the bending strength of the studied sections by modifying the elastic buckling capacity of the studied beams without holes. The presented equations were for all buckling modes of CFSC sections with stiffened perforations. It should be noted that the equations of Dai et al. [59] did not consider the effect of the ratio of hole depth to web height, or the effect of edge stiffener height.

These factors have a noticeable effect on the behavior of the beams investigated in the current study (see Chapter 4), which raises questions about the ability of these equations to predict the buckling strength of CFSC beams with stiffened holes.

A great effort was made by Liu and Duan (2023) [60] to present an analytical method for estimating the bearing capacity for the distortional buckling of CFS channel beams with edge-stiffened rectangular web holes. The proposed method was validated by a comprehensive finite element analysis. The comparison between the analytical results and the finite element results showed quite consistency. Hence, Liu and Duan [60] advise the researchers to pay more attention to more analytical, experimental, and numerical studies on CFS beams with edge-stiffened web holes so that relatively simple calculation formulas for the calculations of the pure buckling critical loads, which are necessary for the DSM design of CFS members, can be obtained.

2.5 Summary and comments

An overview of experimental and theoretical research relevant to this thesis was presented in this chapter. Our knowledge of CFS beams with stiffened holes is largely based on limited data as stated before, and the elastic buckling strength of such beams has not been dealt in depth. Moreover, the existing CFS design criteria handle the moment capacity of CFS members with solid webs and un-stiffened web perforations. Although some previous studies suggested formulas for designing CFS beams with stiffened perforations, they need to be justified to be more applicable, especially for CFSZ beams.

From all previous, the elastic buckling strength of CFS sections with stiffened openings is still poorly understood. Therefore, motivated by the lack of information about CFSZ section beams with stiffened holes, this thesis concentrates on the bending behavior of CFSZ beams with stiffened openings and the elastic distortional buckling moment of such beams.

Chapter 3

FE Analysis and Verification

3Chapter 3 FE Analysis and Verification

3.1 General

This chapter aims to characterize how CFS beams were modelled in this thesis and validate the adopted FE model by employing findings identified in the literature. Several levels of validation were conducted. Several four-point bending tests available from earlier studies were used to check the FE models. According to the experimental findings performed by Pham and Hancock [19], numerical results conducted by Perampalam et al. [58], nonlinear FE analyses reported by Haidarali and Nethercot. [42], and numerical results obtained by Yu [5], all the forthcoming model's features for bending have been evaluated. These previous researches were utilized as a base for creating the FE models.

The numerical analyses in the current chapter were created using the FE software ABAQUS (2020) [61]. The forthcoming sections provide an overview of the FE analysis and the steps applied to FE modeling. At the end, a comparison of numerical and experimental findings is discussed.

3.2 Overview of Finite Element Analysis (FEA)

In engineering applications, the FEA of CFS structures is becoming more and more significant. Comparing it to physical experiments, particularly when a parametric analysis of cross-section is concerned, it is comparatively inexpensive and time-effective. Additionally, it is difficult to conduct experimental tests to examine the impacts of geometric imperfections and residual stresses of members [6] .

Consequently, provided the FE method (FEM) is precise and the findings could be verified by adequate experimental findings, FEA is more cost-effective than physical experiments [6]. The simulation models in this study were performed using ABAQUS software [61]. The software has a predetermined material property database for almost all materials that structural engineers might be interested in [15]. This study took into account nonlinear and buckling analysis; the differences between them and the explanations behind their use are outlined in the following subsections.

3.2.1 Nonlinear analysis

The three nonlinear analyses types available in ABAQUS are as follows:

- Geometric nonlinearity

This source of nonlinearity is connected to modifications made to the structure's geometry during the analysis. Geometric nonlinearity happens whenever the magnitude of the movements influences how the structure reacts. This could be a result of:

1. Large deformations or rotations
2. Stiffening of the load or initial stresses [15].

- Boundary nonlinearity

If the boundary conditions vary throughout the analysis, boundary nonlinearity will happen. Consider, for illustration, the cantilever beam in Figure 3.1 that bends when a load is applied until it comes to a "stop". If the deformation is small, the tip's vertical deformation is linearly connected to the load until it reaches the stop.

The boundary condition then changes, restricting any further vertical deformation at the tip, and so stiffening the response of the beam. [15]

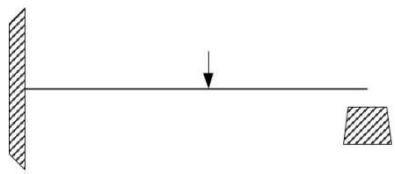

Figure 3.1 An illustration of a cantilever beam used to illustrate boundary nonlinearity [15]

- Material nonlinearity

At small strain values, most metals have a linear stress-strain relationship, but when the material yields, which occurs at more increased strains, the response becomes nonlinear and permanent. Other factors besides strain may be involved in material nonlinearity. Material nonlinearity can take the form of material failure or strain-rate-dependent material data [15].

3.2.2 Buckling analysis

The buckling loads and associated buckling shapes are estimated by the buckling analysis. For the sake of calculating the post-buckling capacity of structures, the buckling load is typically utilized as a parameter. Although the distribution of the imperfection is unknown, its buckling shape is known. In post-buckling analysis, superimposing various buckling shapes could be utilized as the initial geometric imperfection. To analyze the load-deflection behavior, a post-buckling analysis is required. Several strategies are viable based on the algorithm chosen and how the boundary conditions are employed. The increment method, in which proportional displacements are used, is employed when the loads can be added using the defined displacement [6].

In other instances, the modified Rix method, which employs proportional loads, is used to be able to cross boundary points. Both methods are successful in achieving nonlinear static equilibrium conditions throughout the unstable stage of the response. In both methods, it is necessary to introduce initial geometric imperfections to get some response in the buckling shape before reaching the critical load [6].

3.3 Verification Methodology for FE Model

The accuracy of the FE model must be checked prior to the forthcoming parametric investigation on CFSZ sections with stiffened holes in order to obtain accurate results. There are no experimental or numerical findings existing in the literature regarding the behavior of CFSZ sections with stiffened openings. In contrast, the previous research included results regarding CFSZ sections without openings, as well as CFSC sections with stiffened openings that were subjected to bending moment. Accordingly, these findings were utilized to verify the accuracy of the FE model. In the following sections, the ability of the model to simulate the performance of CFS beams with stiffened rectangular openings was validated by the experimental findings of Pham and Hancock [19], and the numerical findings of Perampalam et al. [58]. Furthermore, the accuracy of the model to simulate CFSZ sections under flexural strength was compared to the nonlinear FE analysis of Haidarali and Nethercot [42]. Finally, the behavior of the model of CFSC beams with stiffened circular perforations was checked with the numerical findings of Yu [5].

3.4 Simulation of CFSC Beams; Specimens of Pham and Hancock [19]

The upcoming model characteristics for bending were validated with the experimental findings achieved by Pham and Hancock [19]. The testing was carried out in a four-point bending configuration and composed of 2.6 m long CFSC beams. Figure 3.2 describes the test setup configuration. Six tests for channel sections were selected (using straps only at loading points and supports) to make the validation. The main aim of the straps is to avoid distortion in those regions. Table 3.1 shows the dimensions of the test cross-sections and their yield strength f_y. Figure 3.3 presents the symbols utilized for cross-section dimensions.

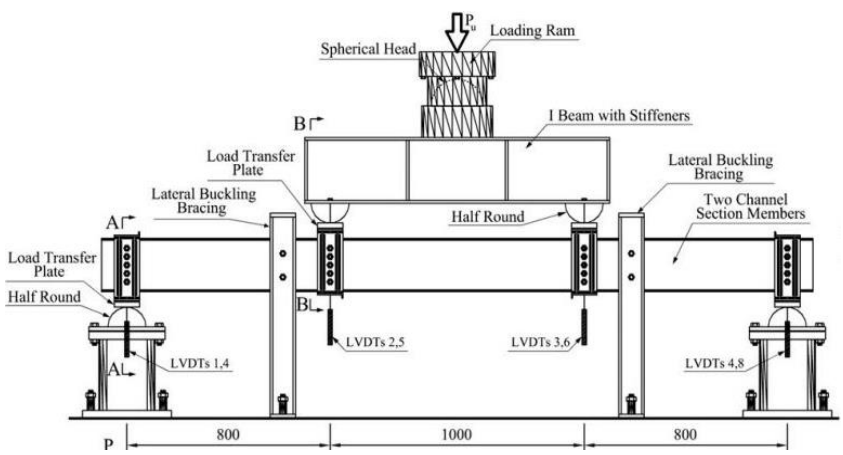

Figure 3.2 Test setup configuration [19]

Table 3.1 Samples dimensions and properties

Samples	*t* (mm)	*H* (mm)	*B* (mm)	*D* (mm)	f_y (MPa)
C15015	1.5	153.0	65.0	17.0	541.1
C15019	1.9	153.4	64.5	16.0	534.5
C15024	2.4	153.0	63.0	20.0	485.3
C20015	1.5	204.0	76.1	16.4	513
C20019	1.9	203.0	78.0	17.3	510.5
C20024	2.4	203.4	77.0	21.0	483.5

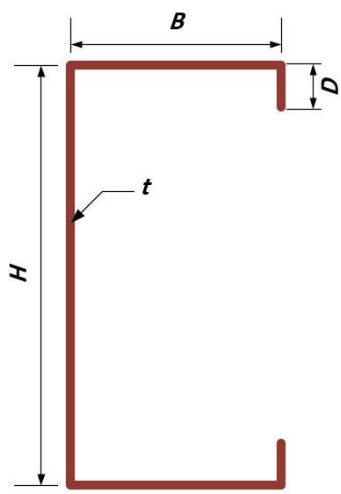

Figure 3.3 Definitions for cross-sectional dimensions

3.4.1 FE model configuration

For the FE model, it was regarded as a model with a single member: just the sample beam was simulated and the other parts of the experiment were modeled using suitable stiffeners and constraints. The general configuration for the model is shown in Figure 3.4. FE model of CFSC sections was as a four-point bending installation with simply supported end conditions. The members have a total length of 2.60 m and a mid-span of 1 m. The loads and supports were generated by assigning web side plates that were 20 mm thick. Each side plate was tied to the web using the tie option with surface-to-surface contact.

The Static, General procedure in ABAQUS was used to solve the nonlinear problem of the models.

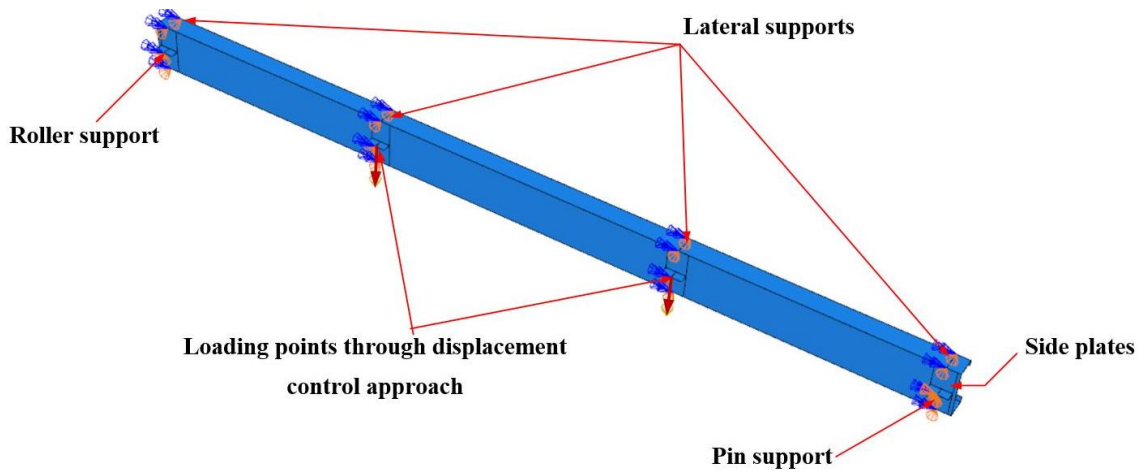

Figure 3.4 FE model configuration

3.4.2 Material Model

The strain hardening of CFS is negligible; then the FE models were performed as perfect plasticity models. The elastic modulus and Poisson's ratio were taken as 210 GPa and 0.3, respectively. All web side plates were assumed as rigid bodies by establishing a high elastic modulus of 2100 GPa.

3.4.3 Loading and supports

At the shear center of channel sections, the points load and simply supported boundary conditions were carried out as illustrated in Figure 3.4 and Figure 3.5. Lateral supports were implemented at the loading and support locations in the both upper and lower flange. Table 3.2 summarizes the FE model boundary conditions.

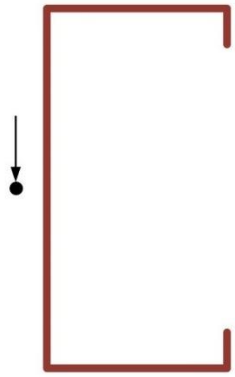

Figure 3.5 Concentrated loads at shear center

Table 3.2 The boundary conditions for the FE model

Locations	U_x	U_y	U_z	UR_x	UR_y	UR_z
Pin support	*C*	*C*	*C*	*F*	*F*	*C*
Roller support	*C*	*C*	*F*	*F*	*F*	*C*
loading points	*C*	*F*	*F*	*F*	*F*	*C*
Lateral support	*C*	*F*	*F*	*F*	*F*	*C*

Note: *C* represented the "constrain" and *F* represented the "free" boundary conditions

3.4.4 Element type and mesh

Since the thickness of CFS sections is considerably lower than the other dimensions, shell elements were utilized for modeling in ABAQUS [61]. The shell element S4R, which is a 4-noded quadrilateral shell element with reduced integration (see Figure 3.6), was used to simulate the entire FE model components. This element is advocated for both elastic buckling and nonlinear analyses in the element library. The mesh size was examined to provide accurate results for test results. The final mesh size was 5x5 mm.

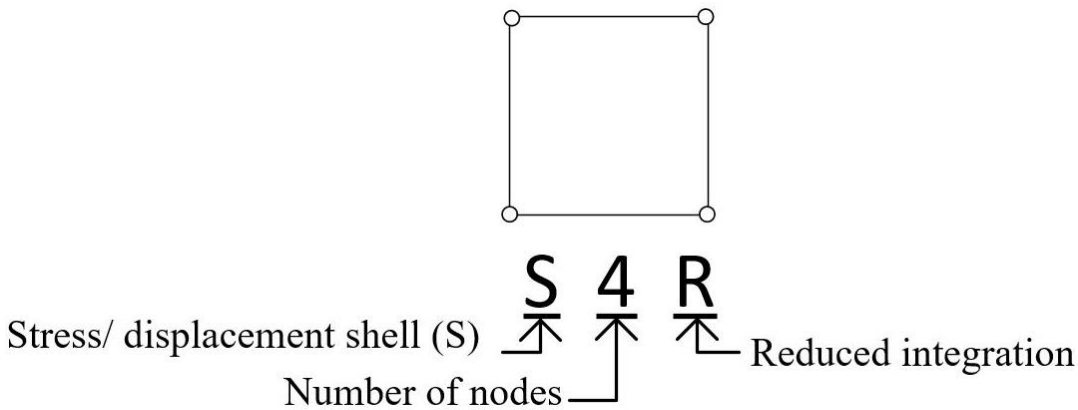

Figure 3.6 Scheme of the S4R shell element

3.4.5 Imperfection

In CFS structures, geometric imperfections can particularly affect the ultimate strength based on their shape and magnitude. The deformations were superimposed on the nonlinear FE model before applying the actual load. The possible buckling modes of the beam were performed by Eigen value linear buckling analysis in ABAQUS [61]. According to the statistical investigation by Schafer and Pekoz [62], the magnitude of the imperfection was set to 0.64 times the beam thickness.

3.4.6 Validation of the FE model

Versus the test findings (Pham and Hancock, 2013) [19] of distortional buckling tests, the previously mentioned FE model characteristics were validated. Table 3.3 demonstrates the comparison of the moment strengths determined from the test and the FE model. The mean and standard deviation (SD) values for the six beams were 0.95 and 0.03, respectively. Those values show an acceptable agreement. Figure 3.7 presents the comparison between the failure mode obtained from the analysis of the test and the FE for tested specimen C20015.

Figure 3.8 illustrates the comparison of load-deflection behavior obtained from the analysis of the test and the FE.

It was found that the load-deflection curves between the test and FE are compatible and suggest the moment strength with a satisfactory agreement. The failure mode between the FE model and the test is also much the same.

Table 3.3 Validation of the FE findings versus the test findings (Pham and Hancock [19])

Sections	M_{test} (kN.m)[19]	M_{FE} (kN.m)	M_{Test}/M_{FE}
C15015	9.47	10.16	0.93
C15019	12.94	14.00	0.92
C15024	17.76	18.00	0.99
C20015	12.20	12.64	0.97
C20019	18.85	20.80	0.91
C20024	27.88	28.32	0.98
Mean	-	-	0.95
SD	-	-	0.03

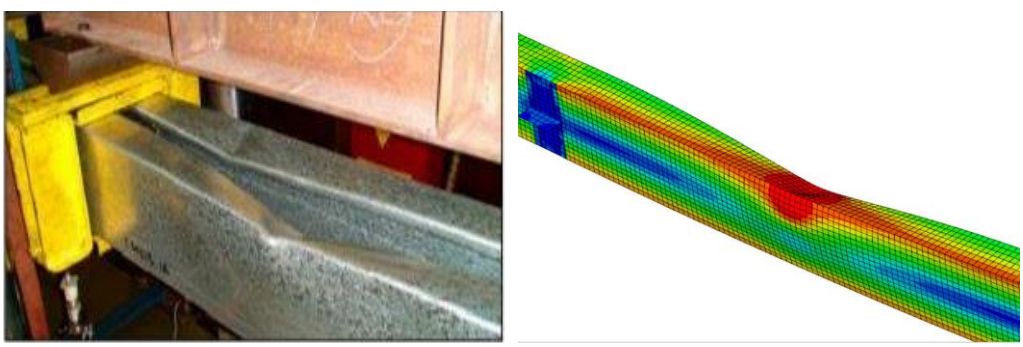

Figure 3.7 The comparison of failure mode between [19] and the FE for C20015

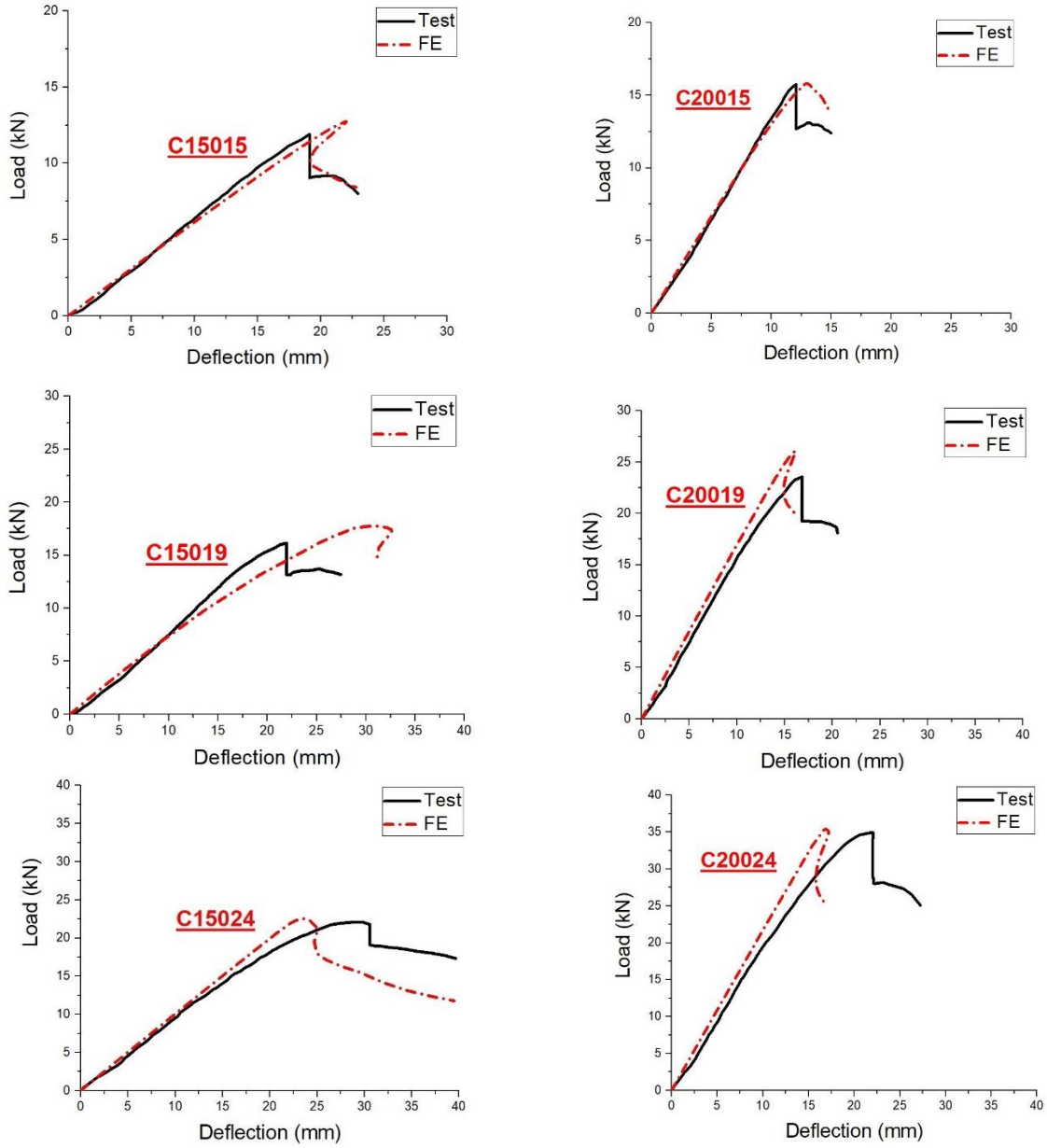

Figure 3.8 The comparison of load-deflection behavior between current FE and test specimens [19]

3.5 Simulation of CFSZ Beams; Specimen of Haidarali and Nethercot [42]

Since the focus of this thesis is the study of the CFSZ beams, this section includes the simulation of Z beam that was validated using a numerical model established by Haidarali and Nethercot [42].

3.5.1 Description of the FE model

For the FE model, section (D8.5Z120-4) has been selected to conduct the verification. Table 3.4 presents the properties of the sample (D8.5Z120-4) and its yield strength f_y. The symbols used for the dimensions are presented in Figure 3.9. FE model of the CFSZ beam was as a four-point bending installation with simply supported end conditions (see Figure 3.10). The sample has a total length of 4.9 m. At the supports and points load, the side plates, with a thickness of 6 mm and a length of 162,7 mm, were connected to the beam web (to prevent localized failure in those zones) using the "Tie" option. All plates were adopted as rigid bodies by establishing a high elastic modulus *E* of 2030 GPa. Whereas *E* of 203 Gpa was assigned to the beam. The loads were implemented at the central nodes of the plates (1/3rd points of the sample). Figure 3.10 demonstrates the details of the FE model.

Table 3.4 Section dimensions

Section	H	B_c	B_t	D_c	D_t	θ^o_c	θ^o_t	t	f_y
D8.5Z120-4	214	67	63	24	25	54.2	50.2	3	422.7

Note= Yield strength in Mpa, and the dimensions in mm.

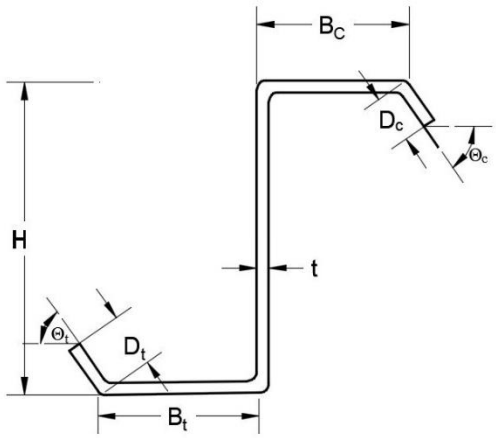

Figure 3.9 The symbols of the Z-section dimensions

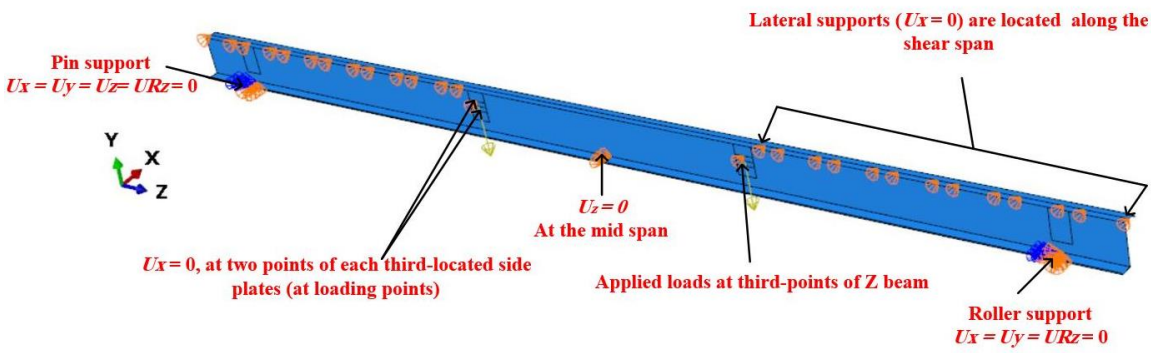

Figure 3.10 The boundary conditions and the configuration of the FE model

According to [42] , the stress-strain curve chosen to represent the material model (Romberg – Osgood model) is shown in Figure 3.11.

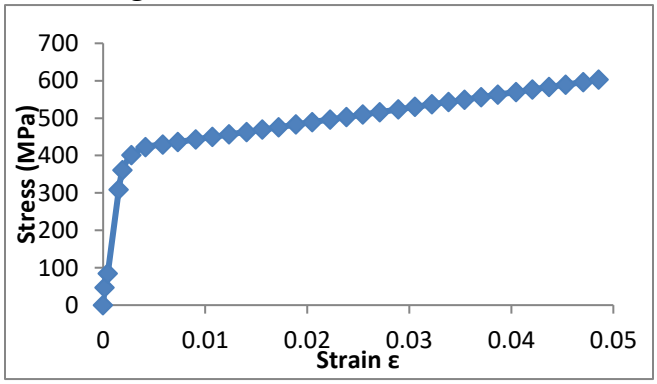

Figure 3.11 Material model for D8.5Z120-4 [42]

The S4R shell element with a mesh size of 10.2 mm was applied to each part of the FE model. The magnitude of the imperfection was set to *0.94t* (*t* is the material thickness). The Static-General procedure in ABAQUS was used to solve the nonlinear FE analysis.

3.5.2 The comparison of the findings

Against the numerical result (Haidarali and Nethercot) [42], the previously mentioned FE model characteristics were verified. Table 3.5 compares the bending strength determined by Haidarali and Nethercot's model and the bending strength estimated by the FE analysis.

Table 3.5 Verification of the FE model against the numerical result of [42]

Section	$M_{Haidarali}$ (kN.m)	M_{FE} (kN.m)
D8.5Z120-4	27.3	28

Figure 3.12 presents the comparison of load-deflection behavior determined from the numerical study of Haidarali and Nethercot [42] and the FE model. As presented in Figure 3.12, the load-deflection curve between Haidarali and Nethercot [42] and the FE is compatible and suggests moment strength with good agreement.

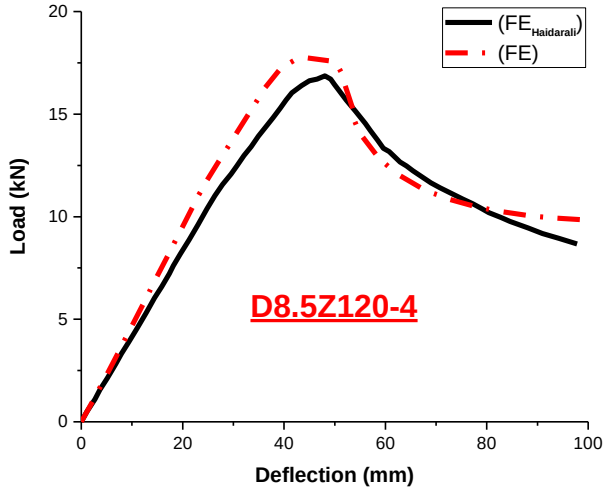

Figure 3.12 The comparison of load-deflection curve obtained from the FE model and those in [42]

3.6 Simulation of CFSC Beams with Rectangular Stiffened Holes; Specimens of Perampalam et. al [58]

In previous studies, stiffened holes have been studied in CFS beams, and one of these studies is the numerical study performed by Perampalam et. al [58], which was selected to perform the verification here.

3.6.1 FE model arrangement

FE model of CFSC beams with rectangular stiffened holes was established. The total span of the model is 2600 mm, two symmetric loads were applied at 800 mm from supports as presented in Figure 3.13. Side plates with a width of 70 mm and a thickness of 5 mm were attached to provide loads and supports. In order to ensure that the rectangular openings would significantly impact bending capacity, they were located in the pure bending region of the beam.

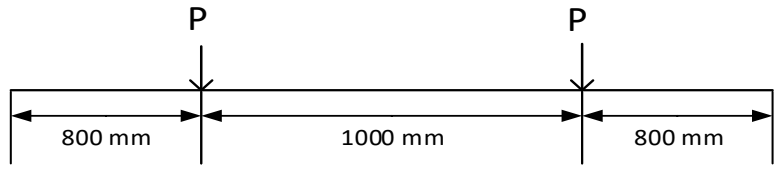

Figure 3.13 The beam with four-point bending arrangement

For verification, one channel section with 1 mm thickness (*t*) was selected (see Figure 3.14). The ratio of perforation depth to web height was 0.6. The width of the hole was 150 mm and the edge stiffener length equals 0, 5, 15, and 20 mm.

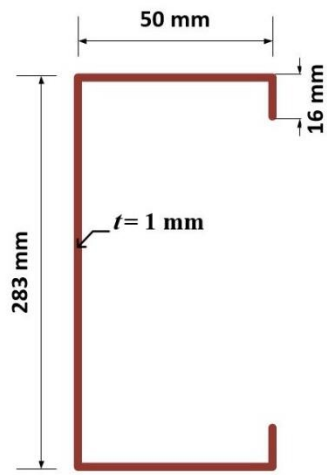

Figure 3.14 Dimensions of channel section

The material of the CFS beam was regarded as perfect plasticity. The yield strength of the FE model was 450MPa, while the yield strength of the side plate was 1350 MPa in order to prevent any failures in side plates. In the FE model, the S4R shell element was used with a 5 mm mesh size. The model was created with simply supported boundary conditions at the middle of the side plates, which are linked to the CFSC model with “tie” constraints. The boundary conditions applied here were the same as the boundary conditions applied in subsection 3.4.3 (see Table 3.6 and Figure 3.15).

Table 3.6 Boundary conditions

Locations	*Ux*	*Uy*	*Uz*	*URx*	*URy*	UR_Z
Pin support	*C*	*C*	*C*	*F*	*F*	*C*
Roller support	*C*	*C*	*F*	*F*	*F*	*C*
loading points	*C*	*F*	*F*	*F*	*F*	*C*
Lateral support	*C*	*F*	*F*	*F*	*F*	*C*

Note: *C* represented the "constrain" and *F* represented the "free" boundary conditions

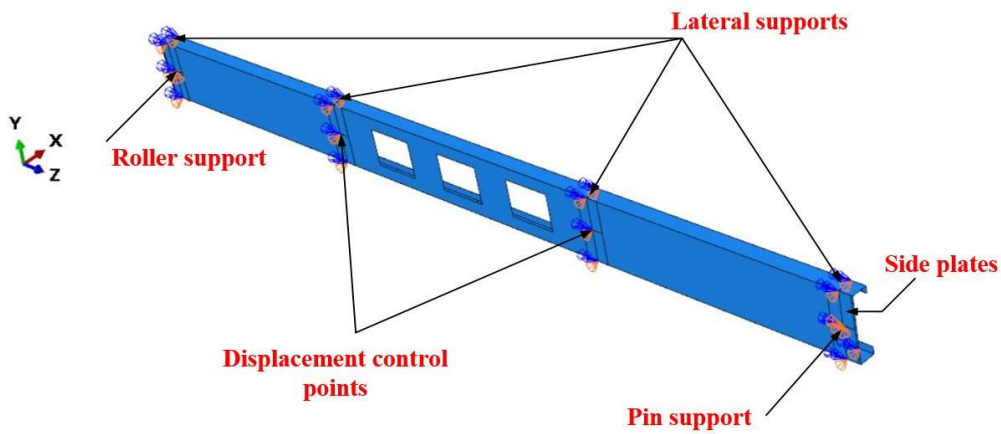

Figure 3.15 The loads and supports of the model

Linear and non-linear analyses were both generated. The linear buckling model was conducted to introduce the initial shape and magnitude of geometric imperfection into the non-linear model. The magnitude of imperfection was considered as *0.64t* (*t* = thickness of CFSC section).

3.6.2 Comparing results

Table 3.7 presents a comparison of the moment strengths determined by Perampalam et al. [58] and FE models. Mean and Standard deviation values of 1.04 and 0.058, respectively, resulted from the validation process for the 4 models. A satisfactory agreement is shown by these values.

Table 3.7 Verification of the FE model against the numerical result (Perampalam et al. [58])

Sections	$M_{Perampalam\ et\ al.}$ [58] (kN.m)	M_{FE} (kN.m)	$M_{Perampalam\ et\ al.} / M_{FE}$
415-O-1-0.6-0	8.41	7.5	1.12
415-O-1-0.6-5	8.8	8.66	1.02
415-O-1-0.6-15	8.85	8.72	1.01
415-O-1-0.6-20	8.96	9.01	0.99
Mean	-	-	1.04
S. D.	-	-	0.058

3.7 Simulation of CFSC Beams with Circular Stiffened Holes; Specimens of Yu [5]

Yu [5] conducted numerically elastic buckling analysis and nonlinear buckling analysis on CFSC beams with circular edge stiffened holes. Both analyses were performed and verified in the following sub-sections.

3.7.1 Description of the elastic buckling model

The S4R shell element with a mesh size of 12.7 mm was utilized to simulate the components of the FE model. Both ends of the model were simply supported. In the middle of the span, the model was restrained against the Z direction. Both ends of the model are subjected to a stress gradient in order to create a uniform moment along the model span. The FE model for the elastic buckling analysis is shown in Figure 3.16. The modulus of elasticity was 203.4 GPa and Poisson's ratio was 0.3. The length of the model was 6100 mm. The opening spacing ranges from 305 mm to 1219 mm; the hole depth/web height ratio was 0.4 and 0.5, and the ratio of the stiffener length/web height was 0.06. The dimensions of the studied beams are shown in

Table 3.8.

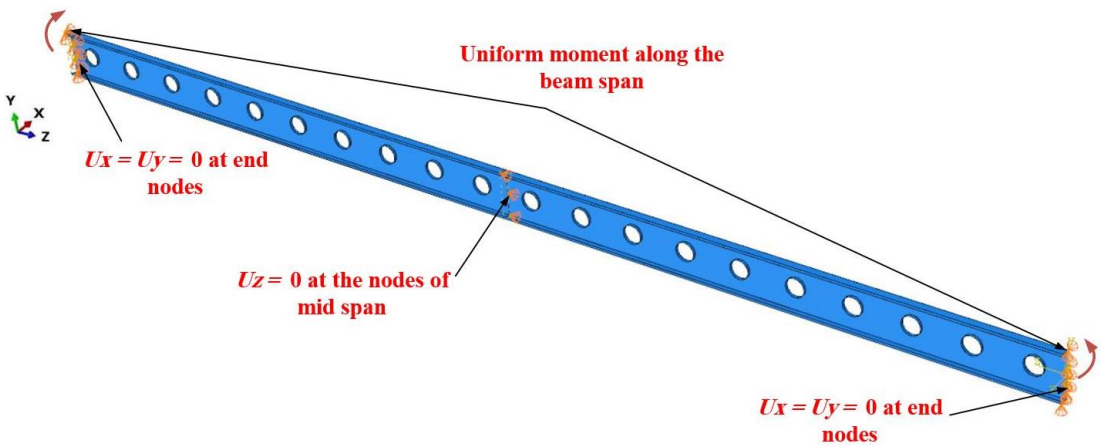

Figure 3.16 Details of FE model of elastic buckling analysis

Table 3.8 Details of Yu's [5] sections

Section	*H*	*B*	*D*	*t*
1000S162-43	254	41.3	12.7	1.1455
1000S250-97	254	63.5	15.9	2.5832

Note: The dimensions in mm.

3.7.1.1 Comparing results

Table 3.9 presents the elastic moment ratios of 1000S162-43 and 1000S250-97 with stiffened holes versus no holes and the comparison between the FE results and Yu results [5]. Moreover, Table 3.10 presents the comparison (mode shape) between the elastic buckling model of Yu [5] and the presented FE for CFSC 1000S162-43 with stiffened circular holes spaced 305 mm. Those values and shapes show an acceptable agreement. From the above, it can be concluded that the FE model is suitable for determining and evaluating the elastic behavior of CFS sections with stiffened holes.

Table 3.9 The comparison between the FE elastic moment ratios and Yu results [5]

1000S162-43 (Hole depth/web height = 0.4)						
S (mm)	$E_{LTB,FE}$	$E_{LTB,Yu}$ [5]	$E_{LTB,FE}/E_{LTB,Yu}$	$E_{LB,FE}$	$E_{LB,Yu}$ [5]	$E_{LB,FE}/E_{LB,Yu}$
305	0.97	0.98	0.99	1.15	1.17	0.98
610	0.98	0.99	0.99	1.04	1.03	1.01
914	0.99	1	0.99	1.02	1.02	1.00
1219	0.99	0.99	1	1.01	1.01	1.00
Mean	-		0.99	-	-	1.00
1000S250-97 (Hole depth/web height = 0.5)						
S (mm)	$E_{LTB,FE}$	$E_{LTB,Yu}$ [5]	$E_{LTB,FE}/E_{LTB,Yu}$	$E_{DB,FE}$	$E_{DB,Yu}$ [5]	$E_{DB,FE}/E_{DB,Yu}$
305	0.93	0.93	1	1.08	1.08	1.00
610	0.96	0.96	1	1.03	1.03	1.00
914	0.97	0.97	1	1.01	1.02	0.99
1219	0.98	0.98	1	1.02	1.02	1.00
Mean	-	-	1	-	-	1.00

Note: E_{LTB} = elastic LTB moment of CFSC section with stiffened holes/ elastic LTB moment of CFSC section without holes ratio, E_{LB} = elastic LB moment of CFSC section with stiffened holes/ elastic LB moment of CFSC section without holes ratio, M_{DB} = elastic DB moment of CFSC section with stiffened holes/ elastic DB moment of CFSC section without holes ratio, S = Hole spacing.

Table 3.10 Comparison between the elastic buckling model of Yu [5] and the presented FE for CFSC 1000S162-43 with stiffened circular holes spaced 305 mm

CFSC 1000S162-43 model	FE presented by Yu		The presented FE model	
	The first eigen mode shape		The first eigen mode shape	
	LTB	LB	LTB	LB
Without holes		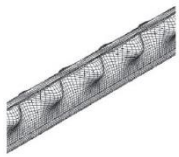		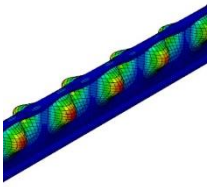
With edge stiffened holes (hole depth/web height =0.5)				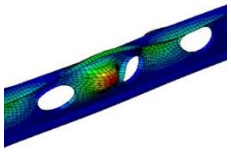
The ratio of elastic moment of CFSC section with stiffened holes/ elastic moment of CFSC section without holes	0.96	1.3	0.96	1.3

3.7.2 Description of the nonlinear buckling model

The model consists of a simply supported CFSC section with stiffened circular holes regularly spaced (S = 305 mm) along the beam span. The 6.1 m long beam is loaded at two 1/3 points of the beam length. The section geometries and the yield stresses of the studied beams are shown in Figure 3.17 and Table 3.11, respectively. The shell element S4R with a mesh size of 12.7 mm was applied to simulate the models. The FE models were generated as perfect plasticity models. 203.4 GPa and 0.3 were chosen as the elastic modulus and Poisson's ratio, respectively.

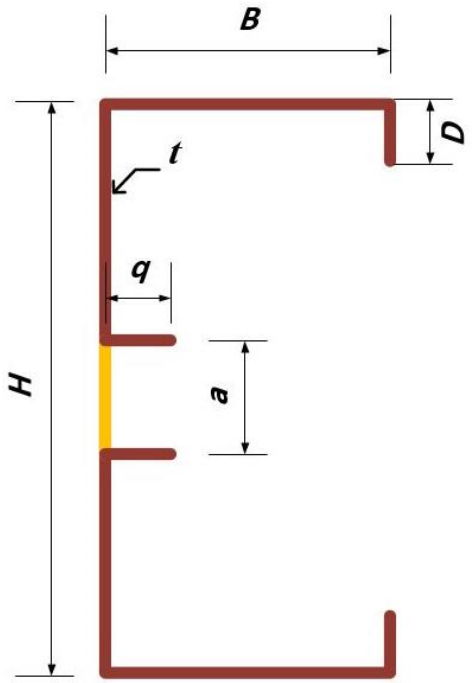

Figure 3.17 Cross-section of CFSC beam with stiffened holes

Table 3.11 The dimensions of the studied beams

Section	*H*	*B*	*D*	*t*	*a*	*q*	f_y (N/mm^2)
600S250-97	152.4	63.5	15.9	2.583	76.2	9.1	345
800S250-97	203.2	63.5	15.9	2.583	101.6	12.2	345
1200S250-97	254.0	63.5	15.9	2.583	152.4	18.3	345

Note: The dimensions in mm.

The possible buckling modes of the beam were performed by Eigen value linear buckling analysis. The magnitude of the imperfection was set to 0.034 times of the beam thickness. Simply supported boundary conditions were located at the ends of the model in the bottom flange. In the meantime, lateral supports were introduced at the corner nodes on the upper flange for each 305 mm. The beam was restrained laterally at the corner nodes on the lower flange at loading locations. The boundary conditions are illustrated in Figure 3.18. The Static, General procedure was utilized to solve the nonlinear buckling analyses of beam models.

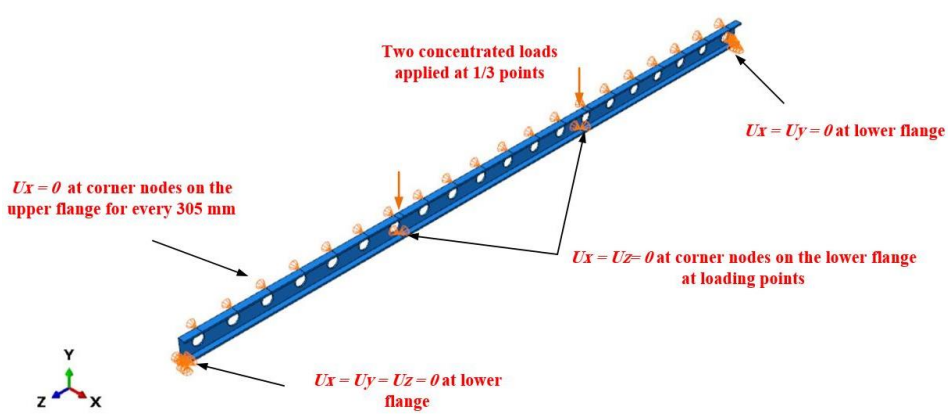

Figure 3.18 The nonlinear buckling model of CFSC beam with stiffened holes

3.7.2.1 Comparing results

The moment strengths predicted by the FE model and Yu's model are compared in Table 3.12. The mean and standard deviation for the three beams were 0.97 and 0.01, respectively. Those values show an acceptable agreement.

Table 3.12 Comparison of the moment strengths determined from the FE and Yu's [5] model.

Section	M_{Yu} [5] (kN.m)	M_{FE} (kN.m)	M_{Yu}/M_{FE}
600S250-97	12.65	12.9	0.98
800S250-97	18.38	18.9	0.97
1200S250-97	30.91	31.8	0.97
Mean	-	-	0.97
S. D.	-	-	0.01

The nonlinear buckling FE model having the desired failure mode stated by Yu [5] (see Figure 3.19) showed that the distortional buckling failure mode of the CFSC beams, stated in Table 3.12, matched with the finding of Yu [5] in his study.

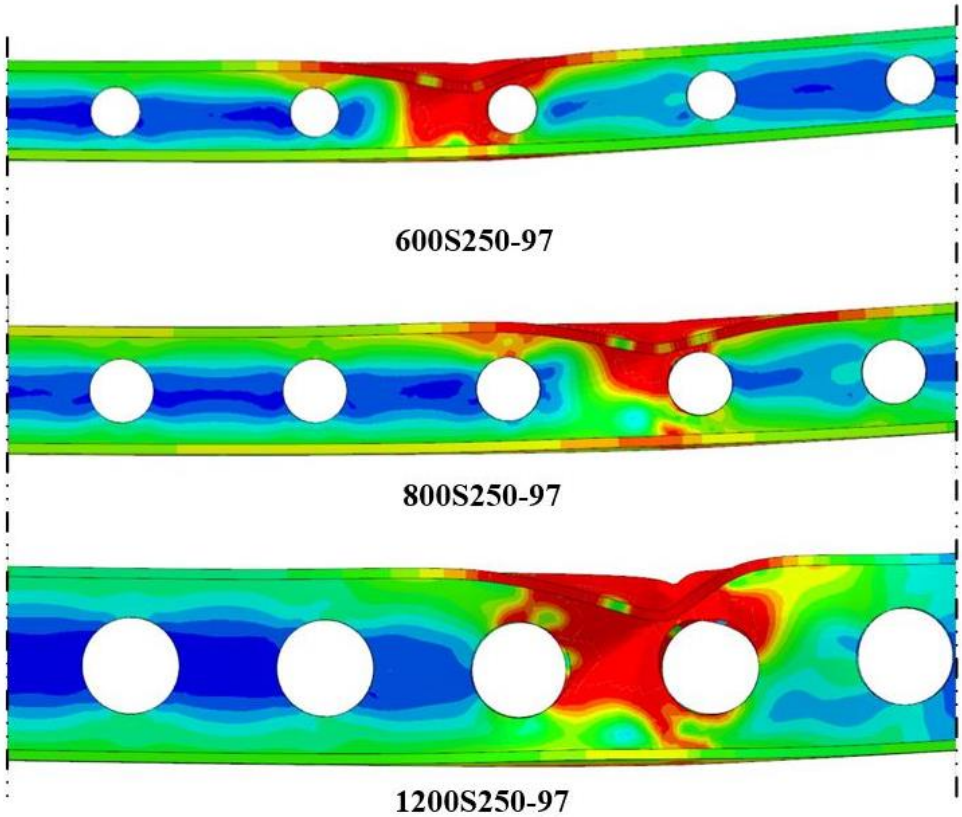

Figure 3.19 Distortional failure for 600S250-97, 800S250-97 and 1200S250-97 beams with stiffened holes

3.8 Summary

A series of analyses carried out in this chapter was verified by a group of previous studies (on the CFSC beams of Pham and Hancock [19], CFSZ beams of Haidarali and Nethercot [42], CFSC beams with stiffened holes of Perampalam et. al [58], and Yu [5]). It can be concluded that the comparison between the FE model and the results reported in the literature are compatible and predict the bending strength with good agreement. Hence, the model's confidence is enhanced by all of the previous results. Throughout this thesis, the validated FE was utilized for parametric study purposes to monitor the key parameters affecting the behavior of CFSZ beams.

Chapter 4

Chapter 4 Parametric Study on CFSZ Sections with Stiffened Holes

4Chapter 4 Parametric Study on CFSZ Sections with Stiffened Holes

4.1 General

Chapter 3 illustrated the FE model that simulated a series of four-point bending tests known from earlier studies. Nevertheless, Chapter 3 only regarded the phases of FE model progression and validation to simulate tests. This chapter, therefore (using the verified FE model) discuss the impact of different variables on the behavior of CFSZ beams with stiffened holes under bending moment.

4.2 Description of FE Model

A series of nonlinear FE models were generated based on the FE models that were validated versus a group of bending tests (Pham and Hancock [19], Haidarali and Nethercot [42], Perampalam et. al [58], and Yu [5]), were utilized for the objectives of the parametric investigation.

The shell element S4R was used to simulate all components of the studied FE models. The mesh size of 5x5 mm was adopted as suggested by [58]. The mesh shape of CFSZ with edge-stiffened holes is shown in Figure 4.1.

To accurately predict the behavior of the studied sections the geometrical and material nonlinearity were formed in the full-scale 3D model. Initial geometric imperfections were considered for an accurate FE with geometrical nonlinear. Two steps were introduced: first, the possible buckling modes of the beam were determined by eigenvalue linear buckling analysis using ABAQUS [61].

Then, deformations of the buckling mode with the lowest positive eigenvalues were superimposed on the FE model, and the nonlinear large deformation analysis was then performed. According to the statistical analysis by Schafer and Pekoz [62], the magnitude of the imperfection was set to 0.64 times the beam thickness (cumulative distribution function = 25%).

To simplify the analysis as well as highlight the impact of the opening size and the edge stiffened dimension on the plate stability, all edges were simulated sharp, as suggested by Yu [5].

Web side plates, with dimensions 70 mm wide and 5 mm thick, were attached to the web. These plates were implemented at the loading and support points, this technique was presented by Haidarali and Nethercot [42] to prevent localized failure in the web plate at these places. Each side plate was tied to the web using the tie option with surface-to-surface contact.

It should be noted that to investigate the impact of edge stiffened openings on the behavior of the CFSZ sections under bending, the stiffened openings were arranged in the mid panel (pure bending region) between the loading points. Hence the end panels have not any web opening to prevent failure at the edge panels and localized failure at the mid panel.

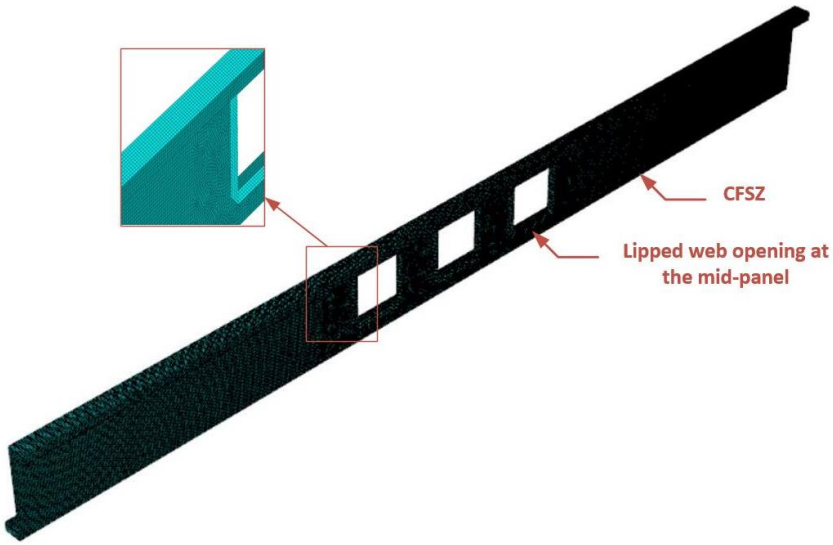

Figure 4.1 Mesh shape of the FE model

Simply supported boundary conditions were at the end of the beam in the mid-point of the web at side plate locations. In the meantime, lateral supports were at the upper and lower flange points at the location of the loading points as well as supports. The beam pinned at one end and rolled at the other. The pinned support was prevented to move in all directions (*Ux*, *Uy*, and *Uz* are prevented) as well as rotation in the direction of the beam span (*Rz* is prevented). The roller support was permitted to move only in the direction of the beam span (*Ux* and *Uy* are prevented), and the rotations were prevented only along the beam direction (*Rz* is prevented). The lateral supports were prevented to move in the out-of-plane direction (*Ux* is prevented) and to rotate along the beam direction (*Rz* is prevented). Figure 4.2 presents the details of the boundary conditions. All the beams were subjected to displacement-controlled loading, which was applied until failure occurred.

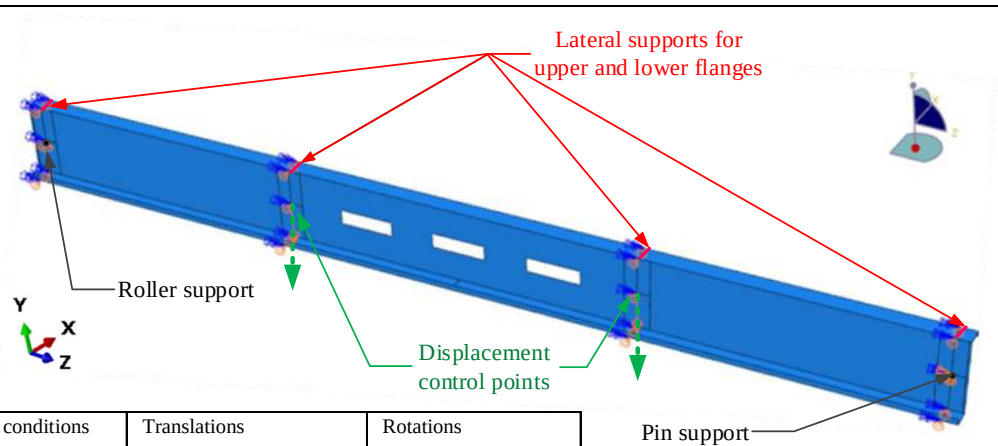

Boundary conditions	Translations			Rotations		
	U_X	U_Y	U_Z	R_X	R_Y	R_Z
Pin support	1	1	1	0	0	1
Roller support	1	1	0	0	0	1
Lateral support	1	0	0	0	0	1

Note: “1” represented the "restrain" and “0” represented the "free".

Figure 4.2 Description of the boundary conditions applied in the FE model

The strain hardening of CFS is negligible; then the FE models were created as perfect plasticity models as mentioned before in Chapter 3. The elastic modulus and Poisson's ratio were taken as 210000 MPa and 0.3, respectively. The elastic modulus of all web side plates was set to 2100000 MPa by assuming they were rigid bodies. The impact of residual stresses and corner strengths on the bending strength of CFS beams has been investigated by some researchers and it was found that residual stresses and corner strengths can be neglected [63][64]. Therefore, they were not incorporated into the FE models.

4.3 Parametric Study

As demonstrated in Chapter 3, the FE model performed for this study could accurately estimate the bending capacity of Z-sections with and without holes. Utilizing the verified FE model, a parametric investigation composed of 104 models was accomplished to examine the impact of section thickness (t), the height of hole edge stiffener (q), hole depth to web height (a/H) ratio as well as the hole shape (rectangular/circular) on the bending strength of such Z- sections.

The main objective of the parametric study is to study the behavior of Z- sections with stiffened holes until failure and to determine the main parameters that affect the bending strength of these sections.

4.3.1 List of key parameters

In the parametric study, full-scale CFSZ beams with steel S450 were considered, and the yield stress is 450 MPa. The CFSZ beams under consideration have the same span length (*L*) equals 2600 mm (1000 mm length for the mid panel), it should be noted that the specified span was successfully utilized in earlier works to model the behavior of CFS beams in both numerically and experimentally [19] [58]. The sections were divided into two groups of beams *G1* and *G2*. Such that the dimensions of the cross-section of each group were selected to have the same coiled length (C), refer to Figure 4.3. The coiled length equals 337 mm and 415 mm for *G1* and *G2*, respectively. Each group has two different cross-sections. The details of the symbols and dimensions of the adopted sections were given in Figure 4.3 and

Table 4.1, respectively.

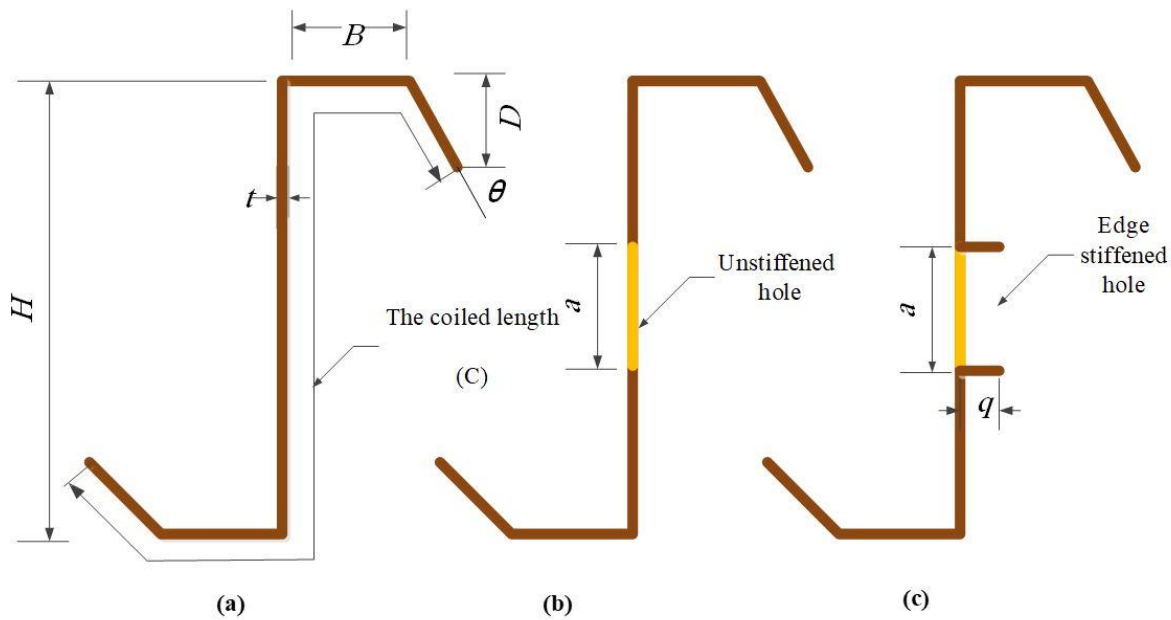

Figure 4.3 Finite element model dimensions (a: cross-section, b: unstiffened holes, c: Stiffened hole)

Table 4.1 Dimensions of the adopted Z- section

No. of Specimens	Groups	CFSZ	Web height *H* (mm)	Flange width *B* (mm)	Edge stiffener depth *D* (mm)	Thickness *t* (mm)	The hole shape	Hole depth/ web height *a/H*	Height of hole edge stiffener *q* (mm)
84	*G1* (C = 337 mm)	*Z1*	205	50	16	1	Rectangular with a width of 150 mm	0.0, 0.2, 0.4, 0.6 and 0.8	0, 5, 10 15 and 20
		Z2	193	50	22	2			
	G2 (C = 415 mm)	*Z3*	283	50	16	1			
		Z4	265	50	25	2			
20	*G2* (C = 415 mm)	*Z3*	283	50	16	1	Circular*	0.52 and 0.64	0, 5, 10 15 and 20
		Z4	265	50	25	2		0.54 and 0.66	

*The diameter of the circular holes was chosen such that the area of the circular holes = the area of rectangular holes with *a/H* = 0.4 and 0.6

As shown in

Table 4.1 the steel thicknesses (*t*) were considered as 1 and 2 mm. The edge stiffener inclination angle (θ) was chosen to be 90 Degree for all studied sections. The web holes were arranged at the mid-panel, and the holes were chosen to be rectangular holes with constant width (150 mm) or circular holes. The hole depth to web height (*a/H*) ratio ranged from 0.2, 0.4, 0.6, to 0.8. It should be noted that the holes were arranged regularly at the mid panel as shown in Figure 4.4. Finally, the parametric study considers the unstiffened hole ($q = 0$ mm) and stiffened holes. The height of the hole edge stiffener (*q*) equals 5, 10, 15, or 20 mm.

Table 4.1 includes details about the parameters that have been employed in this chapter. The Z-sections examined in the parametric analysis were labelled so that the number of the group (*G*), the thickness of the section (*t*), the ratio of hole depth to web height *R* =(*a/H*), and the height of the hole edge (*q*) were specified by the label. For instance, the label "*G1-1-R0.2-q5*" can be explained below:

- The notation "*G1*" means the group number (Group = 1).
- The number "*1*" means the thickness of the specimen ($t = 1$ mm).
- The notation "*R0.2*' means the ratio of hole depth to web height ($a/H = 0.2$).
- The notation "*q5*" means the height of the edge stiffener ($q = 5\ mm$).

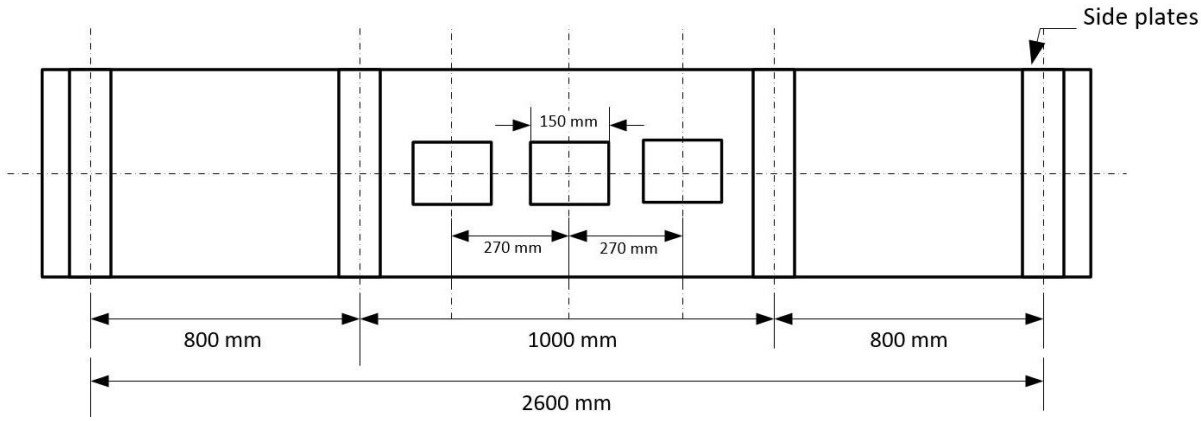

Figure 4.4 The hole location in the beam web

4.4 Examination of The Results

The bending strengths for solid beams without holes (M_{us}) and beams with holes (M_{uh}) were predicted from the nonlinear FE model. Then the impact of each parameter on the moment strength and the modes of failure of CFSZ beams are presented and discussed in the following sub-sections.

4.4.1 Effect of the section thickness (*t*)

The effect of steel thickness on the bending strength of CFSZ beams with rectangular edge stiffened holes was investigated. As can be seen, the studied sections were divided into thin sections ($t = 2$ mm) and very thin sections ($t = 1$ mm). The results shown in Figure 4.5 are for *G1* and *G2* beams. The normalized strength of the CFSZ beams with rectangular holes ($a/H = 0.6$) are presented.

As expected, the presence of the holes affects both thin and very thin sections, such that the reduction in bending strength is higher for thin sections than for very thin sections, as stated in [4]. For example, M_{uh}/M_{us} equals 0.94 and 0.85 for beams *G1-1-R0.6-q0* and *G1-2-R0.6-q0*, respectively.

And for *G2* beams M_{uh}/M_{us} equals 0.94 and 0.88 for beams *G2-1-R0.6-q0* and *G2-2-R0.6-q0*. That can be explained such that the very thin section ($t = 1$) tends to fail under the LB of the web for the solid section or LB of the web in the solid part between the holes. Hence it should be noted that the edge stiffened existence increases the strength of the CFSZ beams with holes and enhance the bending behavior of the beams. And that effect is highly observed for thin sections than for very thin sections due to LB of very thin sections as explained before such that the bending strength of the CFSZ beams with edge stiffened hole can sustain the strength of solid section or higher as for *G1-1-R0.6*.

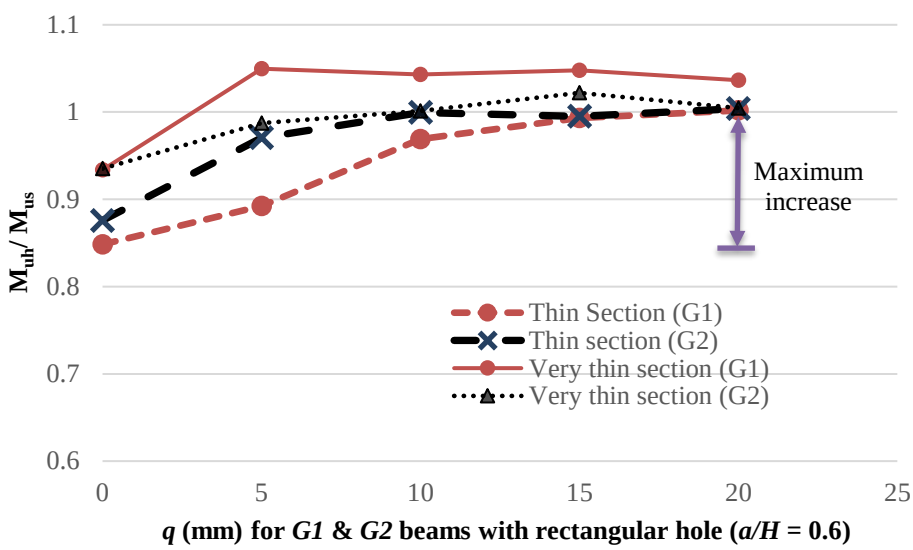

Figure 4.5 Normalized bending strength for studied beams *G1* and *G2* with rectangular holes ($a/H = 0.6$)

The same observations are presented in Figure 4.6, the studied beams have rectangular holes with an edge stiffened height of 10 mm. For very thin sections with edge-stiffened holes, the studied sections can compensate for the resistance of the solid section ($M_{uh}/M_{us} > 1$).

On contrary, for thin sections ($t = 2$) with various (*a/H*) ratios, the influence of holes is observed, such that the studied section can't achieve the solid section strength ($M_{uh}/M_{us} < 1$), especially for bigger holes (*a/H =0.8*). In other meaning, the edge-stiffened holes are unable to regain the original strength for thin sections (2 mm thickness) with rectangular holes, especially for larger holes.

The influence of the thickness (*t*) on the failure is presented in Figure 4.7, where very thin sections with rectangular holes tend to fail due to LB. Whereas the failure of the thin sections with rectangular holes is expected to battle between local or distortional buckling.

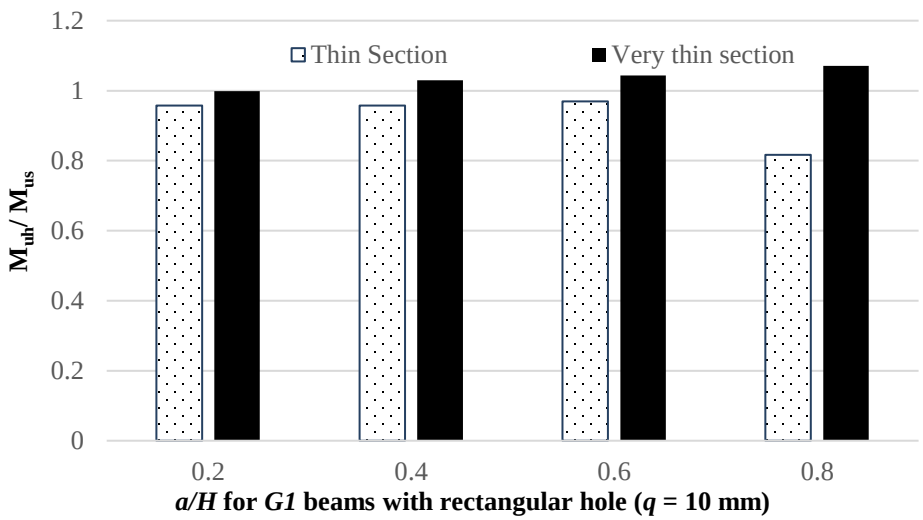

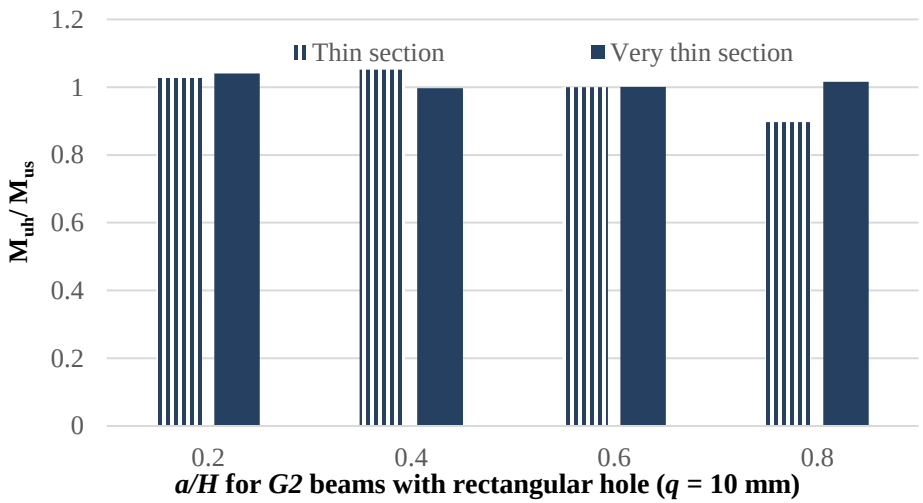

Figure 4.6 Normalized bending strength for sections with edge stiffened holes (*q* = *10* mm)

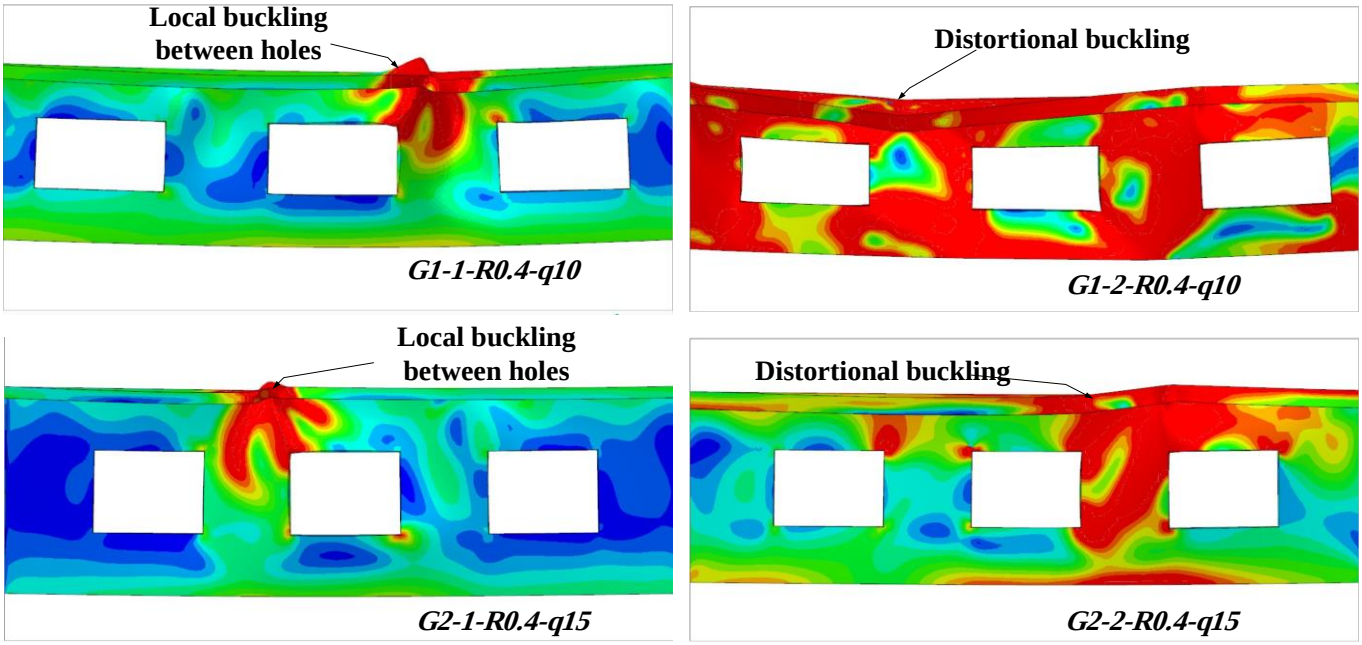

Figure 4.7 The failure modes of CFSZ beams with varying cross-section thickness

4.4.2 Effect of the hole depth to web height ratio (*R=a/H)*

To study the effect of hole depth on the moment strength, the hole depth to web height ratio (*R*) changed from (*R = 0.0*) for solid web to 0.2 then 0.4, 0.6, and 0.8 as indicated in Table 4.2. Table 4.2 demonstrates the reduction in bending strength of CFSZ beams due to the existence of rectangular holes, with unstiffened edges (*q = 0*), and with stiffened edges (*q* = 5 mm and 15 mm). It should be noted that *Z2* and *Z4* beams listed in Table 4.2 indicate that the effect of the hole is more obvious in thin thickness than in very thin thickness as discussed in the previous subsection. As expected for beams with unstiffened holes, increasing hole depth/web height causes a decrease in the bending capacity of the CFSZ beams up to 23%, as for G1-2-R0.8-q0.

However, for beams with stiffened holes, the bending strength of the CFSZ beams was affected by both the hole size (R) and the height of the hole edge stiffener (q), where the reduction in bending strength was obvious for beams with large holes ($R > 0.5$). In other words, for small R ($R < 0.5$) the presence of the hole stiffener enhances the behavior of the section, such that, CFSZ beams with edge-stiffened holes can sustain the bending strength of solid beams.

Table 4.2 Reduction in the bending strength of the CFSZ section with the variation of *R* and *q*

R	***q* = 0 mm**		***q* = 5 mm**		***q* = 15 mm**	
	M_{uh} (kN.m)	**Difference %****	**M_{uh} (kN.m)**	**Difference %****	**M_{uh} (kN.m)**	**Difference %****
for *G1-2* beams (*Z2*)						
0 (Solid web)	16.42*	-	16.42*		16.42*	
0.2	15.69	4.4	16.45	-0.2	15.74	4.1
0.4	14.80	9.9	15.70	4.4	16.00	2.6
0.6	13.93	15.2	14.65	10.8	16.31	0.7
0.8	12.64	23.0	12.98	21.0	13.65	16.9
for *G2-2* beams *(Z4)*						
0 (Solid web)	22.71*	-	22.71*		22.71*	
0.2	22.54	0.7	22.77	-0.3	23.20	-2.2
0.4	21.74	4.3	22.91	-0.9	24.57	-8.2
0.6	19.89	12.4	22.04	3.0	22.60	0.5
0.8	18.29	19.5	19.13	15.8	20.84	8.2

*The given values are the bending strength of solid webs without holes ($a/H = 0$) and so without edge stiffener ($q = 0$)

**Difference between M_{us} and M_{uh} divided by M_{us}.

4.4.3 Effect of edge stiffener height (*q*)

Concerning the impact of the hole edge stiffener height (*q*), the results, shown in Table 4.2, indicate that adding edge stiffener around rectangular holes improves the bending strength of CFSZ beams, and sometimes it can restore the original bending strength of the solid section, or it can increase the bending strength beyond the original strength. In other words, an increase in bending strength is observed when the bending strength of CFSZ beams with unstiffened holes q = 0 (2nd column of Table 3) is compared to the bending strength of the same beams with stiffened holes q = 5 and 15 mm (4th and 6th columns of Table 3). Furthermore, in most cases, as the edge stiffener height increases, the bending behavior of the CFSZ becomes better and the reduction of the bending strength decreases.

The impact of stiffened rectangular holes on the bending strength of CFSZ beams is shown in

Figure 4.8. It was observed that for *G1-1* beams, for example, bending capacity reduced up to 18.21% due to the existence of unstiffened rectangular holes with *R* equals 0.8. Hence for specimen *G1-1-R0.8-q15*, the use of stiffened holes, with an edge stiffener of 15 mm, could raise the bending strength up to 7.78%., when compared with that of the solid specimen.

To statistically analyze the effect of changing the edge stiffened height, a box plot for 80 specimens is presented in Figure 4.9. The given plot analyses the normalized bending strength, of all beams *G1* and *G2* with rectangular holes that have different *R* ratios (0.2: 0.8), when the edge stiffened height varied from $q = 0$ mm to $q = 5, 10, 15,$ and *20* mm. The plot indicates that for CFSZ beams with unstiffened holes (16 specimens), the normalized bending strength is less than 1 with a wider range of data, that means the bending strength of CFSZ beams with unstiffened holes can’t sustain the bending strength of solid sections.

Whereas 75% of CFSZ beams with stiffened rectangular holes of $q = 20$ mm achieve normalized bending strength of more than 1 with a narrow range of data. In other meaning, 75% of CFSZ members with edge-stiffened holes of 20 mm have bending strength higher than the strength of the solid members with the same section. On contrary, by using an edge stiffened height equals to 5 mm nearly 25% of the studied beams have a normalized bending capacity of more than 1, which by attention to the importance of the edge stiffener height on the bending capacity. It should be noted that the *x*-mark in the plot indicates the mean of each group, hence the means of studied beams with q equals 10, 15, and 20 are nearly the same and equal to 1. The average of the bending strength of the studied beams with q = 10, 15, and 20, is equal to the bending strength of the solid beams with the same sections.

Figure 4.10 displays the failure modes of Z beams with varying rectangular hole edge stiffener lengths. DB, LB, and distortional-local buckling interactions were observed. It should be noted that changing the q/H ratio did not affect the failure mode of the very thin section, due to the LB of the solid part between openings as discussed before. Hence the effect of the q/H ratio was observed in the thin section.

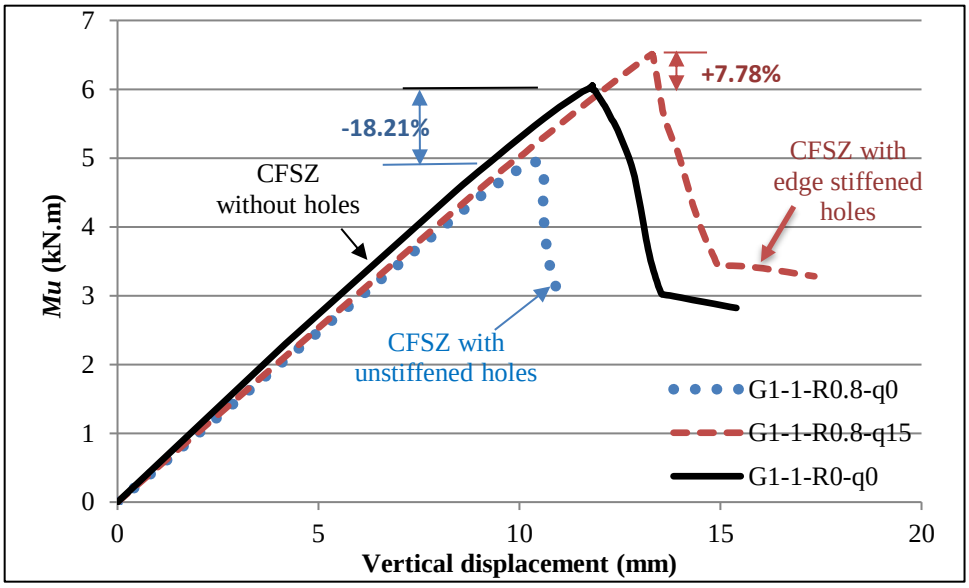

Figure 4.8 Relation between bending strength and displacement for CFSZ without holes, with unstiffened holes, and with stiffened edge holes

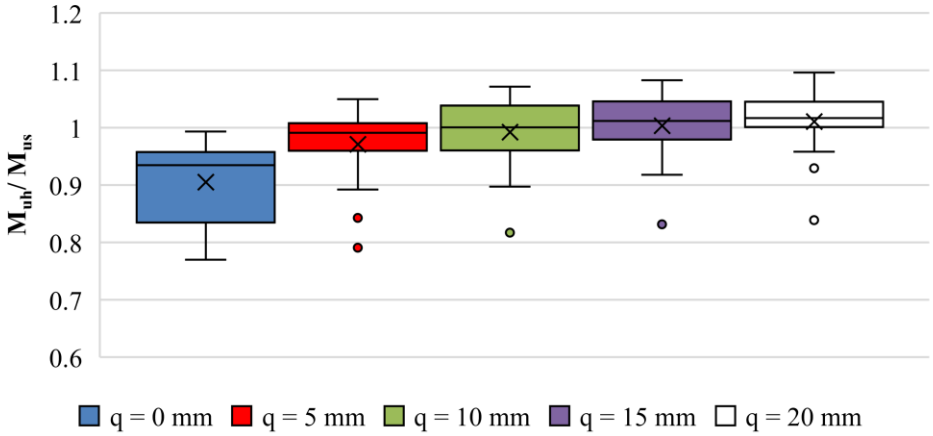

Figure 4.9 Box plot for 80 CFSZ specimens with rectangular web openings showing the effect of edge stiffened height (*q*)

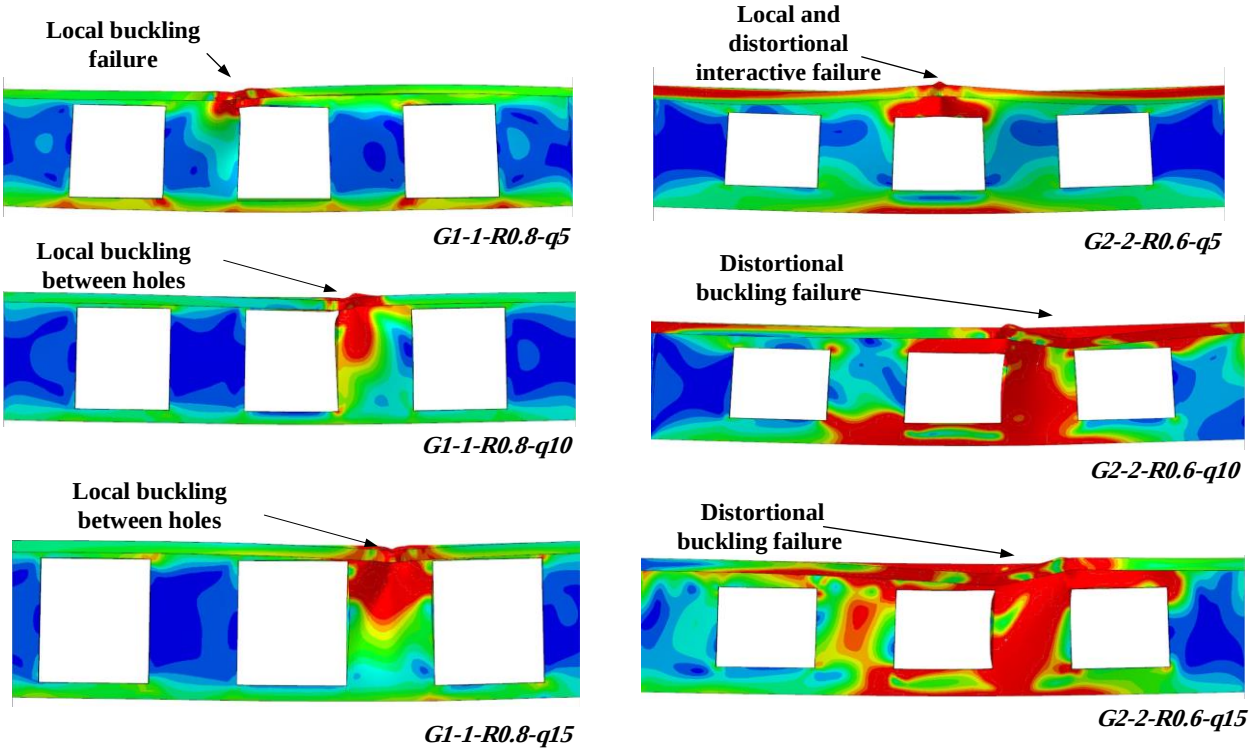

Figure 4.10 The failure modes of the CFSZ section with varying stiffener height

4.4.4 Effect of hole shape (Rectangular/Circular)

The effect of the hole shape on the moment capacity of CFSZ beams with stiffened holes was examined. The findings presented in Table 4.3 are for *Z3* and *Z4* beams. The studied beams had circular holes with *R* equals (0.52, and 0.64) for *Z3* and (0.54, and 0.66) for *Z4*. These beams were compared with rectangular holes having the same hole area such that *R* = 0.4 and 0.6. Also, the studied beams had different hole edge stiffener heights (*q* = 0, 5, 10, 15, and 20 mm). From Table 4.3, it can be noticed that the impact of stiffened circular holes on the compensation of original bending strength (for solid beams) was greater than that of stiffened rectangular holes, especially for *G2-2*. For example, the moment strength was increased by 18.5% for specimen *G2-2-R0.52-q20* with circular holes. On contrary, for *G2-2-R0.4-q20* with rectangular holes, the moment strength was increased by only 9.6%.

Table 4.3 The effect of hole shape on the bending strength

Hole shape	*G2-1* (*Z3*) beams (M_{us} = 8.64 kN.m)				*G2-2* (*Z4*) beams (M_{us} = 22.7 kN.m)			
	Specimen	M_{uh} (kN.m)	M_{uh}/M_{us}	Difference %*	Specimen	M_{uh} (kN.m)	M_{uh}/M_{us}	Difference %*
Circular holes	*G2-1-R0.52-q0*	8.13	0.94	-5.9	*G2-2-R0.52-q0*	21.7	0.96	-04.4
	G2-1-R0.0.52-q5	8.60	0.99	-0.5	*G2-2-R0.52-q5*	25.1	1.11	+10.6
	G2-1-R0.52-q10	8.60	0.99	-0.5	*G2-2-R0.52-q10*	26.5	1.17	+16.7
	G2-1-R0.52-q15	8.60	0.99	-0.5	*G2-2-R0.52-q15*	26.8	1.18	+18.1
	G2-1-R0.52-q20	8.60	0.99	-0.5	*G2-2-R0.52-q20*	26.9	1.19	+18.5
	G2-1-R0.64-q0	8.10	0.94	-6.3	*G2-2-R0.64-q0*	20.0	0.88	-11.8
	G2-1-R0.64-q5	8.60	0.99	-0.5	*G2-2-R0.64-q5*	23.0	1.01	+01.3
	G2-1-R0.64-q10	8.80	1.02	+1.9	*G2-2-R0.64-q10*	24.6	1.08	+08.4
	G2-1-R0.64-q15	8.80	1.02	+1.9	*G2-2-R0.64-q15*	25.3	1.11	+11.5
	G2-1-R0.64-q20	8.80	1.02	+1.9	*G2-2-R0.64-q20*	25.5	1.12	+12.3
Rectangular holes	*G2-1-R0.4-q0*	8.10	0.94	-6.3	*G2-2-R0.4-q0*	21.7	0.96	-04.4
	G2-1-R0.4-q5	8.48	0.98	-1.9	*G2-2-R0.4-q5*	22.9	1.01	+00.9
	G2-1-R0.4-q10	8.61	0.99	-0.4	*G2-2-R0.4-10*	23.8	1.05	+05.2
	G2-1-R0.4-q15	8.65	1.01	+0.1	*G2-2-R0.4-q15*	24.6	1.08	+08.2
	G2-1-R0.4-q20	8.69	1.01	+0.6	*G2-2-R0.4-q20*	24.8	1.10	+09.6
	G2-1-R0.6-q0	8.08	0.94	-6.5	*G2-2-R0.6-q0*	19.8	0.90	-12.4
	G2-1-R0.6-q5	8.53	0.99	-1.3	*G2-2-R0.6-q5*	22.0	0.97	-2.9
	G2-1-R0.6-q10	8.65	1.00	+0.1	*G2-2-R0.6-q10*	22.7	1.00	00.0
	G2-1-R0.6-q1	8.83	1.02	+2.2	*G2-2-R0.6-q15*	22.6	0.99	-00.4
	G2-1-R0.6-q20	8.68	1.00	+0.5	*G2-2-R0.6-q20*	22.8	1.00	+00.4

*Difference between M_{us} and M_{uh} divided by M_{us}.

Table 4.4 shows the influence of the hole shape on the failure mode. It can be noticed that changing edge stiffener heights affect the failure mode of the very thin section (*Z3*) with circular holes but this does not occur in the same section (*Z3*) with rectangular holes. For instance, for *Z3* with circular holes, LB was observed in beams with edge stiffener heights of 0-5 mm. However, for the same section, DB was demonstrated in beams with edge stiffener heights of 10-20 mm. No effect on failure mode was observed for the *Z3* section with rectangular holes with different edge stiffener heights (LB was noted to be the primary failure mode). On the other hand, for thin beams (*Z4*), DB, LB, and distortional-Local buckling interactions were observed in both cases (stiffened circular and rectangular holes).

Table 4.4 Influence of hole shape on failure modes of beams

Hole shape	*G2-1(Z3)*		*G2-2 (Z4)*	
Circular holes	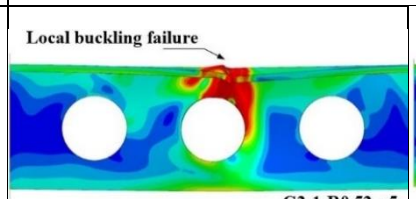 G2-1-R0.52-q5	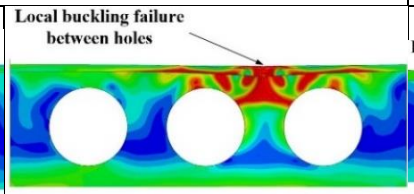 G2-1-R0.64-q5	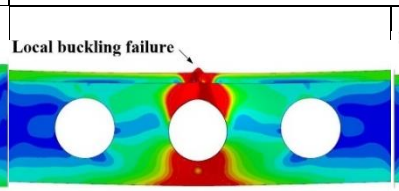 G2-2-R0.54-q5	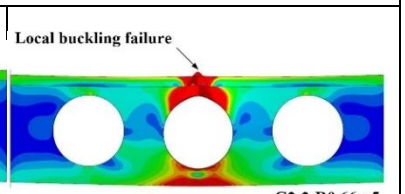 G2-2-R0.66-q5
	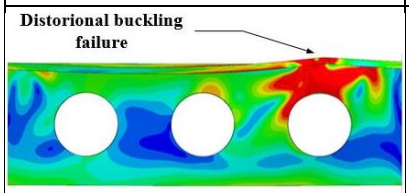 G2-1-R0.52-q20	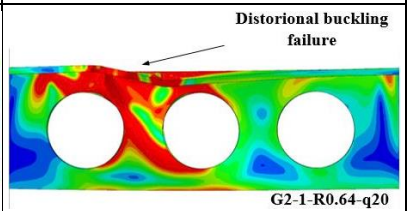 G2-1-R0.64-q20	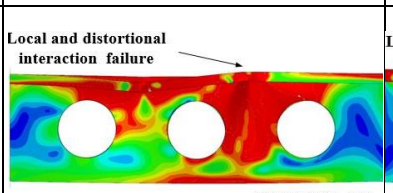 G2-2-R0.54-q20	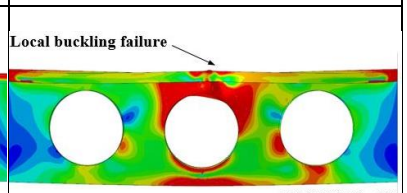 G2-2-R0.66-q20

Table 4.5 (continued)

Hole shape	*G2-1(Z3)*		*G2-2 (Z4)*	
Rectangular holes	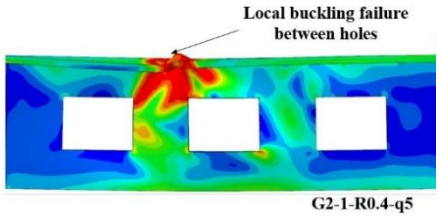	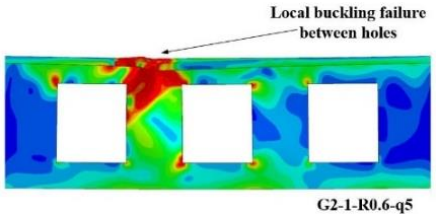	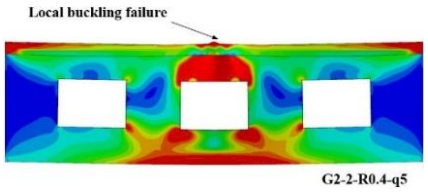	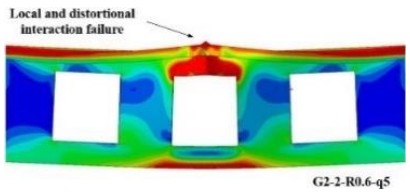
	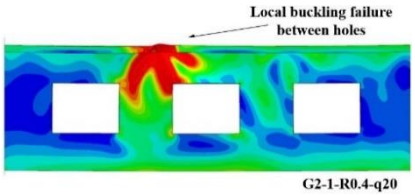	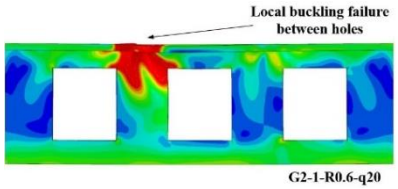	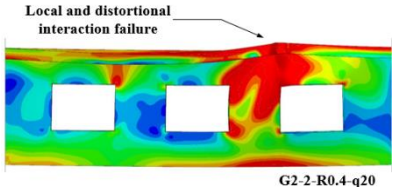	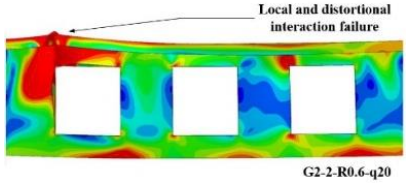

4.5 Summary

The extended parametric study was performed to examine the effect of the thickness of the cross-section, the ratio of hole depth to web height, edge stiffener height, and hole shape on the bending capacity of CFSZ beams.

The findings acquired from the parametric investigation showed that:

- With the presence of holes, thin sections have a higher reduction in bending strength compared to very thin sections. Since the very thin section tends to fail under the LB of the web for the solid section or the LB of the web in the solid part between the holes.
- The bending strength of the CFSZ beams with unstiffened holes decreased up to 23% with an increase of (a/H) ratio.
- The bending strength of CFSZ beams is enhanced by adding edge stiffener around holes. In some cases, this can restore the original bending strength or even increase the strength to become greater than the original strength.
- By increasing the edge stiffener height, the bending strength becomes better and the reduction of strength decreases. The bending strength of 75% of CFSZ beams with 20 mm edge stiffened holes is greater than the capacity of solid beams with the same section. On the other hand, nearly 25% of the examined beams have normalized bending strengths greater than 1 when using an edge stiffener height of 5 mm, drawing attention to the significance of the edge stiffener height on the bending strength.
- Stiffened circular holes have a greater influence than stiffened rectangular holes on compensating for original bending strength.

Chapter 5

Chapter 5 Investigation on the elastic DB moment of CFSZ sections with stiffened openings.

5Chapter 5 Investigation on the elastic DB moment of CFSZ sections with stiffened openings

5.1 General

In this chapter, a numerical technique to estimate the elastic distortional buckling moment of CFSZ with edge-stiffened holes is introduced, as it is necessary for the DSM design of CFS members. Buckling analysis of CFS members without openings and with unstiffened holes using finite strip methods is well-defined and is an effective method studied by previous researchers [41][63][65][66]. However, to the best of our knowledge, the buckling model of CFSZ beams has not been addressed in depth since computational techniques solving buckling modes of CFS with stiffened holes are still unclear. As indicated in Chapter 2, the justification of previous work concerning CFS beams with stiffened holes is thoroughly discussed. Criticism and limitation for the previous techniques for solving buckling modes were also presented.

CFSZ sections are thin sections subjected to local, distortional, and global modes of failure. For our case of study, the global failure mode is ignored assuming the continuous lateral restrain of compression flange by floor (reinforced concrete slab or metal deck). Furthermore, the LB of the CFSZ with stiffened holes is assumed to be the LB capacity of the CFSZ without holes, as edge stiffeners increase web bending stiffness locally and LB occurs between holes[67]. This observation is also indicated by our nonlinear analysis presented in chapter 4. From all the previous, and to prevent the LB mode for all studied beams, the distances between holes were chosen to be 110 mm, which is less than the half-buckling length of the LB mode of the studied sections.

From all previous, the numerical computational method to calculate the elastic DB moment of CFSZ with stiffened openings will be discussed in the next subsections.

5.2 Introduction of Finite Strip Method (FSM)

Finite strip analysis offers a practical and effective way to find out the elastic buckling stress and related modes. The fundamental distinctions between the FSM and the FEM are explained in this section. The FSM could be classified as a section of the FEM. Both methods share the same fundamental theory and methodology. The division of a member is the only distinction between the FEM and FSM. In the FSM, the longitudinal direction is modeled by a single element (strip) (see Figure 5.1). In comparison to a standard finite element solution, the overall number of equations required for the solution is drastically decreased when employing the finite strip method [68].

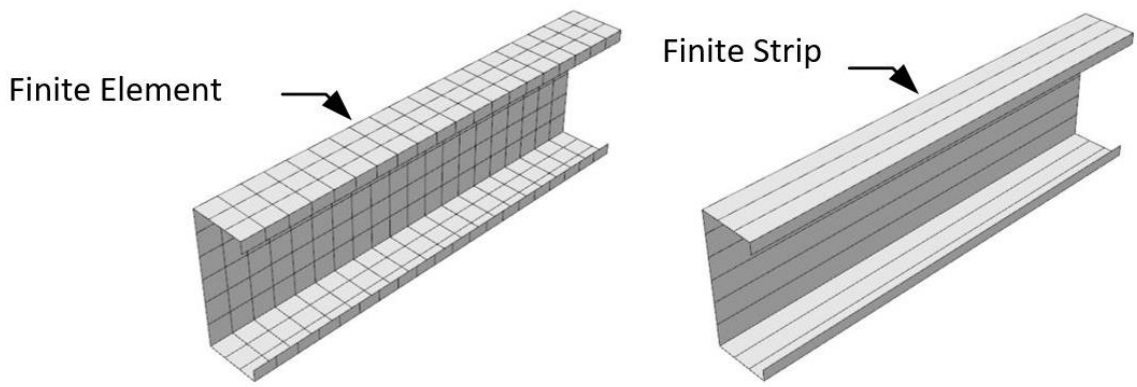

Figure 5.1 Finite strip and finite element discretization.

The finite strip program CUFSM [16] presents an implementation of the semi-analytical finite strip method appropriate for CFS beams with pinned end conditions and subjected to uniform moments. CUFSM program has many capabilities as illustrated by Schafer et al. [63], such as the automatic conversion of FSM cross-sections to shell element meshes appropriate for FEM, and the potential to include holes along the length. It performs a series of eigen-buckling analyses over a range of buckled half-wavelengths. The program can consider the three categories of elastic buckling (local, distortional, and global buckling needed in the DSM) to present the elastic buckling moment and its corresponding half-wavelength. The analysis is conducted to establish the buckling shape and the load factor of a member by methodically increasing half wavelengths [42]. The CUFSM was used in this chapter to obtain the elastic DB moment of the CFSZ beams with stiffened openings. The buckling curve is the main result from the CUFSM. Understanding CUFSM results is illustrated in Figure 5.2 The minimum of this curve is particularly significant because they reveal the load factor and half-wavelength for a specific buckling mode.

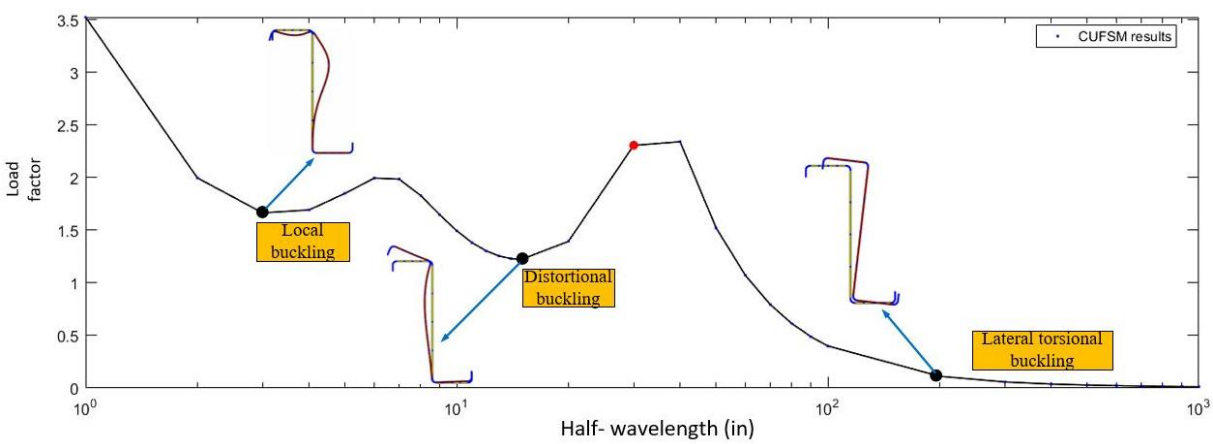

Figure 5.2 The buckling curve in CUFSM

5.3 Calculation of the distortional elastic buckling moment (M_{crd})

The elastic DB moment, M_{crd}, is determined for the CFS beams with holes as:

$$M_{crd} = \min of \begin{cases} M_{crdn} \\ M_{crdw} \end{cases} \qquad \textbf{Eq. (5.1)}$$

where:

M_{crdn} is the DB moment for the studied section with the same dimensions but without holes, which can be determined by FSM in the open source program (CUFSM) [16] or by (AISI-S100 2016) [12]. M_{crdw} is the DB moment for the same studied section including holes. The presented computational method depends on calculating M_{crdw} using CUFSM for unstiffened openings by simulating the influence of the opening with a reduced web thickness (t_r) in a finite strip analysis, as reported by Moen and Schafer [41][69]. The method used to calculate M_{crd} is summarized in the given flow chart shown in Figure 5.3.

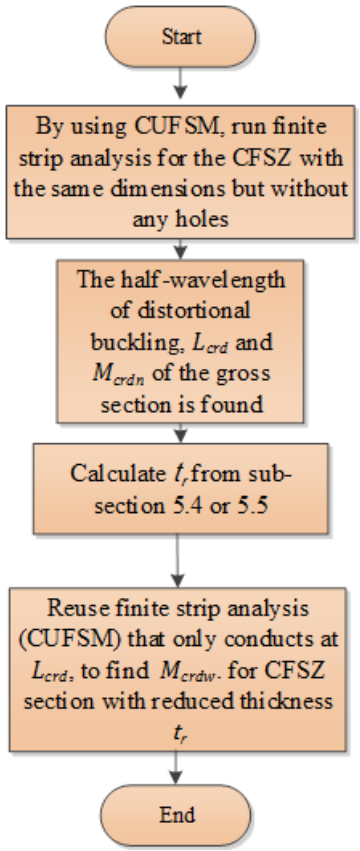

Figure 5.3 Illustration of the numerical model for calculating elastic DB moment

Hence, the influence of an edge stiffener around holes on the elastic DB moment was predicted by varying the web thickness to t_r in CUFSM using two procedures. The first procedure is based on the assumption suggested by Grey and Moen [55]. The second procedure, which is a new procedure for predicting $t_{r,}$ is suggested by the author. Both procedures of predicting t_r, needed to estimate the elastic DB moment of CFSZ beams with stiffened openings, are derived in the next subsections.

5.4 Calculating t_r based on the assumption of Grey and Moen [55]

The First procedure is based on the assumption presented by Grey and Moen [55] along with analytical equations for elastic analysis of CFS, subjected to flexure, and presented by AISI-

S100 2016 [12]. The opening existence reduces the bending stiffness of a web with holes (Eq. (5.2)), while the existence of edge stiffeners around the openings increases the bending stiffness of the web (Eq. (5.4) and Eq. (5.5)). Across a half-wavelength of DB, L_{crd} , the reduced transverse rotational stiffness of a web with an unstiffened hole $K_{\theta,\ hole}$ is reported as:

$$K_{\theta,hole} = \left(1 - \frac{L_h}{L_{crd}}\right) K_\theta \qquad \textbf{Eq. (5.2)}$$

Such that:

K_θ is the accumulative web stiffness without a hole calculated from Eq. (5.3) as stated by AISI-S100 2016 [12]. L_h is the opening length which is calculated as the width of the rectangular openings, or for circular openings, it is determined by supposing that the circular opening area is equal to equivalent rectangular opening area with a depth of opening diameter, a, as presented in Figure 5.4. L_{crd} is the half-wavelength of DB of CFS without holes (gross section) calculated from CUFSM.

$$K_\theta = \left(\frac{Et^3}{12(1-\nu^2)}\right)\left[\frac{3}{H} + \left(\frac{\pi}{L_{crd}}\right)^2 \frac{19H}{60} + \left(\frac{\pi}{L_{crd}}\right)^4 \left(\frac{H^3}{240}\right)\right] L_{crd} \qquad \textbf{Eq. (5.3)}$$

where:

ν is the Poison ratio, E is the elastic modulus of steel.

The two hole edge stiffeners, in the direction of the web height, add rotational restraint $K_{\theta,\ stiffener}$ to the web across L_{crd} [55]. It can be calculated as:

$$K_{\theta,stiffener} = \frac{2Eq^3t}{12\,a}\left(\frac{a}{H}\right)\left(\frac{L_p}{L_{cr}}\right)^3 \qquad \textbf{Eq. (5.4)}$$

Such that:

L_p is the effective hole length, and for circular holes, it is determined as half the perimeter of a circle. Hence, for rectangular holes, it equals the hole length L_h directly.

The equivalent accumulative web rotational stiffness, $K_{\theta,r}$, can be formulated by comprising the loss of web material and the existence of edge stiffeners as:

$$K_{\theta,r} = K_{\theta,hole} + 2K_{\theta,stiffener} \qquad \textbf{Eq. (5.5)}$$

At the same time $K_{\theta,r}$ can be calculated as the transverse rotational stiffness of a web without holes and having a reduced thickness t_r.

$$K_{\theta,r} = \left(\frac{Et_r^3}{12(1-\nu^2)}\right)\left[\frac{3}{H} + \left(\frac{\pi}{L_{crd}}\right)^2 \frac{19H}{60} + \left(\frac{\pi}{L_{crd}}\right)^4 \left(\frac{H^3}{240}\right)\right] L_{crd} \qquad \textbf{Eq. (5.6)}$$

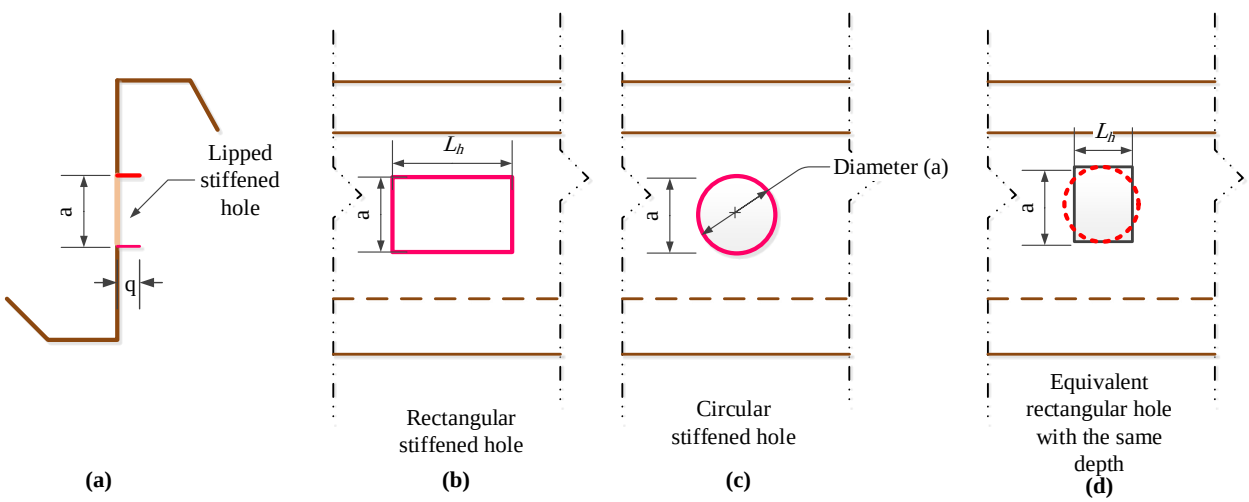

Figure 5.4 Illustration of the web hole: a) cross-section, b) web with a rectangular opening, c) web with a circular opening and equivalent rectangular to the circular opening

Replacing Eq. (5.2) and Eq. (5.4) into Eq. (5.5) and equate with Eq. (5.6)

$$\therefore\ t_r = \left[\left(1 - \frac{L_h}{L_{crd}}\right) t^3 + \left(\frac{(1-\nu^2)}{L_{crd}}\right)\frac{q^3 t}{a}\left(\frac{4}{\left[\frac{3}{H} + \left(\frac{\pi}{L_{crd}}\right)^2 \frac{19H}{60} + \left(\frac{\pi}{L_{crd}}\right)^4 \left(\frac{H^3}{240}\right)\right]}\right)\left(\frac{a}{H}\right)\left(\frac{L_p}{L_{crd}}\right)^3\right]^{1/3} \qquad \textbf{Eq. (5.7)}$$

5.5 A new procedure for calculating t_r

The second procedure is based on the analytical equations for elastic analysis of CFS, presented by AISI-S100 2016 [12]. For a CFSZ section with stiffened holes shown in Figure 5.5, the flange/web juncture is connected to the upper half of the web above the hole (indicated by the red line) and the stiffened flange (indicated by the blue line). Along hole length, the web above the hole and the flange are considered partially stiffened members subjected to compression. From that point of view, the elastic rotational stiffness presented by the web above the hole to the flange/web juncture can be defined as the procedure presented by [12] to the rotational stiffness of the flange.

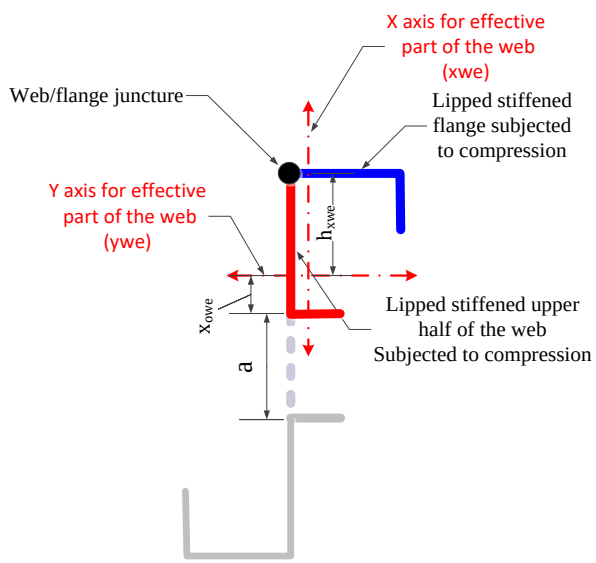

Figure 5.5 Rotational stiffness of the web/flange juncture for CFSZ with stiffened hole

Based on the previous assumption, the elastic rotational stiffness of the effective part of the web above the hole can be defined as:

$$K_{\theta we} = \left[\left(\frac{\pi}{L}\right)^4 \beta + \left(\frac{\pi}{L}\right)^2 GJ_{we}\right] L_p \qquad \textbf{Eq. (5.8)}$$

Where L is the minimum of L_{crd} or L_p, G is the shear modulus for steel, J_{we}, is the St. Venant torsional constant for the web above the hole, and β is coefficient calculated as follows:

$$\beta = EI_{xwe}(x_{owe} - h_{xwe})^2 - E\frac{I^2{}_{xywe}}{I_{ywe}}(x_{owe} - h_{xwe})^2 \qquad \textbf{Eq. (5.9)}$$

$I_{xwe}, x_{owe}, h_{xwe}$ and I_{xywe} are geometric properties for the web above the hole with stiffened edges. To get the reduced effective web thickness (t_r); the transverse rotational stiffness of a web without holes and having a reduced thickness ($K_{\theta,r}$) Eq. (5.6), equalized to the elastic rotational stiffness provided by the effective part of the web ($K_{\theta we}$) Eq. (5.8). Hence t_r can be calculated as:

$$t_r = \left[\left[\left(\frac{\pi}{L}\right)^4 \beta + \left(\frac{\pi}{L}\right)^2 GJ_{we}\right]\left[\frac{L_p 12(1-\mu^2)}{\alpha L_{crd} E}\right]\right]^{1/3} \qquad \textbf{Eq. (5.10)}$$

where α equals $\frac{3}{H} + \left(\frac{\pi}{L_{crd}}\right)^2 \frac{19H}{60} + \left(\frac{\pi}{L_{crd}}\right)^4 \left(\frac{H^3}{240}\right)$

The impact of the edge stiffener around holes on the elastic distortional moment can be predicted by varying the web thickness to t_r in CUFSM, as discussed in the numerical model presented in sub-section 5.3. The validity of the procedures to calculate t_r will be proved in the next sub-sections.

5.6 The validation of the numerical model

Two steps of validation were produced. The first step is that the elastic DB moments for the CFS with stiffened circular openings obtained by Yu [5] are compared with the proposed numerical model presented in sub-section 5.3 and elastic FE eigen buckling analysis in ABAQUS. It should be mentioned that the elastic DB moments estimated by the proposed numerical model were determined twice, with different values of t_r (sub-section 5.4 and 5.5).

The second step is to compare the different procedures of t_r calculation and verify the accuracy of the elastic distortional moments calculated using the two procedures if applied to a variety of CFSZ available on the market and have different cross-sections.

5.6.1 Validation with Yu [5]

The result of the numerical model, illustrated in Figure 5.3 using CUFSM, was compared to the elastic distortional moment stated by Yu [5] ($M_{crd,\ Yu}$) for four channels with stiffened holes. $M_{crd,t1}$ and $M_{crd,t2}$ are the DB moment formulated using the presented numerical model with t_{r1} and t_{r2}, respectively.

Table 5.1 shows that the mean values for $M_{crd,t1}/M_{crd,\ Yu}$ and $M_{crd,t2}/M_{crd,\ Yu}$ are 0.97 with standard deviations 0.04 and 0.07, respectively. Clearly, both approaches show comparable results. In the meantime, linear buckling FE analysis for four specimens of Yu [5] was set (the details of the linear buckling analysis were explained in chapter 3), and the distortional moment determined from the linear buckling FE analysis ($M_{crd,\ FE}$) were compared with Yu's ($M_{crd,\ Yu}$). The mean and standard deviation values for the four beams were 0.99 and 0.02, respectively. Those values show an excellent agreement. In the meantime, the elastic DB moments ($M_{crd,tG}$)

calculated based on the reduced web thickness t_{rG} proposed by Grey and Moen [55] were listed in

Table 5.1. The results of Grey and Moen were compared to the elastic distortional moment given by Yu [5]. The mean value for $M_{crd,tG}/M_{crd,\ Yu}$ is 1.10 with standard deviations of 0.25. This result has further strengthened our confidence in the proposed model to predict the elastic distortional moment more accurately than Grey and Moen's formula.

Table 5.1 Verification of the Numerical model against the results in Yu [5]

Section	***H*** **(mm)**	***B*** **(mm)**	***D*** **(mm)**	***t*** **(mm)**	**Hole depth (diameter)** ***a*** **(mm)**	**Height of hole edge stiffener** ***q*** **(mm)**	$M_{crd,FE}$ **(kN.m)**	$M_{crd,Yu}$ [5] **(kN.m)**	$M_{crd,FE}/M_{crd,Yu}$	t_{r1} **Eq. 5.7 (mm)**	$M_{crd,t1}$ **(kN.m)**	$M_{crd,t1}/M_{crd,Yu}$	t_{r2} **Eq 5.10 (mm)**	$M_{crd,t2}$ **(kN.m)**	$M_{crd,t2}/M_{crd,Yu}$	t_{rG} [55] **(mm)**	$M_{crd,tG}$ **(kN.m)**	$M_{crd,tG}/M_{crd,Yu}$
600S250-97	152.4	63.5	15.9	2.5832	76.2	9.1	24.41	25.13	0.97	2.455	23.50	0.94	2.269	21.50	0.86	٢,٤٤٣	23.0	0.92
800S250-97	203.4	63.5	15.9	2.5832	101.6	12.2	31.00	31.17	0.99	2.441	29.10	0.93	2.474	30.22	0.97	٢,٤٤0	29.0	0.93
1000S250-97	254.0	63.5	15.9	2.5832	127.0	15.2	35.70	35.32	1.01	2.471	33.50	0.95	2.647	35.60	1.01	٢,٧١٨	٣٨,٣	1.08
1200S250-97	304.8	63.5	15.9	2.5832	152.4	18.3	35.51	35.79	0.99	2.584	37.10	1.04	2.817	37.20	1.04	٣,١٦0	٥٢.0	1.45
Mean	-	-	-	-	-	-	-	-	0.99	-	-	0.97	-	-	0.97			1.10
Standard Deviation	-	-	-	-	-	-	-	-	0.02	-	-	0.04	-	-	0.07			0.25

5.6.2 Accuracy of the t_r procedures

The elastic DB moments, for a wide variety of CFSZ sections with stiffened holes illustrated in Table 5.2, were calculated using the presented numerical model with two procedures for calculating t_r. Then, the accuracy of the results was stated by comparing numerical model results with the results of the FE linear buckling analysis. In this sub-section M_{crdn}, M_{crdw}, for beams were identified using numerical analyses, hence M_{crd} is set to be the minimum value as stated by Eq. (5.1). Note that $M_{crdw,tr1}$, and $M_{crdw,tr2}$ were determined with a reduced web thickness t_{r1} (Eq. (5.7)), and t_{r2} (Eq. (5.10)) in CUFSM, respectively. $M_{crdw,FE}$ were calculated with FE linear buckling analysis by simulating the stiffened holes.

For CFSZ beams with stiffened openings regarded in this study, the procedures of t_{r1} (sub-section 5.4), and t_{r2} (sub-section 5.5) are on average an accurate predictor of M_{crd} (mean of 1.05 and 1.07 for the procedures of t_{r1} and t_{r2}, respectively). However, the Standard deviation of the $M_{crd,FE}/M_{crd,tr}$ are 0.04 and 0.13 of t_{r1} and t_{r2}, respectively, which indicates the accuracy of the first procedure and then the second procedure. It is worth mentioning that, the ratios of $M_{crdw,FE}/M_{crdw,tr}$ were introduced to directly justify the numerical calculation of DB moment M_{crdw}. The mean values for $M_{crdw,FE}/M_{crdw,tr1}$, and $M_{crdw,FE}/M_{crdw,tr2}$ are 1.07 and 1.05 with standard deviations 0.05 and 0.31, respectively, that did not affect the accuracy of M_{crd}, as shown in Table 5.2 and discussed for the values of $M_{crd,FE}/M_{crd,tr}$. Since the elastic distortional buckling moment (M_{crd}) is the minimum of M_{crdn} and M_{crdw}. However, it gives an advantage for t_{r1} than t_{r2}.

It should be noted that, as shown in Table 5.2, the second procedure of reduced thickness (t_{r2}) calculation is adequate and accurate in estimating M_{crdw} when the web height is more than 145 mm and (a/H) ratio is larger than 0.3. In addition, the best ratio of (a/H) that makes this procedure more effective is 0.5. Hence on average, both presented procedures are accurate numerical calculations to predict the DB moment of CFSZ beams with stiffened holes, with the privilege of the results of the first procedure.

Table 5.2 The accuracy of the presented model to calculate M_{crd}

Section	H	B	D	t	a/H	q/H	A	θ^o	q	f_y	$M_{crd,n\,FE}$	$M_{crd,w\,FE}$	$M_{crd,FE}$	$M_{crdn,CUFSM}$	t_{r1} Eq. (5.7)	$M_{crdw,tr1}$	$M_{crd,tr1}$	$M_{crd,FE}/M_{crd,tr1}$	$M_{crdw,FE}/M_{crdw,tr1}$	t_{r2} Eq. (5.10	$M_{crdw,tr2}$	$M_{crd,tr2}$	$M_{crd,FE}/M_{crd,tr2}$	$M_{crdw,FE}/M_{crdw,tr2}$
	mm	mm	mm	mm			mm	degree	mm	MPa	kN.m	kN.m	kN.m	kN.m	mm	kN.m	kN.m			mm	kN.m	kN.m		
Z14620	145.00	62.5	20.0	2.00	0.5	0.06	72.5		8.7		18.2	18.9	18.2	16.5	1.928	16.5	16.5	1.10	1.15	1.646	14.0	14.0	1.30	1.35
Z17625	175.00	62.5	20.0	2.50	0.3	0.08	52.5		14.0		32.3	32.3	32.3	31.8	2.433	30.6	30.6	1.06	1.06	3.888	58.0	31.8	1.02	0.56
					0.5	0.06	87.5		10.5		32.3	33.7	32.3	31.8	2.387	30.0	30.0	1.08	1.12	2.184	27.2	27.2	1.19	1.24
					0.7	0.08	122.5		14.0		32.3	35.0	32.3	31.8	2.379	29.7	29.7	1.09	1.18	1.810	22.3	22.3	1.45	1.57
Z20620	200.00	65.0	20.0	2.00	0.5	0.06	100.0		12.0		21.8	21.8	21.8	21.3	1.916	20.0	20.0	1.09	1.09	1.850	19.4	19.4	1.12	1.12
Z26625	225.00	65.0	20.0	2.50	0.5	0.06	112.5		13.5		36.9	37.1	36.9	36.3	2.377	34.1	34.1	1.08	1.09	2.388	34.4	34.4	1.07	1.08
Z24623	240.00	65.0	20.0	2.30	0.3	0.08	72.0		19.2		31.7	31.1	31.1	31.4	2.236	30.2	30.2	1.03	1.03	4.574	85.2	31.4	0.99	0.37
					0.5	0.06	120.0	90	14.4	450.0	31.7	33.0	31.7	31.4	2.196	29.6	29.6	1.07	1.11	2.265	31.9	31.4	1.01	1.03
					0.7	0.08	168.0		19.2		31.7	33.1	31.7	31.4	2.329	29.2	29.2	1.09	1.13	1.917	27.5	27.5	1.15	1.20
Z26630	265.00	65.0	20.0	3.00	0.5	0.06	132.5		15.9		59.6	62.4	59.6	58.9	2.844	54.9	54.9	1.09	1.14	2.966	60.0	58.9	1.01	1.04
Z30725	300.00	75.0	20.0	2.30	0.3	0.08	90.0		24.0		38.8	37.2	37.2	39.4	2.439	37.6	37.6	0.99	0.99	5.317	123.6	39.4	0.94	0.30
					0.5	0.06	150.0		18.0		38.8	40.3	38.8	39.4	2.410	37.1	37.1	1.05	1.09	2.462	38.7	38.7	1.00	1.04
					0.7	0.08	210.0		24.0		38.8	48.0	38.8	39.4	2.747	45.1	39.4	0.98	1.06	2.113	31.5	31.5	1.23	1.52
Z30730	300.00	75.0	20.0	3.00	0.5	0.06	150.0		18.0		59.3	59.3	59.3	58.5	2.868	55.5	55.5	1.07	1.07	3.065	61.2	58.5	1.01	0.97
Z34130	345.00	100	30.0	3.00	0.5	0.06	172.5		20.7		77.7	77.7	77.7	76.4	2.876	72.2	72.2	1.08	1.08	2.927	74.2	74.2	1.05	1.05
Z20312	203.20	58.4	22.8	1.27	0.5	0.06	101.6	50	12.2		6.5	6.3	6.3	6.5	1.229	6.3	6.3	1.00	1.00	1.301	6.7	6.5	0.97	0.94
Z21517	215.90	63.5	22.8	1.77	0.5	0.06	107.9	50	13.0		12.4	12.9	12.4	13.6	1.707	12.9	12.9	0.96	1.00	1.750	13.4	13.4	0.93	0.96
Z29202	292.10	88.9	22.8	2.03	0.5	0.06	146.1	50	17.5		19.2	19.6	19.2	19.2	1.962	18.3	18.3	1.05	1.07	2.136	20.5	19.2	1.00	0.96
Z21322	213.36	66.0	22.8	2.28	0.5	0.06	106.6	51	12.8	303.4	25.3	22.3	22.3	24.3	2.179	22.2	22.2	1.00	1.00	2.162	22.2	22.2	1.00	1.00
Z21529	215.90	66.0	25.4	2.98	0.5	0.06	107.9	48	12.9		40.8	41.4	40.8	42.6	2.829	39.7	39.7	1.03	1.04	2.754	38.5	38.5	1.06	1.08
Z21402	214.88	63.5	24.1	2.05	0.5	0.06	107.4	49	12.8		17.2	17.9	17.2	18.6	1.958	17.5	17.5	0.98	1.02	1.964	17.6	17.6	0.98	1.02
Mean																		1.05	1.07				1.07	1.01
S. D.																		0.04	0.05				0.13	0.31

5.7 Summary

In this chapter, a numerical method with two procedures for calculating t_r was proposed to estimate the elastic DB moment for a wide variety of CFSZ sections with stiffened holes using CUFSM. The accuracy of the findings was then determined by comparing the findings of the numerical model with that of the FE linear buckling analysis. Upon comparison, the elastic DB moment of CFSZ sections with stiffened holes was predicted accurately with the two procedures.

Chapter 6

Chapter 6 Conclusions and Trends for Future Research

6Chapter 6 Conclusions and Trends for Future Research

6.1 General

The manufacturing of CFS beams often involves openings for multiple reasons. Even so, because of openings in the web, the web area is reduced and their bending strength is decreased. To improve the bending strength of flexural members, edge stiffeners have now been added around the openings. Accordingly, this thesis presents a numerical investigation of CFSZ beams with stiffened openings. The thesis primarily focused only on the bending capacity of the prementioned beams.

Thus, a numerical investigation was performed, utilizing the ABAQUS program, on CFSZ beams with different parameters. These parameters were generally, steel thickness, edge stiffener height, hole depth to web height ratio, and hole shape. Finally, a numerical model using FSM was carried out with two procedures for defining the critical elastic DB moment of the studied sections.

6.2 Conclusions

The key conclusions that can be drawn from the examination conducted in this thesis are as follows:

1. With the presence of holes, very thin sections have a lower reduction in bending capacity compared to thin sections. A possible explanation is that the middle portion of the web of the very thin sections contributes less to maximum moment strength, as the middle portion experiences less stress because of the web buckling. As a result, cutting out areas with low stress would be less likely to affect the maximum strength of the beams.

2. The very thin sections with edge-stiffened rectangular holes can make up for the strength of the solid sections ($M_{uh}/M_{us} > 1$).
3. The edge-stiffened rectangular holes are incapable to recover the original strength for thin sections, especially for large holes ($R = 0.8$).
4. Generally, very thin sections with rectangular holes fail due to local buckling while thin sections with rectangular holes typically fail due to distortional buckling.
5. Adding edge stiffener around holes enhances the bending strength of CFSZ beams. The strength can be restored to the original value or even increased in some cases to become greater than the original value, especially for small R ($R < 0.5$).
6. The bending capacity becomes better and the reduction in capacity decreases as the height of the edge stiffener increases. The capacity of 75% of CFSZ beams with 20 mm edge stiffened holes is greater than the capacity of solid ones with the same section. On contrary, about 25% of the investigated beams have capacities greater than 1 when the edge stiffener height was 5 mm, attracting attention to the significance of the stiffener height on the bending capacity.
7. LB, DB, and the combination of DB and LB were noted in the examined beams with stiffened rectangular holes. changing the q/H ratio did not affect the failure mode of the very thin section, whereas, affected the failure mode of the thin section.
8. Stiffened circular holes have a more significant influence than stiffened rectangular holes on compensating for the original bending strength. Sections with circular holes that have edge-stiffening experienced an average increase in bending strength of 9.3% (when compared to solid sections). In contrast, sections with rectangular holes that have edge-stiffening experienced an average increase in bending strength of 2.78%.

9. The DB moment, for a wide variety of CFSZ sections with stiffened holes, was predicted with the two procedures. Therefore, on average both suggested approaches are accurate and suitable numerical calculations to predict the distortional moment of CFSZ beams with stiffened openings (mean of 1.05 and 1.07 for the procedures of $t_{r1}$and t_{r2}, respectively), with the privilege of the results of the first procedure.

6.3 Future works

The theoretical and experimental research in CFSZ sections with stiffened perforations can be further extended to:

1. Further study using the proposed FE model and the numerical method to consider a broader range of dimensions is required.
2. Study the impact of edge stiffener around perforations on the bending resistance about the minor axis of the Z section.
3. Determine the impact of stiffened openings on the Z- beam deflection with long spans.
4. Evaluate the impact of stiffened openings on the LTB moment of Z-beams.

References

7References

[1] B. H. S. Rad, “Experiments on Cold-Formed Steel Beams with Holes,” Thesis, *Virginia Polytechnic Institute and State University*, 2010.

[2] K. Mathivanan and M. H. Santhi, “FE Analysis of Hollow Flanged Cold-Formed Steel ‘ Z ’ Beams,” *International Journal of Civil Engineering and Applications*, vol. 3, pp. 1-6, 2013.

[3] T. Anapayan, “Flexural Behavior and Design of Hollow Flange Steel Beams,” *Queensland University of Technology*, no. March, p. 435, 2010.

[4] S. R. Acharya, “Reinforcement Schemes for Cold-Formed Steel Joists Having Web Openings,” *McMaster University*, no. August, 2009.

[5] C. Yu, “Cold-Formed Steel Flexural Member with Edge Stiffened Holes: Behavior, Optimization, and Design,” *Journal of Constructional Steel Ressearch*, vol. 71, pp. 210–218, 2012, doi: 10.1016/j.jcsr.2011.09.008.

[6] S. Wanniarachchi, “Flexural Behaviour and Design of Cold- formed Steel Beams with Rectangular Hollow Flanges,” *Queensland University of Technology*, no. December, p. 354, 2005.

[7] W. W. Yu and R. A. LaBoube, “Cold-Formed Steel Design,” *John Wiley & Sons*, Fourth Edition, 2010.

[8] F. Ljubinkovi, “Structural Behaviour of Cold-Formed Steel Beams Subjected to Fire,” *Coimbra University*, 2016.

[9] M. Ghannam, “Bending Moment Capacity of Cold-Formed Steel Built-Up Beams,” *International Journal of Steel Structures*, vol. 19, no. 2, pp. 660–671, 2019, doi: 10.1007/s13296-018-0155-2.

[10] B. Chea, “Cold-Formed Steel Built-Up Box Beams with Different Sections by Experimental and Numercal Study on Cold-Formed Steel Built-Up Box Beams with Different Sections,” Thesis, *Thammasat University*, 2016.

[11] G. J. Hancock, T. Murray, and D. S. Ellifrit, “Cold-Formed Steel Structures to the AISI Specification,” *CRC Press*, 2001.

[12] “AISI Standard S100-16: North American Specification for the Design of Cold-Formed Steel Structural Members ,” *American Iron and Steel Institute*, 2016.

[13] “Eurocode 3 - Design of steel structures - Part 1-3: General rules - Supplementary rules for cold-formed members and sheeting,” vol. 1, no. 2005, 2011.

[14] “Australian / New Zealand Standard ™ Cold-formed steel structures 4600:2005,” vol. 2005, no. 1, p. 153, 2005.

[15] A. Basta, “Behaviour of Stainless Steel and Cold Formed C Sections with Large Web Openings in Bending and Shear,” *Surrey University*, no. 6015142, 2017.

[16] Ben Shafer, “CUFSM.” Department of Civil Engineering, *Johns Hoplcins University*, 2006, [Online]. Available: http://www.ce.jhu.edu/bschafer/cufsm/.

[17] C. Yu and B. W. Schafer, “Local Buckling Tests on Cold-Formed Steel Beams,” *Journal of Structural Engineering*, no. December, pp. 127–144, 2002, doi: 10.1061/(ASCE)0733-9445(2003)129:12(1596).

[18] N. T. B. Nguyen, T. C. Fung, and B. Young, “ Strength and Behavior of Cold-Formed Steel Z -Sections Subjected to Major Axis Bending ,” *Journal of Structural Engineering*, vol. 132, no. 10, pp. 1632–1640, 2006, doi: 10.1061/(ASCE)0733-9445(2006)132:10(1632).

[19] C. H. Pham and G. J. Hancock, “Experimental Investigation and Direct Strength Design of High Strength Complex C-Sections in Pure Bending,” *Journal of Structural Engineering*, no. 925, pp. 1–27, 2013, doi: 10.1061/(ASCE)ST.1943-541X.0000736.

[20] Luís Laím, J. P. C. Rodrigues, and L. S. da Silva, “Flexural Behaviour of Cold-Formed Steel Beams,” *International Conference on Design, Fabrication and Economy of Metal Structures*, no. April 2014, 2013, doi: 10.1007/978-3-642-36691-8.

[21] K. S. Wanniarachchi and M. Mahendran, “Experimental Study of The Section Moment Capacity of Cold-Formed and Screw-Fastened Rectangular Hollow Flange Beams,” *Thin-Walled Structures*, vol. 119, no. March, pp. 499–509, 2017, doi: 10.1016/j.tws.2017.05.033

[22] H. T. Li and B. Young, “Tests of Cold-Formed High Strength Steel Tubular Sections Undergoing Web Crippling,” *Engineering Structures*, vol. 141, pp. 571–583, 2017, doi: 10.1016/j.engstruct.2017.03.051.

[23] F. Muftah, M. S. H. Mohd Sani, and M. M. Mohd Kamal, “Flexural Strength Behaviour of Bolted Built-Up Cold-Formed Steel Beam with Outstand and Extended Stiffener,” *International Journal of Steel Structures*, vol. 19, no. 3, pp. 719–732, 2019, doi: 10.1007/s13296-018-0157-0.

[24] M. T. Chen and B. Young, “Structural Behavior of Cold-Formed Steel Semi-Oval Hollow Section Beams,” *Engineering Structures*, vol. 185, no. January, pp. 400–411, 2019, doi: 10.1016/j.engstruct.2019.01.069.

[25] P. Manikandan and M. Thulasi, “Investigation on Cold-Formed Steel Lipped Channel Built-up I Beam with Intermediate Web Stiffener,” *International Journal of Advanced Structural Engineering*, vol. 11, no. 1, pp. 97–107, 2019, doi: 10.1007/s40091-019-0220-x.

[26] D. K. Phan and K. J. R. Rasmussen, “Flexural Rigidity of Cold-Formed Steel Built-Up Members,” *Thin-Walled Structures*, vol. 140, no. March, pp. 438–449, 2019, doi: 10.1016/j.tws.2019.03.051.

[27] A. Schudlich, A. Von der Heyden, and C. D. Moen, “Distortional Buckling Experiments on Cold-Formed Steel Joists with Unstiffened Holes,” *The 6th International Conference on Thin Walled Structures*, 2011.

[28] A. Uzzaman, J. B. P. Lim, D. Nash, J. Rhodes, and B. Young, "Web Crippling Behaviour of Cold-Formed Steel Channel Sections with Offset Web Holes Subjected to Interior-TwoFlange Loading," *Thin-Walled Structures*, vol. 50, no. 1, pp. 76–86, 2012, doi: 10.1016/j.tws.2011.09.009.

[29] P. Keerthan and M. Mahendran, "Experimental Studies of The Shear Behaviour and Strength of Lipped Channel Beams with Web Openings," *Thin-Walled Structures*, vol. 73, pp. 131–144, 2013, doi: 10.1016/j.tws.2013.06.018.

[30] C. D. Moen, A. Schudlich, and A. von der Heyden, "Experiments on Cold-Formed Steel C-Section Joists with Unstiffened Web Holes," *Journal of Structural Engineering*, vol. 139, no. 5, pp. 695–704, 2013, doi: 10.1061/(ASCE)ST.1943-541X.0000652.

[31] C. Wang, R. Liang, L. Jia, and H. Liu, "Experiments on Cold-Formed Steel Lipped Channel Beams with Complex Edge Stiffeners and Web Holes," *In Advanced Materials Research*, vol. 671–674, pp. 461–464, 2013, doi: 10.4028/www.scientific.net/AMR.671-674.461.

[32] M. Karmazínová, "Lateral Flexural-Torsion Buckling of Thin-Walled Cold-Formed Steel Beams with Holes-Design Resistance Evaluation Based on Test Results," *In Applied Mechanics and Materials*, vol. 368–370, no. 1, pp. 1683–1687, 2013, doi: 10.4028/www.scientific.net/AMM.368-370.1683.

[33] A. Uzzaman, J. B. P. Lim, D. Nash, J. Rhodes, and B. Young, "Effect of Offset Web Holes on Web Crippling Strength of Cold-Formed Steel Channel Sections Under End-Two-Flange Loading Condition," *Thin-Walled Structures*, vol. 65, pp. 34–48, 2013, doi: 10.1016/j.tws.2012.12.003.

[34] P. Keerthan and M. Mahendran, "Improved Shear Design Rules for Lipped Channel Beams with Web Openings," *Journal of Constructional Steel Research*, vol. 97, pp. 127–142, 2014, doi: 10.1016/j.jcsr.2014.01.011.

[35] L. Wang and B. Young, "Beam Tests of Cold-Formed Steel Built-Up Sections with Web Perforations," *Journal of Constructional Steel Research*, vol. 115, pp. 18–33, 2015, doi: 10.1016/j.jcsr.2015.08.001.

[36] N. V. Degtyareva and V. V. Degtyarev, "Experimental Investigation of Cold-Formed Steel Channels with Slotted Webs in Shear," *Thin-Walled Structures*, vol. 102, pp. 30–42, 2016, doi: 10.1016/j.tws.2016.01.012.

[37] J. Zhao, K. Sun, C. Yu, and J. Wang, "Tests and Direct Strength Design on Cold-Formed Steel Channel Beams with Web Holes," *Engineering Structures*, vol. 184, no. December 2018, pp. 434–446, 2019, doi: 10.1016/j.engstruct.2019.01.062.

[38] K. S. Sivakumaran, M. Y. Ng, and S. R. Fox, "Flexural Strength of Cold-Formed Steel Joists with Reinforced Web Openings," *Canadian Journal of Civil Engineering*, vol. 33, no. 9, pp. 1195–1208, 2006, doi: 10.1139/L06-064.

[39] P. Keerthan and M. Mahendran, "Improving the Shear Capacities of Lipped Channel Beams with Web Openings Using Plate Stiffeners," *Journal of Structural Engineering*, vol. 141, no. 11, pp. 1–15, 2015, doi: 10.1061/(ASCE)ST.1943-541X.0001199.

[40] B. Chen, K. Roy, A. Uzzaman, and J. B. P. Lim, "Moment Capacity of Cold-Formed Channel Beams with Edge-Stiffened Web Holes, Un-Stiffened Web Holes and Plain Webs," *Thin-Walled Structures*, vol. 157, no. August, p. 107070, 2020, doi: 10.1016/j.tws.2020.107

[41] C. D. Moen and B. W. Schafer, "Extending Direct Strength Design to Cold-Formed Steel Beams with Holes," *20th International Specialty Conference on Cold-Formed Steel Structures*, pp. 171–183, 2010.

[42] M. R. Haidarali and D. A. Nethercot, "Finite Element Modelling of Cold-Formed Steel Beams Under Local Buckling or Combined Local/Distortional Buckling," *Thin-Walled Structures*, vol. 49, no. 12, pp. 1554–1562, 2011, doi: 10.1016/j.tws.2011.08.003.

[43] M. R. Haidarali and D. A. Nethercot, "Local and Distortional Buckling of Cold-Formed Steel Beams with Both Edge and Intermediate Stiffeners in Their Compression Flanges," *Thin-Walled Structures*, vol. 54, pp. 106–112, 2012, doi: 10.1016/j.tws.2012.02.013.

[44] K. Law, Y. Zhao, W. Yan, and C. Yu, "Simplified Method for Critical Elastic Distortional Buckling of Cold-Formed Steel C and Z Sections," *Advances in Structural Engineering*, vol. 15, no. 12, pp. 2013–2019, 2012, doi: 10.1260/1369-4332.15.12.2013.

[45] D. S. Yerudkar and G. R. Vesmawala, "Finite Element Simulation of Cold Formed Steel Stiffened Zed Sections for Local , Distortional and Lateral Torsional Buckling," *American Journal of Engineering Research*, no. 1, pp. 249–255, 2017.

[46] J. Ye, S. M. Mojtabaei, I. Hajirasouliha, P. Shepherd, and K. Pilakoutas, "Strength and Deflection Behaviour of Cold-Formed Steel Back-to-Back Channels," *Engineering Structures*, vol. 177, no. July, pp. 641–654, 2018, doi: 10.1016/j.engstruct.2018.09.064.

[47] Jun Ye, "More Efficient Cold-Formed Steel Elements and Bolted Connections," Thesis, *Sheffield University*, 2016.

[48] J. Y. Ling, S. L. Kong, and F. De'nan, "Numerical Study of Buckling Behaviour of Cold-Formed C-Channel Steel Purlin with Perforation," *Procedia Engineering*, vol. 125, pp. 1135–1141, 2015, doi: 10.1016/j.proeng.2015.11.140.

[49] Wei-bin Yuan, Nan-ting Yu, and Long-yuan Li, "Distortional Buckling of Perforated Cold-Formed Steel Channel-Section Beams with Circular Holes in Web," *International Journal of Mechanical Sciences*, vol. 126, no. March, pp. 255–260, 2017, doi: 10.1016/j.ijmecsci.2017.04.001.

[50] L. Wang and B. Young, "Design of Cold-Formed Steel Built-Up Sections with Web Perforations Subjected to Bending," *Thin-Walled Structures*, vol. 120, no. June, pp. 458–469, 2017, doi: 10.1016/j.tws.2017.06.016.

[51] F. De'nan, C. K. Keong, N. S. Hashim, and N. Yuting, "A Numerical Study on Shear Buckling Capacity of Z-Section Steel Purlin with Opening," *AIP Conference Proceedings*, vol. 1892, 2017, doi: 10.1063/1.5005664.

[52] N. A. Kumar, D. A. Yogesh, K. Akshay, and H. A. L. Swinton, "Cold Formed Steel Lipped Zed Section with and Without Web Holes – Web Crippling Behaviour," *International Research Journal of Engineering and Technology*, vol. 05, no. 04, pp. 997–1001, 2018.

[53] R. M. Lawson and A. Basta, “Deflection of C Section Beams with Circular Web Openings,” *Thin-Walled Structures*, vol. 134, no. April 2018, pp. 277–290, 2019, doi: 10.1016/j.tws.2018.10.010.

[54] Nan-ting Yu, Boksun Kim, Wei-bin Yuan, Long-yuan Li, and Feng Yu, “An Analytical Solution of Distortional Buckling Resistance of Cold-Formed Steel Channel-Section Beams with Web Openings,” *Thin-Walled Structures*, vol. 135, no. October 2018, pp. 446–452, 2019, doi: 10.1016/j.tws.2018.11.012.

[55] C. N. Grey and C. D. Moen, “Elastic Buckling Simplified Methods for Cold-Formed Columns and Beams with Edge-Stiffened Holes,” *In Proceedings of The Annual Stability Conference Structural Stability Research Council*, no. January, pp. 92–103, 2011.

[56] M. Garifullin, D. Trubina, and N. Vatin, “Local Buckling of Cold-Formed Steel Members with Edge Stiffened Holes,” *Applied Mechanics and Material*, vol. 725–726, pp. 697–702, 2015, doi: 10.4028/www.scientific.net/amm.725-726.697.

[57] A. Uzzaman, J. B. P. Lim, D. Nash, and B. Young, “Effects of Edge-Stiffened Circular Holes on The Web Crippling Strength of Cold-Formed Steel Channel Sections Under One-Flange Loading Conditions,” *Engineering Structures*, vol. 139, pp. 96–107, 2017, doi: 10.1016/j.engstruct.2017.02.042.

[58] G. Perampalam, K. Poologanathan, S. Gunalan, K. Tsavdaridis, and B. Nagaratnam, “Flexural Behaviour of optimised Cold-Formed Steel Beams with Sleeve Stiffened Web Openings,” *10th International Conference on Structural Engineering and Construction Management, Kandy, Sri Lanka*, no. November, 2019.

[59] Y. Dai, K. Roy, Z. Fang, B. Chen, G. M. Raftery, and J. B. P. Lim, “A Novel Machine Learning Model to Predict The Moment Capacity of Cold-Formed Steel Channel Beams with Edge-Stiffened and Un-Stiffened Web Holes,” *Journal of Building Engineering*, vol. 53, no. February, p. 104592, 2022, doi: 10.1016/j.jobe.2022.104592.

[60] C. Liu and L. Duan, “Analytical Prediction of the Distortional Buckling Loads for Cold-Formed Channel Beams with Edge-Stiffened Rectangular Web Openings,” *Buildings*, vol. 13, no. 1, 2023, doi: 10.3390/buildings13010101.

[61] “ABAQUS Standard User’s Manual, The Abaqus Software is a product of Dassault Systèmes Simulia Crop, DassaultSystèmes,” *Providence*, RI, USA, 2008.

[62] B. W. Schafer and T. Peköz, “Computational Modeling of Cold-Formed Steel: Characterizing Geometric Imperfections and Residual Stresses,” *Journal of Constructional Steel Research* , vol. 47, no. 3, pp. 193–210, 1998, doi: 10.1016/S0143-974X(98)00007-8.

[63] B. W. Schafer, Z. Li, and C. D. Moen, “Computational Modeling of Cold-Formed Steel,” *Thin-Walled Structures*, vol. 48, no. 10–11, pp. 752–762, 2010, doi: 10.1016/j.tws.2010.04.008.

[64] C. D. Moen, T. Igusa, and B. W. Schafer, “Prediction of Residual Stresses and Strains in Cold-Formed Steel Members,” *Thin-Walled Structures*, vol. 46, no. 11, pp. 1274–1289, 2008, doi: 10.1016/j.tws.2008.02.002.

[65] B. W. Schafer, “Advances in the Direct Strength Method of Cold-Formed Steel Design,” *Thin-Walled Structures*, vol. 140, no. December 2018, pp. 533–541, 2019, doi: 10.1016/j.tws.2019.03.001.

[66] B. W. Schafer, “Review: The Direct Strength Method of Cold-Formed Steel Member Design,” *Journal of Constructional Steel Research*, vol. 64, no. 7–8, pp. 766–778, 2008, doi: 10.1016/j.jcsr.2008.01.022.

[67] C. D. Moen and C. Yu, “Elastic Buckling of Thin-Walled Structural Components with Edge-Stiffened Holes,” Structures, *Structural Dynamics, and Materials Conference, Orlando, Florida*, no. April, pp. 1–10, 2010, doi: 10.2514/6.2010-2613.

[68] B. W. Schafer, “Cold-Formed Steel Behavior and Design: Analytical and Numerical Modeling of Elements and Members with Longitudinal Stiffeners,” Ph.D. Thesis, *Cornell University*, 1997.

[69] C. D. Moen and B. W. Schafer, “Elastic Buckling of Cold-Formed Steel Columns and Beams with Holes,” *Engineering Structures*, vol. 31, no. 12, pp. 2812–2824, 2009, doi: 10.1016/j.engstruct.2009.07.007.